UNIVERSIDAD POLITÉCNICA DE MADRID

ESCUELA TÉCNICA SUPERIOR DE INGENIEROS INDUSTRIALES

WIRELESS COMMUNICATION ENHANCEMENT METHODS FOR MOBILE ROBOTS IN RADIATION ENVIRONMENTS

RAMVIYAS NATTANMAI PARASURAMAN

M.Tech. Instrument Technology

October, 2014

DEPARTAMENTO DE AUTOMÁTICA, INGENIERÍA ELECTRÓNICA E INFORMÁTICA INDUSTRIAL
ESCUELA TÉCNICA SUPERIOR DE INGENIEROS INDUSTRIALES

WIRELESS COMMUNICATION ENHANCEMENT METHODS FOR MOBILE ROBOTS IN RADIATION ENVIRONMENTS

PhD Thesis

Author: Ramviyas Nattanmai Parasuraman
M.Tech. Instrument Technology

Advisors: Manuel Ferre Perez, PhD
PhD in Automation and Robotics

Alessandro Masi, PhD
PhD in Automatic Controls and Computer Science

October, 2014

WIRELESS COMMUNICATION ENHANCEMENT METHODS FOR MOBILE ROBOTS IN RADIATION ENVIRONMENTS

Author: Ramviyas Nattanmai Parasuraman

Tribunal:

Presidente:	Ernesto Gambao
Secretario:	Claudio Rossi
Vocal A:	Pierre Bonnal
Vocal B:	Antonio Giménez
Vocal C:	Raul Marín
Suplente A:	Concha Monge
Suplente B:	Raul Suárez

Acuerdan otorgar la calificación de:

Madrid,   de   de October, 2014

Acknowledgements

I express my profound sense of gratitude to my advisors Prof.Manuel Ferre at UPM and Dr. Alessandro Masi at CERN for their immense interest, invaluable guidance, moral support and constant encouragement during the tenure of this work. I'm highly indebted to CERN supervisors Mr.Keith Kershaw and Mr.Mario Di Castro for their invaluable supervision and guidance in all ways of my term at CERN.

I express my deepest thanks to thank all my colleagues and graduate students at ROMINS lab in UPM for their support, comments and feedback in my work. Special mention goes to my colleagues Thomas Fabry, Luca Molinari, Denis Paulic, Mathieu Baudin at CERN and Prithvi Pagala, Francisco Suárez, Alex Owen-Hill, Jose Breñosa, Javier Rojo, José Maria Sebastien and all the members of the group of Robots and Intelligent Machines (ROMIN) at the Centro de Automática y Robótica (CAR) in UPM and all PURESAFE researchers and their supervisors.

It wouldn't go without saying my wife's moral support and encouragement during the course of this work. I am very grateful to my parents, without whom none of this world is possible. I'm also thankful to my sister, who has always played the roles of both an adviser and a best friend in my life. They are all an unbelievable inspiration to me for instilling the love of learning in me and for teaching me about integrity, dignity and respect.

My sincere thanks to all my friends especially Lakshmi Prabha, Mythra Nemallapudi, Raja Sripada and Amitabh Srinivas for their immense help and support during the course of my PhD.

Reader's guide

This page is intended to guide the readers in understanding the logical organisation of the thesis chapters to boost reader's comprehension. While this thesis is no exception to the typical convention (in which consecutive reading order is used to provide incremental understandability while reading the chapters successively), readers can make discontinuity at some chapters without loosing the readability. A dependency graph is shown below to help the readers. A detailed outline of the thesis organization is presented in section 1.4 concentrating on the technical flow but this guide concentrates only on the logical flow.
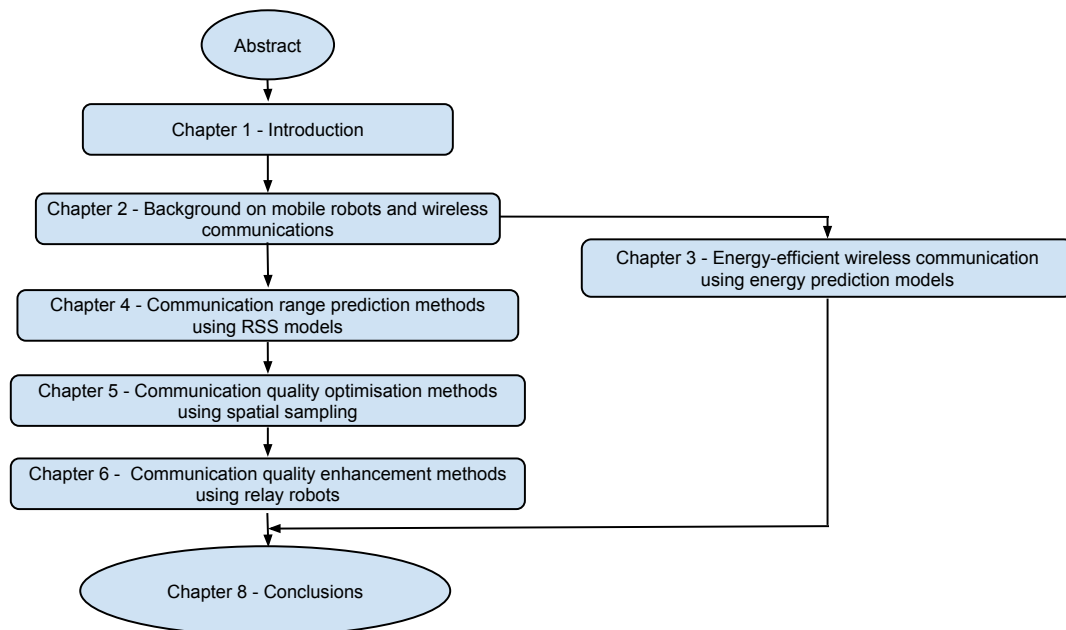
Abstract

In hostile environments such as in scientific facilities where ionising radiation is a dominant hazard, reducing human interventions by increasing robotic operations are desirable. CERN, the European Organization for Nuclear Research, has around 50 km of underground scientific facilities, where wireless mobile robots could help in the operation of the accelerator complex, e.g. in conducting remote inspections and radiation surveys in different areas. The main challenges to be considered here are not only that the robots should be able to go over long distances and operate for relatively long periods, but also the underground tunnel environment, the possible presence of electromagnetic fields, radiation effects, and the fact that the robots shall in no way interrupt the operation of the accelerators.

Having a reliable and robust wireless communication system is essential for successful execution of such robotic missions and to avoid situations of manual recovery of the robots in the event that the robot runs out of energy or when the robot loses its communication link. The goal of this thesis is to provide means to reduce risk of mission failure and maximise mission capabilities of wireless mobile robots with finite energy storage capacity working in a radiation environment with non-line-of-sight (NLOS) communications by employing enhanced wireless communication methods. Towards this goal, the following research objectives are addressed in this thesis: predict the communication range before and during robotic missions; optimise and enhance wireless communication qualities of mobile robots by using robot mobility and employing multi-robot network.

This thesis provides introductory information on the infrastructures where mobile robots will need to operate, the tasks to be carried out by mobile robots and the problems encountered in these environments. The reporting of research work carried out to improve wireless communication comprises an introduction to the relevant radio signal propagation theory and technology followed by explanation of the research in the following stages: An analysis of the wireless communication requirements for mobile robot for different tasks in a selection of CERN facilities; predictions of energy and communication autonomies (in terms of distance and time) to reduce risk of energy and communication related failures during missions; autonomous navigation of a mobile robot to find zone(s) of maximum radio signal strength to improve communication

coverage area; and autonomous navigation of one or more mobile robots acting as mobile wireless relay (repeater) points in order to provide a tethered wireless connection to a teleoperated mobile robot carrying out inspection or radiation monitoring activities in a challenging radio environment. The specific contributions of this thesis are outlined below.

The first sets of contributions are novel methods for predicting the energy autonomy and communication range(s) before and after deployment of the mobile robots in the intended environments. This is important in order to provide situational awareness and avoid mission failures. The energy consumption is predicted by using power consumption models of different components in a mobile robot. This energy prediction model will pave the way for choosing energy-efficient wireless communication strategies. The communication range prediction is performed using radio signal propagation models and applies radio signal strength (RSS) filtering and estimation techniques with the help of Kalman filters and Gaussian process models.

The second set of contributions are methods to optimise the wireless communication qualities by using novel spatial sampling based techniques that are robust to sensing and radio field noises and provide redundancy features. Central finite difference (CFD) methods are employed to determine the 2-D RSS gradients and use robot mobility to optimise the communication quality and the network throughput. This method is also validated with a case study application involving superior haptic teleoperation of wireless mobile robots where an operator from a remote location can smoothly navigate a mobile robot in an environment with low-wireless signals.

The third contribution is a robust stochastic position optimisation algorithm for multiple autonomous relay robots which are used for wireless tethering of radio signals and thereby to enhance the wireless communication qualities. All the proposed methods and algorithms are verified and validated using simulations and field experiments with a variety of mobile robots available at CERN.

In summary, this thesis offers novel methods and demonstrates their use to predict energy autonomy and wireless communication range, optimise robots position to improve communication quality and enhance communication range and wireless network qualities of mobile robots for use in applications in hostile environmental characteristics such as scientific facilities emitting ionising radiations. In simpler terms, a set of tools are developed in this thesis for improving, easing and making safer robotic missions in hostile environments.

This thesis validates both in theory and experiments that mobile robots can improve wireless communication quality by exploiting robots mobility to dynamically optimise their positions and maintain connectivity even when the (radio signal) environment possess non-line-of-sight characteristics. The methods developed in this thesis are well-suited for easier integration in mobile robots and can be applied directly at the application layer of the wireless network. The results of the proposed methods have outperformed other comparable state-of-the-art methods.

Resumen

En entornos hostiles tales como aquellas instalaciones científicas donde la radiación ionizante es el principal peligro, el hecho de reducir las intervenciones humanas mediante el incremento de las operaciones robotizadas está siendo cada vez más de especial interés. CERN, la Organización Europea para la Investigación Nuclear, tiene alrededor de unos 50 km de superficie subterránea donde robots móviles controlador de forma remota podrían ayudar en su funcionamiento, por ejemplo, a la hora de llevar a cabo inspecciones remotas sobre radiación en los diferentes áreas destinados al efecto. No solo es preciso considerar que los robots deben ser capaces de recorrer largas distancias y operar durante largos periodos de tiempo, sino que deben saber desenvolverse en los correspondientes túneles subterráneos, tener en cuenta la presencia de campos electromagnéticos, radiación ionizante, etc. y finalmente, el hecho de que los robots no deben interrumpir el funcionamiento de los aceleradores.

El hecho de disponer de un sistema de comunicaciones inalámbrico fiable y robusto es esencial para la correcta ejecución de las misiones que los robots deben afrontar y por supuesto, para evitar tales situaciones en las que es necesario la recuperación manual de los robots al agotarse su energía o al perder el enlace de comunicaciones. El objetivo de esta Tesis es proveer de las directrices y los medios necesarios para reducir el riesgo de fallo en la misión y maximizar las capacidades de los robots móviles inalámbricos los cuales disponen de almacenamiento finito de energía al trabajar en entornos peligrosos donde no se dispone de línea de vista directa. Para ello se proponen y muestran diferentes estrategias y métodos de comunicación inalámbrica. Teniendo esto en cuenta, se presentan a continuación los objetivos de investigación a seguir a lo largo de la Tesis: predecir la cobertura de comunicaciones antes y durante las misiones robotizadas; optimizar la capacidad de red inalámbrica de los robots móviles con respecto a su posición; y mejorar el rango operacional de esta clase de robots. Por su parte, las contribuciones a la Tesis se citan más abajo.

El primer conjunto de contribuciones son métodos novedosos para predecir el consumo de energía y la autonomía en la comunicación antes y después de disponer de los robots en el entorno seleccionado. Esto es importante para proporcionar conciencia de la situación del robot y evitar fallos en la misión. El consumo de energía se predice usando una estrategia propuesta la cual

usa modelos de consumo provenientes de diferentes componentes en un robot. La predicción para la cobertura de comunicaciones se desarrolla usando un nuevo filtro de RSS (Radio Signal Strength) y técnicas de estimación con la ayuda de Filtros de Kalman.

El segundo conjunto de contribuciones son métodos para optimizar el rango de comunicaciones usando novedosas técnicas basadas en muestreo espacial que son robustas frente a ruidos de campos de detección y radio y que proporcionan redundancia. Se emplean métodos de diferencia central finitos para determinar los gradientes 2D RSS y se usa la movilidad del robot para optimizar el rango de comunicaciones y la capacidad de red. Este método también se valida con un caso de estudio centrado en la teleoperación háptica de robots móviles inalámbricos.

La tercera contribución es un algoritmo robusto y estocástico descentralizado para la optimización de la posición al considerar múltiples robots autónomos usados principalmente para extender el rango de comunicaciones desde la estación de control al robot que está desarrollando la tarea. Todos los métodos y algoritmos propuestos se verifican y validan usando simulaciones y experimentos de campo con variedad de robots móviles disponibles en CERN.

En resumen, esta Tesis ofrece métodos novedosos y demuestra su uso para: predecir RSS; optimizar la posición del robot; extender el rango de las comunicaciones inalámbricas; y mejorar las capacidades de red de los robots móviles inalámbricos para su uso en aplicaciones dentro de entornos peligrosos, que como ya se mencionó anteriormente, se destacan las instalaciones científicas con emisión de radiación ionizante. En otros términos, se ha desarrollado un conjunto de herramientas para mejorar, facilitar y hacer más seguras las misiones de los robots en entornos hostiles.

Esta Tesis demuestra tanto en teoría como en práctica que los robots móviles pueden mejorar la calidad de las comunicaciones inalámbricas mediante la profundización en el estudio de su movilidad para optimizar dinámicamente sus posiciones y mantener conectividad incluso cuando no existe línea de vista. Los métodos desarrollados en la Tesis son especialmente adecuados para su fácil integración en robots móviles y pueden ser aplicados directamente en la capa de aplicación de la red inalámbrica.

Contents

List of Figures

List of Tables

Terms and Definitions

CERN   The European Organization for Nuclear Research (French: Conseil Européen pour la Recherche Nucléaire).

LHC   The Large Hadron Collider.

ISOLDE   Isotope Separator On Line DEvice.

RP   Radiation Protection.

ALARA   As Low As Reasonably Achievable

RH   Remote Handling.

RSP   Radio Signal Propagation.

RSS   Radio Signal Strength (also, Received Signal Strength).

RSSI   Received Signal Strength Indicator.

LQI   Link Quality Indicator.

RTT   Round Trip Time.

SNR   Signal to Noise Ratio.

PL   Path Loss.

ELNSM   Extended Log-Normal Shadowing Model.

WNC   Wireless Network Capacity.

LOS   Line-of-Sight.

NLOS   Non-Line-of-Sight or Near-Line-of-Sight.

LFC   Leaky Feeder Cable.

RBF   Radial Basis Function.

DKF   Discrete Kalman Filter.

MWN   Mobile Wireless Nodes.

RSO   Robust Stochastic Optimisation.

SGA   Stochastic Gradient Ascent.

CFD   Central Finite Difference.

IIR   Infinite Impulse Response.

EMA   Exponential Moving Average.

SRC   Server-Relay-Client framework.

Chapter 1

Introduction

This chapter will introduce the objectives and motivations of the thesis, the problems and challenges considered and will provide the requirements for a solution. Then a solution proposed to meet the needs and requirements will be presented along with the application scenarios where the solution will be implemented. Afterwards, the research questions and objectives this thesis aims to solve while establishing the proposed solution will be discussed. Finally, the organisation of the thesis and the contributions in each chapter will be outlined.

1.1   Motivation

Robots are increasingly considered in applications in hostile and hazardous environments where humans cannot perform some tasks due to safety issues such as high radiation levels or because of challenges in the environments [1], [2]. Furthermore, there exist a special category of robots known as rescue robots, which are meant to intensify rescue efforts during a disaster situation where human may not be fully able to perform the tasks due to harmful or risky environments.

There are two important motivations behind this thesis.

- First motivation is from the European Organization for Nuclear Research (CERN[1]), which has identified the need for and is in the process of developing several devices for remote inspection and radiation survey for different areas of its accelerator complex to avoid/minimise the need for personnel to go into radiation areas [3]. The remote operation devices capable of the before mentioned tasks typically possess some autonomy capabilities to ease part of the workload for human operators conducting the remote operation.

- Second motivation comes from the potential applications of robots in urban search and rescue (USAR) during disaster situations, where mobile robots could certainly assist humans in search and rescue operations especially in changing environmental conditions [4].

In the applications emerging from both of the above motivations, the primary objective is to reduce the risk of robotic mission failure and maximise robotic mission capabilities given the conditions that the robot has finite energy storage capacity, deployed in a hazardous environment and encounters non-line-of-sight wireless communication.

Most of the discussions in this thesis are inclined towards the first motivation for two elementary reasons: this thesis is carried out at CERN and the outcome of this research will be exploited immediately at CERN. An important application using robots at CERN is the remote radiation measurement and survey. If the radiation survey task is done remotely, significantly reduction in radiation exposure to humans can be achieved and hence can greatly benefit the radiation protection (RP) operations at CERN. The following section provides more details on the background of ionising radiation at CERN, the radiation protection, and the operations involved.

---

[1]At CERN, the world's largest and most complex scientific instruments are used to study the basic constituents of matter, the fundamental particles. The particles are made to collide together at close to the speed of light. The process gives the physicists clues about how the particles interact, and provides insights into the fundamental laws of nature. The instruments used at CERN are purpose-built particle accelerators and detectors. Accelerators boost beams of particles to high energies before the beams are made to collide with each other or with stationary targets. Detectors observe and record the results of these collisions. Founded in 1954, the CERN laboratory sits astride the Franco-Swiss border near Geneva. It is one of Europe's first joint ventures and now has 21 member states.

1.1.1   Radiation protection

A dominant hazard in the environment considered in this thesis is the hazard due to ionising radiation which has impact in both biological and non-biological elements. Ionisation is an process in which an atom becomes an ion by gaining or losing electrons due to the energy carried by the radiation. There are many sources of radiations such as the background cosmic radiation that are abundant in nature, and artificially created radiations by particle accelerators, for instance. Sources for ionising radiations are mainly alpha particles (protons and neutrons), beta particles (electrons and positrons), and photons (gamma rays, X-rays). The ionising radiation can affect humans with deterministic (high radiation exposure) and stochastically (low level of exposure). The ionising radiation is measured and quantised using the following quantities:

Absorbed dose: The absorbed dose, or energy, is the fundamental physical quantity that is used as the basis for all subsequent radiation protection quantities that are used in radiation protection. The absorbed dose, abbreviated as D, is the amount of energy locally deposited at a given location in matter. It is defined as the deposited energy (ΔE) per unit of mass of material (Δm).

$$D = \frac{\Delta E}{\Delta m} \qquad [\text{Gy} = \text{J.kg}^{-1}]. \qquad (1.1)$$

The unit of absorbed dose is the gray (equivalent to 100 rads). The absorbed dose not only depends on the incident radiation, but also on the absorbing material (depending on their mass). The energy deposited in material due to ionising radiation is measured in gray(Gy). To use the absorbed dose in practical radiation protection applications on humans, doses have to be averaged over tissue volumes (i.e. organs) according to the recommendations of the International Commission on Radiation Protection (ICRP) [5].

Effective dose: The effective dose is then defined as follows:

$$H_{eff} = \sum_T w_T H_T = \sum_T w_T \sum_R w_R D_{T,R} \qquad [Sv]; \qquad (1.2)$$

where, w_T is the tissue weighting factor for tissue T [5] and $\sum w_T = 1$, H_T is the equivalent dose received by tissue T, w_R is the weighing factor for radiation type R [5], $D_{T,R}$ is the equivalent dose received by tissue T for radiation type R. The unit of effective dose is "Sievert" (Sv = J.kg^{-1}).

Dose rate: The dose rate is defined as the dose of ionising radiation delivered per unit time.

$$\dot{H} = \frac{H_{eff}}{\Delta t} \qquad [Sv.h^{-1}]. \qquad (1.3)$$

The term Δt is the accumulation time while measuring radiation dosage.

Radiation protection (RP) [6], sometimes also called as radiological protection (RP), is the science and practice of protecting people and the environment from the harmful effects of ionising radiation. RP also includes the technology and its implementation in measuring radiation levels. As the goal of RP is to protect human beings from the damaging biological effects of ionising radiation, RP is concerned about the radiation effects on humans, the effective dose and dose rate are primarily used in the RP applications.

Human intervention is often required for repairing/maintenance when there is a planned technical stop or shutdown or when there is failure of equipment inside the scientific facility. There exist legal bodies that provide rules and recommendations to restrict the operational radiation exposure to humans. The prevalent method for implementing the justification, optimisation and limitation of the radiation exposure to people is the so-called ALARP or ALARA approach (As Low As Reasonably Practicable or Achievable [7]). In [8], ALARA is explained as follows: "ALARA is an acronym for the ICRP recommendation on the optimisation of radiation protection, namely, that radiation doses be kept as low as reasonably achievable, social and economic considerations being taken into account". Also at CERN, the ALARA principle is adopted [9], [10].

Figure 1.1 provides an example of life-cycle of operations of CERN's beam facilities and situation that necessitate implementation of the ALARA approach. The following criteria apply depending on whether the particle accelerator machines (and so the beams in the machine) are running:

- Beam ON: No personnel access is possible when particle beams are circulating in the accelerator. This is because of high levels of radiations that will affect both humans and electronics inside the facilities. For the same reason, electronics devices (including mobile robots) cannot be permanently fixed/placed inside the beam facilities.

- Beam OFF: Personnel access and human intervention are usually possible only after a "cool down" period (when the residual activity is below certain legal and admissible threshold) depending on the facility. This is because there are residual radioactivity from the activated components when the beam is "off". Radiation tolerance in robot components are generally more than four orders of magnitude higher than in humans [11]–[13]. For this reason, electronic devices (and mobile robots) can be used inside the beam facilities during (and also after) the cool down period when human access is restricted [13].

CERN has a legislation to protect the public and persons working on its site from any unjustified exposure to ionising radiation. For this purpose, CERN's Occupational Health and Safety and Environmental Protection (HSE) Unit monitors ambient dose equivalent rates inside and outside CERN's perimeter and releases of radioactivity in air and water. The results of the measurements
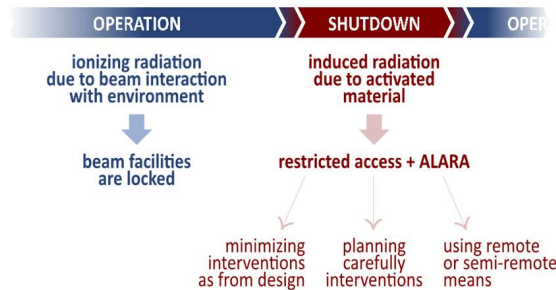
Figure 1.1: Application of ALARA and intervention operation restrictions in scientific facilities.

allow the preventive assessment of radiological risks and the minimisation of individual and collective doses.

CERN's HSE Unit currently operates two radiation monitoring systems: ARCON (ARea CONtroller) [14], which was developed at CERN for the Large Electron-Positron (LEP) collider and has been in use since 1988 and RAMSES (RAdiation Monitoring System for the Environment and Safety) [15], which was designed for the Large Hadron Collider (LHC[2]) based on current industry standards and has been in use since 2007.

About 800 monitors are employed in ARCON and RAMSES, about 400 for each system. Both installations comprise data acquisition, data storage, and the triggering of radiation alarms and beam interlocks. The most recent CERN facilities (the LHC, for example) are equipped with RAMSES, whereas the entire LHC injector chain, the remaining facilities, and all experimental areas are still equipped with ARCON. In the long run, it is envisaged that ARCON will be replaced by the more recent RAMSES technology [14], [15].

Before permitting any personnel inside the facilities for intervention or maintenance tasks, there is a need for radiation survey to be conducted by the RP personnel. Therefore, the purpose of the radiation surveys is to provide radiation measurements before interventions and the results are used to calculate the dose rate data required for maintenance or intervention job and dose planning of the intervention based on the ALARA (As Low as Reasonably Achievable) principle.

While automatic radiation data gathering at CERN is performed through a state-of-the-art RAMSES system, the obtained data is sparse and more detailed measurements (called as "RP Survey") are often done manually by the radiation protection technicians at CERN (see figure 1.2). Even though the conventional (personnel access) RP survey is easy to perform, there are some restrictions associated with it. They are,

- Dose to RP personnel shall be kept as low as reasonably possible

---

[2]The LHC is the largest particle accelerator in the world. It was built by CERN between 1998 and 2008. It is located in a tunnel of 27 km in circumference, at a depth of 175 meters near Geneva, on the French-Swiss border.

- Long waiting time before RP access because of long time of cool down of some activated equipment

- Need to do RP survey quickly so as to minimise the exposure to RP personnel.

- Limited number of RP personnel available at a time.

Figure 1.2: Radiation Protection (RP) personnel performing a RP survey manually.

After conducting the RP survey at each access to the radioactive areas, the measured dose rates and visual inspection together helps the RP personnel plan the intervention and optimise human exposure. For instance, the dose limit for a person conducting intervention at CERN is 6 mSv per year and for normal employees at CERN is 2 mSv per year [9].

1.1.2   Need for mobile robots

The needs and benefits of having a robotic means for remote handling or remote measurement/inspection application are described in this section. As already detailed, conducting the radiation survey and visual inspection tasks from a remote location (to reduce radiation exposure to humans) are of great benefit to the RP personnel. This remote operation can be realised with a robotic solution. Generally, electronics can tolerate a radiation dosage of up to 100 Sv, which is more than 10^4 times the maximum dose limit (6 mSv) for RP personnel at CERN [9]. This fact supports the need for using robots instead of humans for radiation survey, visual inspection and robotic interventions in radiation environments.

There are existing systems at CERN for conducting remote measurement and handling systems such as a radiation monitoring system (RAMSES) that consists of fixed radiation sensors stationed sparsely inside most of the CERN facilities including the LHC [14], the "Train Inspection

Monorail" (TIM) robotic platform [16] and overhead cranes for conducting remote handling operations. These existing remote operation solutions have either cost limitations or infrastructure limitations [17]. This factor too promotes the necessity of having mobile robots inside CERN facilities for performing simple remote radiation measurements and visual checks of radioactive equipments.

The principal benefits of using a mobile robot at CERN are outlined below.

- Reduce radiation exposure of radiation protection personnel by reducing their time in radioactive areas.

- Permit measurements when manual radiation measurements are needed but not possible due to ALARA (As Low as Reasonably Achievable) constraint.

- Save waiting time at the beginning of an intervention (e.g.: in ISOLDE area at CERN, the waiting time before human intervention can be up to 5 days)

The use of mobile robots would strongly reduce the dose given to personnel and the waiting time required to manually perform visual inspection of highly radioactive components (for instance, in ISOLDE area). Especially in cases of machine failures during beam operation, the cool down period can be quite long (several days) before an access for a visual check of the equipment can be granted. One can also consider to extend the use of mobile robots for remote handling and maintenance tasks in hostile facilities. Besides, mobile robots could help in the planning of a human intervention for repair or maintenance of some equipment of the accelerators by providing detailed radiation measurements and visual checks of faulty equipments. Moreover, a mobile robot would allow performing more accurate measurements or visual inspections since time limits (for humans) in high radiation places will not pose a problem any more.

As the radiation measurements need to be conducted in many locations, mobility is vital for a robot performing a RP survey, and this makes the "mobile robots" essential in such applications. Any locomotion on a robotic platform materialises energy limitations. Internal combustion engines cannot be used inside a scientific facility due to the constraints in the environment and hence only batteries with limited energy storage capacity can be used for driving the mobile robot. The chapter 3 discusses the role of managing energy consumption in mobile robots and the use of predicting energy consumption beforehand in optimising the wireless communication devices of the mobile robot.

As the mobile robots are intended for remote measurements and operations, they are usually controlled from a command station, by employing wired or wireless communication means. The wired communication (E.g. optical fibre cables) generally poses a lot of problems [1], [4] such as being fragile or can easily be run over, broken or damaged and can clutter the environment. For example, the most significant problem in the Quince robot that was used in radiation

measurement application at the Fukushima Daiichi nuclear disaster area, was the communication cable where the cable-rewinding device on the Quince robot did not work properly at the end of the sixth mission and in the end, the cable became useless and the Quince robot can not retrieved for several months from the radiation area [4]. Hence there is an undoubted need for wireless communication for the mobile robot.

In the next section, the problems, challenges and constraints at CERN associated with the development of mobile robot based solutions are discussed.

1.2   Problems and challenges

The solution of using a wireless mobile robot is of great interest to specifically RP personnel. It is wise to implement a robotic solution after considering the constraints and challenges applicable in the intended hostile and cluttered environments. Therefore, a deep insight of the real application environments and the associated challenges are required before conducting the research as the practical use of the robots at CERN is the aim. Detailed specifications of the requirements and constraints for the robot itself are presented in (the) appendix A, where (the) table A.1 summarises the needs gathered from the Radiation Protection (RP) group at CERN for the desired applications. For instance, some of the basic requirements for the robotic platform are that the robot should be able to go over long distances (> 200 m) and for relatively longer periods (> 2 hours) [18], only batteries having limited energy storage capacity can be used owing to safety issues, and the robot could be employed only when the accelerator machines are not in operation because of dangerous levels of radiation even to the electronics.

Radiation tolerance of components and systems should also be taken into consideration when deploying a mobile robot consisting of multiple electronic components. The total energy deposition and particle fluence suffered by electronic devices before they fail depend on the type and mass of the material. Therefore, if the robot is used in high energy particle environments or facilities where discharge of ionising radiations are prominent, there are chances of wireless communication device failures due to radiation effects on electronics [19], [20]. Radiation effects in electronics cause increase in conductivity, hence potentially permitting to dangerous current levels. The radiation effects are usually single event effects (SEEs) or cumulative effects and a way to impede these effects is by radiation hardening of the electronics in the robot [11], which usually comes at high cost and is normally incompatible with most of the commercial off the shelf (COTS) wireless devices. Therefore, instead of radiation hardening, fail-safe software routines and fault-tolerant hardware modules can be devised in the mobile robots. This aspect requires the need of having redundancy in communication methods and hence the redundancy in wireless devices is envisaged and considered in this thesis.

Another important aspect to be considered is that the mobile robot deployed for remote inspection, surveying or rescue missions can fail due to various possibilities such as hardware or software failure, especially the effects of ionising radiation on the electronics on-board the robot. One can refer to [21], [22] for a detailed analysis on the categories of failure scenarios, how and when a mobile robot could fail providing experimental studies. These failure scenarios necessitate manual recovery (self-rescue) of the robot from the environment. It would bring unforeseen challenges to recover the mobile robot if the environment where the robot is deployed has hazardous or harmful conditions. While it is not fully possible to prevent the failures in the robot, equipping the mobile robots with means to avoid the recovery situations or predict the failure status could certainly help.

The foremost research challenges (even) for a mobile robot deployed in hostile environments are the management of energy and communication. Particularly, research in wireless communication for mobile robots has been studied in the past decade and is compelling because of two major reasons: the existing wireless technology solutions cannot be well-suited to the application requirements as explained (later) in section 2.4; and the wireless communication has shown issues in hostile environments because of the fundamental dynamic nature of the radio signals [23]. As most of the facilities at CERN are underground tunnels, the propagation of radio signals is even more challenging [24].

1.2.1 Application environments

The environments where mobile robots could be employed are shown in the following figures. It includes the ISOLDE (Isotope Separator On Line DEvice) target area, the AD (Anti-proton Decelerator) target area, the ECN3 underground experimental hall (where a primary proton beam with high intensity can be received [25]), the SPS (Super Proton Synchrotron) accelerator machine areas, the TCC2 and TDC2 beamline[3] areas in the north of SPS, and some areas in the LHC machine. Further information on the areas used in the experimental validation of the proposed methods in this thesis are provided in relevant sections.

The figures presented before provide examples of the type of environments and its constraints such as in space and surfaces for a mobile robot operation. As the presence of large metallic objects and cluttered environment can be observed from these figures, a preliminary conclusion is that, the environments are not friendly for radio signals propagation. Figure 1.9 provides a map of accelerator facilities at CERN and the intended application environments are highlighted.

The LHC is the biggest accelerator machine at CERN. The main application of the mobile robots for radiation survey applications will be at the beam facilities other than the LHC because, the

---

[3]In accelerator physics, a beamline refers to the particle trajectory, including the overall construction of the path segment (vacuum tube, magnets, diagnostic devices) along a specific path of an accelerator facility

Figure 1.3: A view of the TCC2 experimental hall.

Figure 1.4: A view of the TDC2 experimental hall.

Figure 1.5: A view of the ECN3 underground experimental hall.
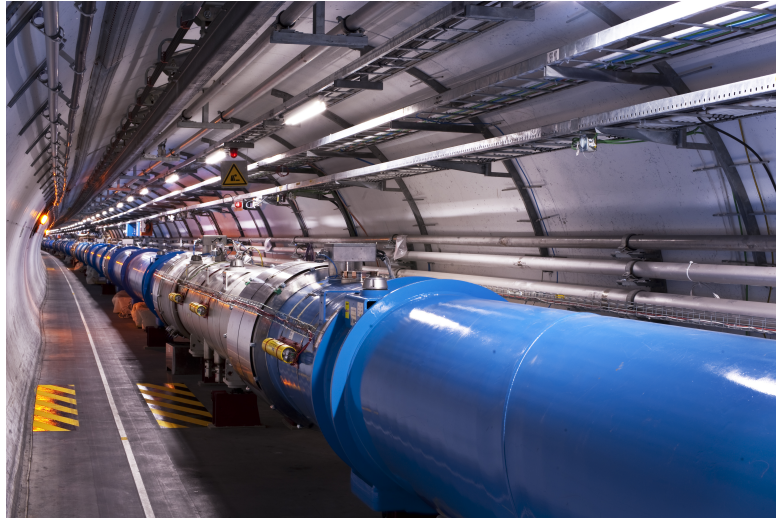
Figure 1.6: A view of the Large Hadron Collider (LHC) machine.
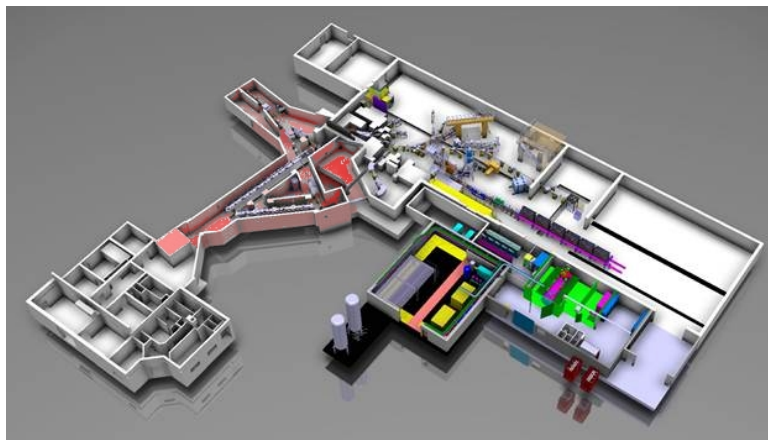
(a) An artistic 3D view of the ISOLDE target area.

(b) A view of the ISOLDE target area showing the KUKA industrial robots for handling radiation targets.

Figure 1.7: Views of ISOLDE (Isotope Separator On Line DEvice) areas

TIM [3] is being specifically designed to be used for conducting remote radiation surveys and inspections in the LHC. Ground mobile robots are not suitable for the LHC as there are several

(a) A view of the SPS north area.

(b) A view of the AD machine area.

Figure 1.8: Views of SPS (Super Proton Synchrotron) and AD (Anti-proton Decelerator) areas
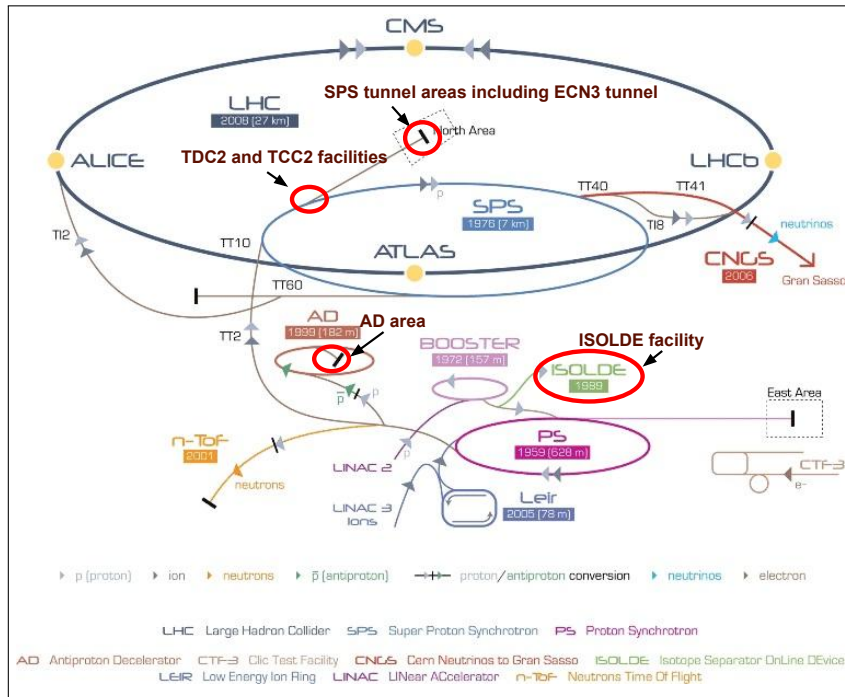
Figure 1.9: Map of particle accelerator machines at CERN.

manual door passages which the mobile robot cannot pass through without human interventions. Therefore, the main environments intended for mobile robot applications are areas around SPS machine and ISOLDE facilities illustrated in the figures 1.10 and 1.7 respectively.

In figure 1.11, examples of radiation levels obtained using FLUKA (a fully integrated particle physics Monte-Carlo simulation package [26]) simulations are shown for ISOLDE target and TDC2-+TCC2 beamline areas. These two areas are among high radiation areas at CERN [27], [28]. For instance, it is mentioned in [27] that, the TCC2 facility can be used for final tests of
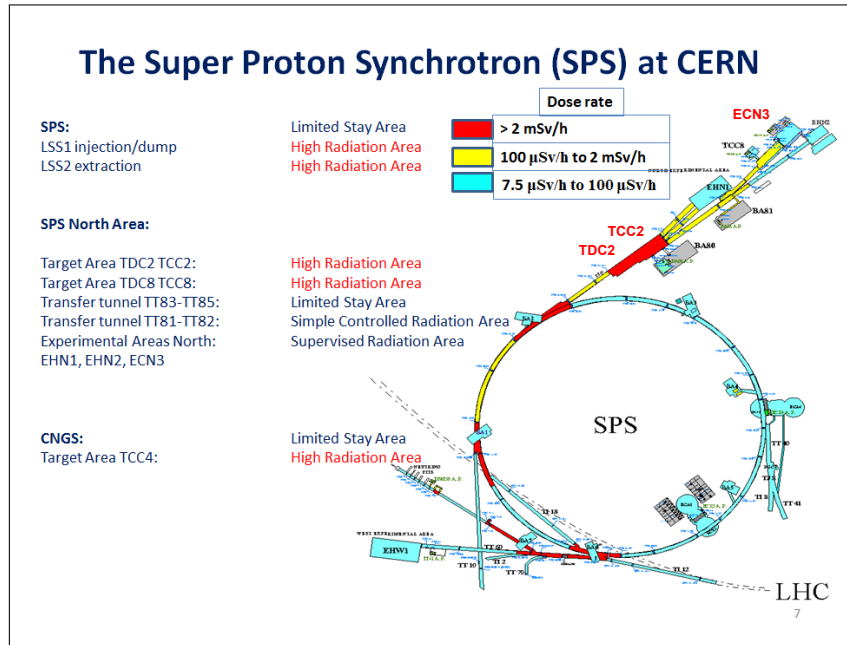
Figure 1.10: Experimental areas around the SPS machine.

remote handling (or robotic) solutions because the radiation doses accumulated in TCC2 for a day is equivalent to radiation doses accumulated in the LHC for a year under certain conditions. In ISOLDE primary area, the radiation levels can reach as high as 100mSv/h [28].
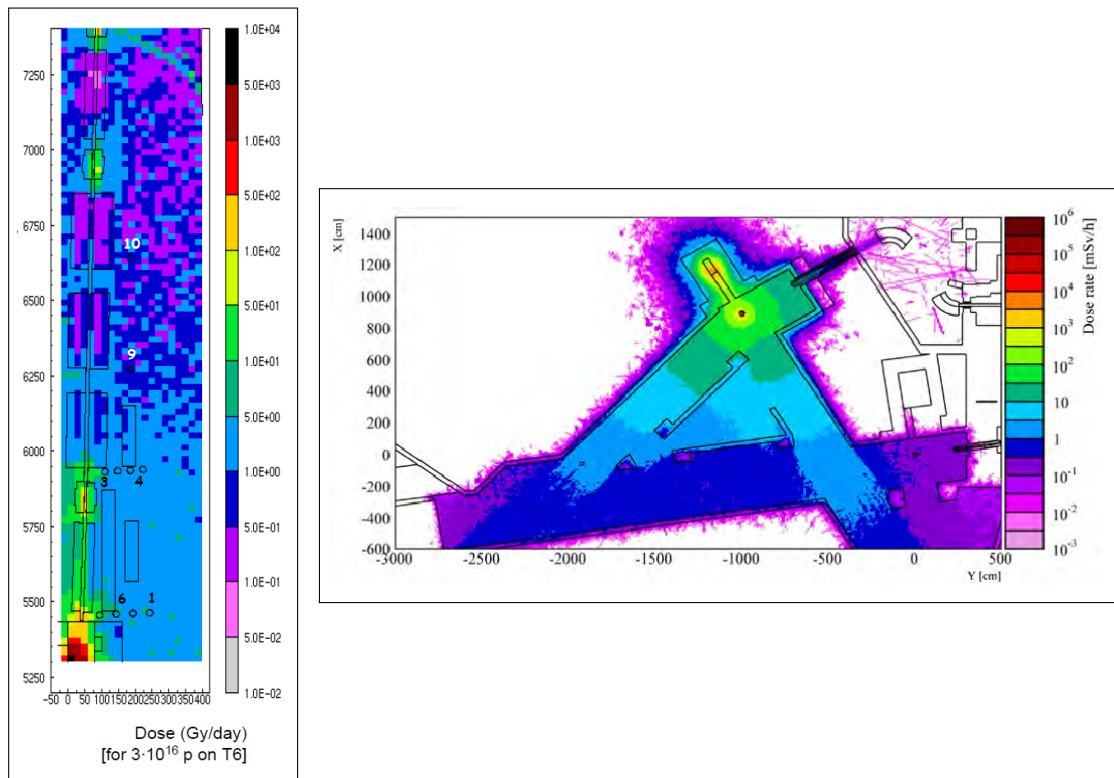
Figure 1.11: FLUKA simulations of radiation levels in TCC2 on T6 beamline [27] (left) and in ISOLDE target area [28] (right).

1.3   Research objectives

The research work reported in this thesis had been carried out as part of the EU-funded PURE-SAFE research programme. The basic idea of the PURESAFE research projects is to carry out robotics research work to address problems associated with scientific facilities emitting ionising radiations such as CERN. Particular features of PURESAFE includes the incorporation of systems engineering [29] techniques in the research work and consideration of reliability, availability, maintainability and safety (RAMS) issues. PURESAFE research project 6 [30], which is covered by this thesis focussed on improving the capabilities of mobile robots for use in CERN's accelerator tunnels where the presence of ionising radiation and the nature of the infrastructure and experimental structures lead to problems with the deployment of mobile robots.

After an initial needs gathering phase [31], the project work focussed on remote visual inspection and remote radiation survey task applications. The main research aims are to increase operating range and to avoid the need to send personnel into radiation areas to recover mobile robots in the event of failure during missions. The particular issues identified and addressed are wireless communication in curved and obstructed underground tunnels and problems encountered due to the relatively limited energy storage capabilities of batteries used in mobile robots. It should be noted that the problems have many similarities with those encountered during robotic search and rescue interventions [32].

This thesis provides introductory information on the infrastructures where mobile robots will need to operate, the tasks to be carried out by mobile robots in these environments and the problems encountered that are addressed in the research reported here. The reporting of research work carried out to improve wireless communication (the main subject of this work) comprises an introduction to the relevant radio signal propagation theory and technology followed by explanation of the research in the following stages:

- An analysis of the wireless communication requirements for mobile robot for different tasks in a selection of CERN facilities;

- Predictions of energy and communication autonomies (in terms of distance and time) to reduce risk of energy and communication related failures during missions;

- Autonomous navigation of a mobile robot to find zone(s) of maximum radio signal strength to improve communication coverage area;

- Autonomous navigation of one or more mobile robots acting as mobile wireless relay (repeater) points in order to provide a tethered wireless connection to a teleoperated mobile robot carrying out inspection or radiation monitoring activities in the challenging environment of CERN's accelerator tunnels.

The challenges in wireless communications for mobile robots are raised in the previous section, especially given the underground and tunnel environments with large metallic objects and non-line-of-sight (NLOS) conditions. Therefore, this thesis researches methods for enhancing wireless communication range and quality for a mobile robot application in radiation facilities.

To tackle the challenges mentioned above, an ever increasing network of researchers has been placing substantial attempts in the development of mobile robot systems for wireless teleoperation, in the last decade. Particularly, the interest in the use of multiple mobile robots for the applications in hostile environments is motivated by the fact that, when dealing with dedicated and complex tasks, it is preferable to exploit the potentialities of a team of robots supporting a main robot, instead of coming up with a ultra-capable individual robot. It is, in fact, more practical from both technological and economical point of view, to incorporate a group of simple robots for wireless tethering and possibly also to assist the main robot. In addition, adding redundancy to the mobile robot systems makes them inherently more reliable.

As the telerobotic operations in hostile or radioactive environments are difficult to fully automate, the robots are usually equipped with teleoperation capabilities, and some autonomy (intelligence) features may be added to ease the operator overload [33]. The main research objectives of this thesis are thus to investigate novels tools and methods that add intelligence features in teleoperated mobile robots by enhancing the reliability and redundancy in wireless communication for mobile robots and possibly employing multi-robot system. This can be achieved by developing novel methods for the prediction, optimisation and extension of wireless communication network capacity for a mobile robot operating in hostile environments including ionising radiations. A part of the thesis is also devoted to predicting the energy consumption of the mobile robots for a particular assigned tasks in advance so that any optimisation of the task including wireless communication methods can be made possible. The research objectives should also consider the fact that the proposed methods should suit the requirements and constraints mentioned in the appendix A.

The research questions this thesis aims to address are follows:

- How to predict the energy consumption of a mobile robot for an assigned tasks? How can such an energy prediction method be useful to optimise wireless communication strategies? (Answered in Chapter 3);

- How to predict the operational range of wireless communication on a mobile robot both before and during execution of some tasks? How can such prediction method be useful in determining the spatial range where the robot can safely operate without losing its communication with its control station? (Answered in Chapter 4);

- How to optimise the communication capabilities in a robot using its mobility, given the fact that the there are harsh environmental constraints with potentially no line-of-sight conditions for radio communication? (Answered in Chapter 5);

- How to extend the operational range of wireless communications, possibly with the use of multiple mobile robot system (by making use of relay robots for wireless tethering) in a robust manner? (Answered in Chapter 6).

Answers to each of the questions is addressed in the following chapters. The research solutions proposed in this thesis such as the communication enhancement methods can be used for other applications at CERN such as a remote collimator exchange system and robotic manipulation of equipments. Also that the proposed methods can be used in other existing mobile robots at CERN or hostile environments where the energy-aware robotic operation is a pre-requisite.

1.4   Thesis outline and contributions

This organisation of the thesis is described here. Firstly, the introduction chapter gives a brief idea about the objectives and research contributions of this thesis. An outline and the contributions of the successive chapters are outlined below.

Chapter 2: In this chapter, wireless communication fundamentals and the background in wireless mobile robots are presented along with the requirements for telerobotic applications in hostile environments. The main contributions of this chapter are the presentation of wireless communication requirements for mobile robots in radiation environments and a comparison of various wireless technologies, especially the available ones at CERN. Parts of this chapter are published in [18], [34].

Chapter 3: This chapter proposes a decentralised method to predict and optimise the energy consumption in a mobile robot. The proposed method predicts the mobile robots energy autonomy for a particular task. The concept of power modelling used for energy prediction is presented. The proposed approach uses real-time measurement of voltage, current at the battery and the time information of activity at each components in a mobile robots are used for the prediction process. The outcome of this method can help in optimising and choosing the wireless communication technology on the mobile robot that can best suit the task requirements. The method is first presented in [35] and then extended and published in [36].

Chapter 4: The radio signal strength (RSS) is an important parameter that determines the operational wireless communication range of the mobile robot. It is important to predict the RSS which can help in predicting the space and time when the communication link between the operator and the mobile robot. This is needed as the loss in communication link be predicted and

thereby avoided by taking appropriate actions. A novel method for on-line prediction of the radio signal strength in space and time using a discrete Kalman filter is presented in this chapter. A detailed analysis of radio signal strength propagation in hostile environments is conducted and the results are published in [18]. The proposed solution for the real-time RSS prediction is published in [37].

Chapter 5: Optimising the network capacity in a wireless communication link is vital for remote operation of mobile robots. Towards this goal, a decentralised algorithm for optimising the network capacity and the communication range using spatial diversity based methods is presented in this chapter. A case study application (haptic teleoperation of mobile robots) that makes use of this algorithm in a real-time scenario is also considered. The proposed algorithm is published in [38] and a novel implementation of this algorithm considering a haptic teleoperation application is published in [39] .

Chapter 6: Extending the coverage area of a radio communication system has always been given priority in the intended applications. A framework for wireless communication range extension called as "Server-Relay-Client (SRC) framework" is presented in this chapter. In addition, a robust stochastic optimisation (RSO) algorithm for SRC framework that optimises position of a relay robot to enhance the RSS between a server and client robots is proposed followed by the evaluation of this RSO algorithm in both simulations and field experiments. The contributions in this chapter are published in [40].

Finally, chapter 7 concludes this thesis (along) with its impact and the contributions to the state of the art and presents some avenue for future research.

1.5 Summary

The goal of this thesis is to advance the state of the art in enhancement of wireless communication methods such as prediction, optimisation and enhancement of wireless communication qualities in mobile robots applied in hostile or radiation environments. This chapter presented an overall introduction to this thesis, introduced the problems in the intended applications such as remote radiation measurement and inspection applications in large scientific facilities with ionising radiation environments. The use and challenges of wireless mobile robots for telerobotic applications were presented in this chapter. The research objectives aiming to tackle the challenges in using wireless communications for mobile robots were established. Finally, the contributions of each chapter were outlined.

Chapter 2

Background on mobile robots and wireless communications

This chapter first will provide essential background on mobile robots, radio signal propagation and characteristics of wireless networks. The communication requirements for typical telerobotic applications will be discussed, assisted with a comparison of various wireless technologies and their relevance to telerobotic applications at CERN. Wireless tethering of mobile robots, which is the predominant concept used in this thesis will be introduced in the last section of this chapter.

2.1   Mobile robots preliminaries

"Mobile robot" is defined as an automatic machine that is capable of locomotion and therefore able to move into the surrounding environment [41]–[46]. In contrast to industrial robots [32] such as the KUKA robots at ISOLDE target area at CERN [17] (which are usually stationary, consisting of a jointed arm (multi-linked manipulator) and gripper assembly (or end effector), and attached to a fixed surface), mobile robots are used to replace humans in case of repetitive or easy tasks and possibly in hazardous environments [41]. Mobile robots are used in military and security applications, though most of the commercial mobile robots are deployed in domestic and service applications. Mobile robots applied in different surfaces or environments and classified under more than one categories [47], [48]. A general classification of mobile robots is provided below.

Unmanned Ground Vehicles (UGVs):   land or domestic robots are usually referred to as unmanned ground vehicles. They are most commonly wheeled or tracked, but also include legged robots with two or more legs (humanoid, or resembling animals or insects) [49].

Unmanned Aerial Vehicles (UAVs):   aerial robots (robots that can fly) such as quad-rotors and autonomous helicopters, are usually referred to as unmanned aerial vehicles (UAVs) [50].

Unmanned Surface vehicles (USVs):   mobile robots operating on the surface of water are usually called as unmanned surface vehicles [51].

A mobile robot or a mobile platform is a platform with a large mobility within its environment (air, land, underwater) and comprises a system with the following functional characteristics.

- *Mobility*: Total mobility relative to the environment. The level of mobility also varies, for example from two-dimensional movement (using wheels or tracks) to three-dimensional movement (using propellers). Mobile robot navigation can be aided by self-localisation, path planning and navigation algorithms [44], [48], [52].

- *Autonomy*: A certain level of autonomy or intelligence to enhance the capabilities and enable enhanced human interaction [45], [53]. The level of autonomy ranges from teleoperation (operated completely manually) to fully autonomous (with intelligence and decision-making abilities) [54].

- *Perception*:   The ability to sense and react to changes in the environment [55]. The level of perception in mobile robots can vary from pure sensing (using fusion of sensors information [56]) to active perception [57] (sensing and actuation are combined).

Telerobotics is the area of robotics concerned with the control of manually operated and/or semi-autonomous robots from a distance, chiefly using wired (such as Ethernet, EtherCAT, or similar communication channels) or wireless network (such as Wi-Fi, Bluetooth). The robot used for the telerobotic application is called a telerobot or sometimes, a teleoperator [13] and the human controlling the telerobot is usually referred to as an operator.

This thesis examines the use of UGVs with basic navigation, localisation, sensing and control strategies. The following wheeled mobile robot platforms are used for experimental demonstration of the algorithms and methods proposed in this thesis.

youBot: The KUKA youBot [58] is a research and educational mobile robot usually accompanied with an arm and its the ideal platform for developing applications in service robotics. It has omnidirectional mobility (the robot can move in both transversal and longitudinal directions at the same time), thanks to the specially designed Swedish wheels [59].

Khepera III: Khepera [60] is a miniature mobile robot, functionally similar to larger robots used in research and education. It allows real world testing of algorithms developed in simulation for trajectory planning, obstacle avoidance, preprocessing of sensory information, and hypotheses on behaviour processing, among others [61].

TIM: The TIM platform [16], abbreviated for the "Train Inspection Monorail" is a remote inspection train that has been developed for the LHC tunnel and is capable of carrying out remote visual inspections as well as taking measurements of radiation and oxygen levels along the tunnel. The train runs on a monorail beam secured to the roof of the tunnel [17].

The youBot mobile robot platform [58] developed by KUKA Robotics laboratories and manufactured by Locomotec GmBH is used for most of the experimental demonstration purposes in

Figure 2.1: Design of the youBot mobile robot platform with arm. Source: youBot-stores GmBH.

this thesis except for the energy prediction method in chapter 3. The figure 2.1 shows the design of the youBot. The youBot usually is accompanied with a 5 degrees of freedom (DoF) robot arm for mobile manipulation.

The other two robots (TIM [62] and Khepera [61]) used for conducting experiments on energy prediction algorithms are introduced and referred in the relevant sections of chapter 3.

2.2   Radio propagation and the Radio Signal Strength (RSS)

When a radio signal travels from a transmitter to a receiver through multiple paths subjected to reflections, diffractions and refractions in the surrounding environment, a phenomenon called multipath propagation occurs. This leads to multipath fading and constructive or destructive interference [63]. The multipath fading can be either long-scale fading due to the shadowing effects caused by the obstacles or small-scale fading due to interferences of the multipath components [64].

The variation of the radio signal strength in space and time is partly a deterministic and partly a stochastic process [64] because the signal propagates through a multipath fading channel (radio signals from the transmitter arriving at the receiver through multiple paths and the signal strength fades with the distance travelled).

The attenuation in the power of the radio signal is defined as the path loss PL. It is caused by many factors such as distance (free space loss), penetration losses through walls and floors and multipath propagation effects [65]. In particular, all walls, ceilings, and other objects that affect the propagation of radio waves will directly impact the signal strength and the directions from which radio signals are received.

The loss in the radio signal strength (RSS[1]) can be regarded as a sum of deterministic effects (modelled using a logarithmic function) and stochastic effects (modelled using random Gaussian variables [63]) as shown in the equation below.

$$PL_d = \underbrace{PL_{d_0} + 10 \cdot \eta \log_{10}\left(\frac{d}{d_0}\right)}_{\text{Deterministic effect}} + \underbrace{\mathcal{X}_\sigma}_{\text{Stochastic effect}} \qquad [\text{dBm}^2]. \qquad (2.1)$$

Where $\|d\| = \sqrt{(x_t - x_r)^2 + (y_t - y_r)^2}$ is the l^2-norm (Euclidean) distance between the transmitter at $p_t = (x_t, y_t)$ and the receiver at $p_r = (x_r, y_r)$. PL_d is the loss in the RSS at distance

---

[1]RSS usually refers to the received radio signal strength at the receiver. RSS is an abbreviation for Radio Signal Strength or for Received Signal Strength.
[2]dBm (dBmW) is the power ratio in decibels (dB) of the measured power referenced to one milliwatt (mW) of absolute signal power.

d, PL_{d_0} is the path loss at a reference distance d_0 and $\eta \geq 2$ is an environment specific propagation constant. $\mathcal{X}_\sigma = \chi_\sigma + \sum_{i=1}^{N} k_i L_i$ is the stochastic part of the RSS and is generally termed as a wide-sense stationary process (the channel is time invariant). Here, the χ_σ models the stochastic nature of the signal attenuation and can be represented using a zero mean Gaussian random variable with variance σ^2, L_i is the loss due to walls and ceilings where k_i is a parameter depending on the type of such obstruction. However, it can be seen later that this generalisation is invalid when the multipath fading effects are included because the multipath channel is time-variant [23] and hence be modelled using a non-stationary process. Hence, the stochastic nature of the RSS variations can be generalised with shadowing and multipath fading effects using equation (2.3).

The RSS at the receiver is the difference between the transmitted power P_T and the path loss PL_d over a distance d. Moreover, the path loss PL_d is composed of three main components as shown in the following equations:

$$RSS(d,t) \;=\; P_T - PL_d = P_T - (PL_d^{pl} + PL_d^{sh} + PL_{(d,t)}^{mp}) \quad [dBm], \qquad (2.2)$$

$$RSS(d,t) \;=\; RSS_{d_0} - \underbrace{10\eta \log_{10}(\frac{d}{d_0})}_{\text{Path loss}} - \underbrace{\Psi_{dBm}(d)}_{\text{Shadowing}} - \underbrace{\Omega_{dBm}(d,t)}_{\text{Multipath}}, \qquad (2.3)$$

where $PL_d^{pl} = PL_{d0}^{pl} + 10\eta \log_{10}(\frac{d}{d_0})$ is the distance-dependent path loss component due to environmental factors such as the size and shape of the environment. PL_d^{sh} is the shadow fading component of the path loss accounting for attenuation due to obstacles in the environment including walls and ceilings. $PL_{(d,t)}^{mp}$ is the multipath faded component accounting for attenuation due to dynamic multipath fading effects.

A commonly used model for radio signal propagation as a function of distance and time is the extended log-normal shadowing model (ELNSM) as shown in the equation (2.3). The path loss fading is a slow process (large-scale), whereas the fading due to shadowing and multipath effects are relatively medium-scale and fast processes respectively. As explained earlier, the path loss fading is deterministic, but the shadowing and multipath fading are Gaussian (stochastic) variables. The signal loss due to shadowing effects $RSS^{sh} = \psi_{dBm} = 10\log_{10}(\psi_{mW})$. $\psi \sim \mathcal{N}(0, \sigma_\psi^2)$ is a zero mean Gaussian distribution with variance σ_ψ^2. The parameters η and σ_ψ together define the environment [64]. The multipath fading effect in the received signal is a function of both space and time; $RSS^{mp} = \Omega_{dBm} = 10\log_{10}(\Omega_{mW})$ and can be represented by a Gaussian random variable $\Omega \sim \mathcal{N}(0, \sigma_\Omega^2)$ with zero mean and variance σ_Ω^2. The probability density function (pdf) of the RSS^{mp} can be modelled using Rician fading (for LOS), Rayleigh fading (for NLOS), and Nakagami-m fading (for indoor) distributions [63].

A radio environment usually contains noise signals (PN_{dBm}) from other radio sources operating in the same frequency band or higher power signals operating at any radio frequency nearby the

radio receivers. As the noise in the environment is not a stationary process because of many factors including the mobility of the node, it is highly unpredictable and cannot usually be modelled. The Signal to Noise Ratio (SNR) is defined as follows:

$$SNR = \frac{RSS_{mW}}{PN_{mW}} = 10^{(\frac{SNR_{dBm}}{10})}, \text{ where } SNR_{dBm} = RSS_{dBm} - PN_{dBm}. \qquad (2.4)$$

The RSS_{mW} is the absolute RSS expressed absolute power (in mW) whereas, the RSS_{dBm} = $10 \log(RSS_{mW})$ is the RSS ratio in decibels referenced to the RSS of one milliwatt. This concept applies also to SNR. While the RSS is an indicator of the intended signal's absolute power, the SNR is an indicator of the intended signal power with respect to noise power in the environment. The RSS can be measured directly in most of the commercial wireless devices using a metric called Received Signal Strength Indicator (RSSI [66]), however this is not the case for the SNR measurement. Some devices report noise power level (which is usually inaccurate [66]) and hence the SNR can be calculated using both RSS and Noise levels. To avoid device dependency, only the RSS information will be considered in developing the algorithms to widen the applicability of the wireless communications enhancement methods to be proposed later in this thesis.

2.2.1 Radio signal propagation in tunnels

Scientific facilities such as those at CERN exhibit the characteristics of underground tunnel structures and complete non-line-of-sight (NLOS) conditions with special properties such as heavy metal objects in the surroundings. The presence of thick concrete blocks (for radiation shielding, which also makes it difficult for the radio waves to penetrate) and large objects with metallic surfaces such as the dipole or quadrupole magnets, contribute to the characteristics of these environments. All these characteristics have different effects on radio signals [23]. For the facilities having obstructed indoor environments, multipath effects have to be taken into account in the propagation of radio waves [64].

Much literature exists for radio signal propagation in tunnel environments [2], [23], [24], [67], [68]. Experimental studies on radio propagation characteristics in tunnel like environments date back to 1975; Emslie et al [69], focus on path loss of radio signal at frequencies in the range of 0.2 to $4GHz$ along a tunnel, and from one tunnel to another around a corner. Reference [23] provides a detailed analysis of wired and radio communication systems in underground mines or tunnel facilities where the tunnels are not straight leading to different forms of turns (e.g., U turn, angle turn). In [2], the authors investigate the communication considerations from the perspective of in-mine and mine to surface communications separately and provide a detailed overview of all types of possible communication systems.

In underground mining and other tunnel environments, leaky feeder cables (LFC) can be used to establish radio communications system [70]. A leaky feeder communication system consists of a coaxial cable run along tunnels which emits and receives (radiates) radio waves, functioning as an extended antenna. The system has a limited range and because of the frequency it uses (typically within 2 GHz range), transmissions cannot pass through solid rock, which limits the system to a line-of-sight application. It does, however, allow two-way mobile communication [71]. CERN also uses leaky feeder system for mobile telephony inside its underground tunnel facilities.

In [68], the authors recommend a wireless system operating at a frequency greater that $2GHz$ in underground tunnel facilities because the transmission loss becomes very small over a frequency of $2GHz$ in a coal mine tunnel of width $4m$ and height $3m$. Therefore, a Wi-Fi system operating at $2.4GHz$ should be a reasonable choice for underground scientific facilities. Also, as the intended radio frequencies are greater than $2\,\mathrm{GHz}$, which exceeds the limits of typical leaky feeder systems, this thesis concentrates on alternative solutions such as wireless systems with mobile robot networks and robotic repeater systems.

2.3 Wireless network characteristics

According to Shannon's capacity theorem [72], in a wireless channel c, the maximum communication channel capacity C_c and the data throughput T_c is related to the SNR as follows:

$$C_c = B\log_2(1+SNR) = B\log_2(1+10^{\frac{RSS_{dBm}-PN_{dBm}}{10}}) \; [\mathrm{Mb/s}], \qquad (2.5)$$

$$T_c = \alpha_T C_c \; [\mathrm{Mb/s}], \qquad (2.6)$$

where B is the frequency bandwidth of the channel in MHz. The data throughput T_c is a factor (by α_T) of the maximum capacity C_c because the capacity is determined at the physical layer whereas the throughput is determined at the transport layer which includes data link, network and physical layers in the Open Systems Interconnection (OSI[1]) reference model [73].

However, as the objectives of the enhancement methods are to implement the algorithms at the application-level, the metric "goodput" G_c (application-level data throughput) of a network which is measured right at the application layer (includes the data transport through all the other layers) is considered.

---

[1]The OSI model maintained by the identification ISO/IEC 7498-1 [73] is a conceptual model that characterises and standardises the internal functions of a communication system by partitioning it into 7 abstraction layers in the following hierarchy: Physical layer, Data link (MAC) layer, Network layer, Transport layer, Session Layer, Presentation layer, and Application layer. The application layer is the top layer that defines the language and syntax that programs use to communicate with other programs and is the closest layer to the end user. Besides, the physical layer is responsible for passing bits onto and receiving them from the physical transmission medium (cable, radio, etc.) and defines the electrical and physical specifications (such as USB and Wi-Fi) of the data connection [74].

The goodput can be modelled with the equation (2.7). α_G is a parameter that determines the proportionality of goodput with throughput.

$$G_c(RSS) = \begin{cases} \alpha_G T_c(RSS) & \text{when } RSS < RSS_{\text{Threshold}}, \\ G_{max} & \text{when } RSS \geq RSS_{\text{Threshold}}. \end{cases} \quad (2.7)$$

This indicates that the goodput of the wireless network, which has a linear relationship with the maximum channel capacity C_c, depends on the RSS and becomes saturated when the RSS reaches a threshold $RSS_{\text{threshold}}$. The usable range of the RSS values that can be improved (enhanced) can be obtained by considering the sensitivity value (R_S) of the used wireless device (the lower bound of the usable RSS) and the empirical value of the $RSS_{\text{threshold}}$ (the upper bound of the usable RSS). The model in equation (2.7) is verified with the experimental data presented in figure 2.2 where the $RSS_{\text{threshold}}$ is -55 dBm (upper threshold) and the sensitivity value of the wireless device used (Zyxel NWD2105) is -81 dBm (lower threshold). The figure 2.2 also shows a linear fit for the RSS and goodput relation using a Minimum Least Squares Error (MLSE) technique. The goodput model is considered in this work as it is a more practical model than Shannon's capacity model.
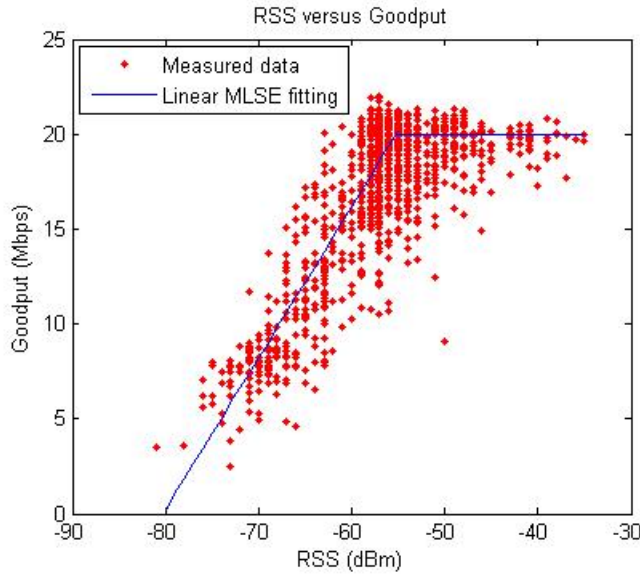
Figure 2.2: Scatter plot depicting the goodput measures against the RSS values in various receivers at different time instants.

In general, higher frequency channels perform better in heavy traffic conditions. It is assumed in this thesis that the best channel based on the traffic conditions is pre-selected to avoid adjacent and co-channel interference and therefore the channel optimisation is assumed to be done beforehand.

2.4 Communication requirements for mobile robot teleoperation

According to the systems engineering approach [29], the user needs are studied first before identifying a solution. Therefore, the first goal is to obtain the requirements of wireless communication system for various possible applications at CERN from the people who need these robotic applications. Each application has different requirements for establishing a point-to-point wireless network between the telerobot and the operator command station. The three main parameters which define these requirements are:

- Maximum admissible system latency (in milliseconds);

- Minimum data transfer rate (in Megabits/second);

- Maximum distance to be covered (in meters).

The system latency is a critical parameter in a real-time application. It is the amount of time taken by a data packet to travel from a source to a destination (host processing latency + network latency). It depends on the number of buffers between communication ends [75]. Network topology and coverage distance requirements (which are relevant to latency) are decided by the type of the application. These values are obtained by interviewing people requiring such applications.

The data transfer rate is defined as the speed with which the data can be transmitted and is decided by the amount of data to be transmitted. For video transmission, one can refer to [76] to find a relation between the quality of the video and data rate required. It is necessary that at least two live video transmissions are recommended for a vision system used for remote handling [77].

An example application is considered to illustrate the requirements. The communication requirements for this application (given in table 2.1) are based on HD transmission of two good quality videos so that the operator can observe the environment more in detail including small sparks in the Faraday cages inside the ISOLDE facility.

Therefore, considering the need of having two good VGA quality videos and using H.264 coding at 30 $frames/s$, the data rate required will be $1.7\ Mbit/s$ [76] per video. Similarly, for other applications, the appropriate data rate is calculated assuming typical data requirements. Table 2.1 summarises the wireless communication requirements for various mobile robot applications at CERN.

	Application	Max distance	Min data rate	Max latency	Comments
1.	Remote measurements	500 m	512 Kbit/s	1000 ms	For measurements of radiation levels, temperature, oxygen and other sensory data transmission [16]
2.	Remote Handling (RH) tasks without haptic feedback	200 m	64 Kbit/s	100 ms	Remote control of robots in scientific facilities [16], [33]
3.	Vision system for RH	200 m	3480 Kbit/s	200 ms	For transmission of two good quality video with VGA resolution [76], [77]
4.	RH with Haptic feedback	200 m	128 Kbit/s	25 ms	Teleoperation with force feedback [78]
5.	An example application	40 m	5120 Kbit/s	200 ms	For transmission of two good quality video with HD resolution (refer section 4.1.1.2 and [76])

Table 2.1: Communication requirements for some telerobotic applications at CERN.

2.5   Comparison of various wireless technologies

Comparison of different wireless technologies is discussed in [79]–[84] . Table 2.2 shows a brief summary of specifications of some wireless technologies with the advantages and disadvantages with respect to the example application mentioned in table 2.1.

Out of these available systems, Wi-Fi based system had been selected for first trials as it was readily available, widely studied and well used technology. Coded Orthogonal Frequency Division Multiplexing (COFDM[2]) based Wi-Fi technology can be well-suited for tunnel environments [86] because it is specifically designed to combat the effects of multipath interference (see section 2.2.1). However, owing to availability and cost limitations, a standard Wi-Fi system has been chosen for the experiments.

---

[2]COFDM is a form of modulation which is particularly well-suited to the needs of the terrestrial broadcasting channel. The key features which make it work, include: orthogonality; the addition of a guard interval; the use of error coding, interleaving and channel-state information (CSI). COFDM can cope with high levels of multipath propagation, with a wide spread of delays between the received signals, co-channel narrow-band interference, as may be caused by the carriers of existing analogue services. The special performance of COFDM in respect of multipath and interference is only achieved by a careful choice of parameters and with attention to detail in the way in which the forward error-correction coding is applied [85].

	Wireless Technology	Max data rate	Max distance	Average Latency	Merits	Demerits	Cost (€)	Typical applications
					Wireless Local Area Networks (WLAN)			
1.	Wi-Fi 802.11n	108-600 Mbit/s	100 m	1-100 ms	Readily available, High data rate	Latency can be high	10x	Internet
2.	Wi-Fi with COFDM [86]	18Mbit/s	5 Km	50 ms	Long range, Low latency	Expensive	1000x	Communication in Tunnels
3.	WirelessHD [87]	1 Gbps	20 m	1 ms	Very low latency, Very high data rate	Short range	100x	HD video transmission
4.	Bluetooth v2.0	1 Mbit/s	10 m	10 ms	Low latency	Low data rate, Short distance	10x	Fast data sharing
5.	Zigbee	250 Kbit/s	70-100 m	5 ms	Very Low latency	Low data rate	10x	Wireless sensor networks
6.	WiMAX	75 Mbit/s	50 Km	10-50 ms	Very Long distance, High data rate	Infrastructure limitations	10000x	Wireless broadband

	Cellular Technology	Max downlink data rate	Max distance	Average Latency	Merits	Demerits	Availability
					Cellular Networks		
1.	2.5G (EDGE)	236.8 Kbits/s	>1 Km	1000 ms	Long range	Low data rate, High Latency	Presently available in CERN underground facilities using LFC
2.	3G (UMTS)	2 Mbit/s	>1 Km	200 ms	Long range	Low data rate, High Latency	Presently available in CERN underground facilities using LFC
3.	4G (LTE)	100 Mbit/s	>1 km	20 ms	Long range, Low latency	Infrastructure limitations	Not available in CERN facilities

Table 2.2: Performance characteristics of commercially available wireless and cellular communication systems with reference to CERN requirements.

2.6   Wireless tethering of mobile robots

Multiple mobile robots can be used to extend the communication range capabilities by tethering[3] the wireless signals. Such amalgamation of mobile robots are called as wireless tethered robots or wireless relay robots and the process is called as wireless tethering or wireless relaying or sometimes even called as wireless multi-hop relaying [88], [89]. Generally in wireless tethering, at least three mobile robots are involved. The first one is called the server robot (it can also be simply a basic computer) that acts as a control or command station for the human interface. There will be a client robot which is the main robot (end user) performing the robotic operations such as remote handling or manipulation. Another robot called "relay robot" is used in the middle of the server and client robots and does the actual relaying of wireless signals from server robot to the client robot. Motion control for wireless tethering robots are well-studied in the literature [89]–[91].
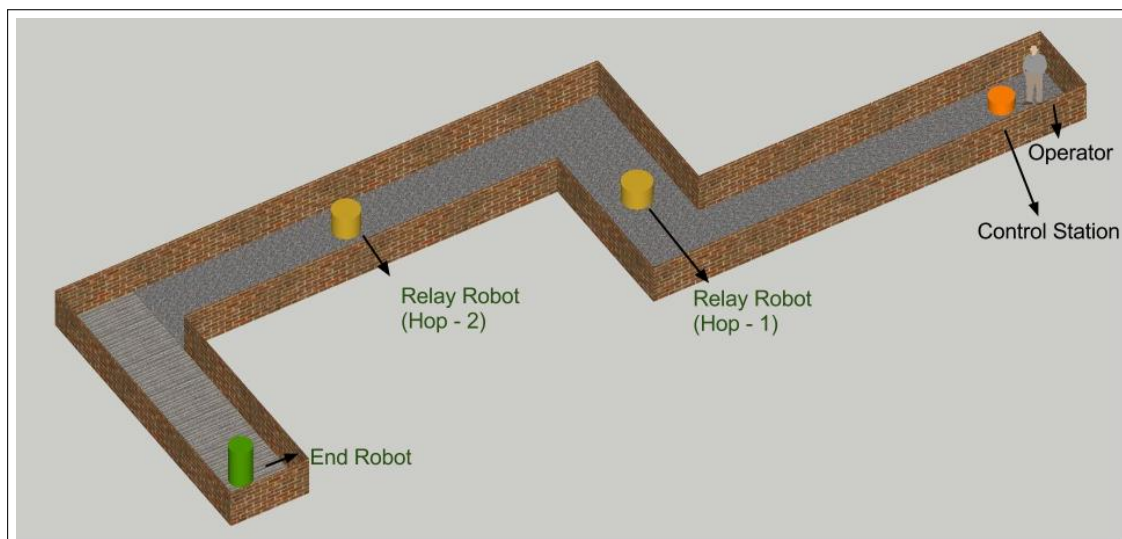
Figure 2.3: Network of robots for extending energy and communication autonomy of mobile robots in telerobotic applications.

In order to achieve higher operational distance range requirement for the mobile robot applications at CERN, a multi-robot network solution is proposed and conceptualised in this later part of the thesis. A scenario of several robots working together for a given teleoperation mission, of the type illustrated in figure 2.3 is considered. A multi-robot network following the Server-Relay-Client (SRC) framework is assumed, in which the client robot (the robot performing the actual remote operation task) is controlled by an operator (a human, who is assigned the teleoperation mission) remotely at the control station or the server robot. The other robots, referred as "relay robots", help the main robot by repeating the wireless signals from their neighbour robots

---

[3]Tethering refers to connecting one device to another either via a physical medium such as a cable or via a radio medium such as a wireless repeater

targeting the end robot. They also send video streams to an operator and exchange information to coordinate within the group.

The needs gathered from the end users suggest that the client robot be teleoperated because the manipulations or remote handling operations are complicated and will be better done with manual control [1]. Moreover, an important constraint in this system is that the operator should not be overloaded with controlling multiple robots at once. This suggests an intelligent relay robotic architecture where the relay robots plan their motion and their position autonomously, thereby not overloading the operator in his task of controlling the main robot. In this regard, solutions are proposed for communication-aware self-positioning of relay robots in order to maximise communication autonomy and to ensure successful mission by predicting the wireless signal strength in advance. Thus this thesis assumes that the client robot is manually teleoperated and the relay robots are autonomous.

2.7   Summary

In this chapter, after introducing the pre-requisites on mobile robots, the fundamentals on radio signal propagation especially in tunnels were presented. Also, the communication requirements of typical telerobotic applications in a scientific facility such as at CERN were discussed so as to understand the needs from an end user perspective. Different wireless technologies currently commercialised were compared with regard to the telerobotic applications in order to obtain the research and developments needed in this field. Lastly, the concept of wireless tethering using mobile relay robots were described.

Chapter 3

Energy-efficient wireless communication using energy prediction models

The primary goal of this chapter is to propose strategies for energy-efficient wireless communication in mobile robots. This chapter will present a novel energy prediction system using power models and real-time activity information. Then the available literature regarding energy management in mobile robots will be reviewed. Subsequently, the theoretical basis behind this work will be discussed, and then the experimental validation of the proposed energy prediction algorithm will be presented and the experimental results will be discussed. Finally, the use of energy prediction models in the optimisation of wireless communication strategies will be presented with examples where energy savings can be obtained by choosing different communication methods.

The robots need to manage their energy consumption[1] to avoid running out of energy as this would mean personnel access to retrieve or recover the robot from the hazardous (e.g. radiation) area where it is deployed (e.g. [1]). Therefore the motivation behind this work is that a mobile robot should be aware of situation that the energy level is too low or the remaining energy is not enough to get the robot back home, especially in radiation environments. This can be engineered by employing on-line energy monitoring and warning system in the robot. The solution proposed in this chapter should allow mission planning considering energy and communication constraints.

Mobile robots are used in various applications such as remote inspection, survey and defence applications. The robot's energy consumption is dependent on the nature of tasks to be performed and the time to complete the assigned mission. Since robots deployed in hazardous environments usually carry a finite power source such as batteries (because of environmental constraints), it is critical to ensure before executing the mission that the robot has sufficient energy to complete the task by predicting the energy requirements beforehand. In addition, the robot should be able to take actions before the remaining energy in the robot is not enough to make a return trip to its charging station.

The robot's energy autonomy should also be optimised to provide more flexibility in possible robotic interventions (in terms of distance travelled and mission time). Predicting the energy consumption requirements of various components in a robot before and during the robot deployment in the application environment will be useful in pre-optimising the mission including the optimisation of wireless communication strategies. It is important to develop energy-efficient designs considering multiple components together. Towards this goal, in this chapter, an energy prediction modelling approach for a small-scale mobile robot platform which can be extended to other mobile platforms is conceptualised.

3.1   Related works in energy prediction methods

The significance of power management for long-term operation of autonomous robots is discussed in the work by Deshmukh et al. [92], with challenges in terms of battery technology, power estimation and automatic recharging abilities. In [93], a robot with an auto-recharging system is proposed with emphasis on the aspects improving the robustness (or reliability) of the system. A method for automatically recharging the batteries using the robot's built-in sensors to control docking with a recharging station is proposed in [94]. Much research has been conducted on mobile robot motion energy optimisation through motion planning [95], [96] and path

---

[1]The terms "Power" and "Energy" used in this thesis always refer to the electrical input power and the electrical energy used by any component. Power (W) = Voltage (V) * Current (A); Energy (J) = Power (W) * Time (s) ; 1 Joule (J) = 1 Ws.

planning [97], [98] techniques. Models for locomotion power and dynamics have been widely studied. Wei Yu et al [99] emphasise that power models of motors are needed for the locomotion planning to complete time or energy constrained missions. Power models for skid-steer wheeled vehicles [99], [100] and tracked vehicles [101] are proposed for various turning radius and surface conditions.

Some works analyse the energy consumption of different components in robots. Liu et al. [102] present an energy breakdown table of a Mars rover. Michaud et al. [103] estimate the energy consumption of a rover including the communication power. However, they do not build power models for each component. A study [104] indicates that sensing, computation and communication consume significant amounts of power compared to locomotion power. Therefore, management of all power consuming modules is important. In [105], power models are used to optimise the deployment of robots under energy and timing constraints. The MarXbot [106] can auto-replace its batteries with hot swapping capability. In [106], it is proposed that power models of various components allow the robot to estimate when the robot should exchange its battery. A nice behavioural model for finding the optimal time at which a robot (or the mobile agent) should go back to recharge is presented in [107].

Hostile or scientific facilities (such as at CERN) generally are not designed to accommodate mobile teleoperated robots. It is complicated to navigate the mobile robot to the work site due to the compact spaces and unstructured sections. For instance, special provisions are made for the TIM robot [3] to pass through the sector doors in the Large Hadron Collider at CERN. Because of such restrictions, auto-recharging techniques [92]–[94], [107] cannot generally be used for telerobotic applications in scientific facilities emitting ionising radiations.

Table 3.1 gives a comparison of selected mobile robot's mass and power consumption considering the maximum power for each component. It can be observed that as the robot becomes heavier; the locomotion power accounts for higher percentage of the total power because the locomotion power depends on the size and the mass of the robot while the computers and sensors are relatively independent of the robot's size and mass. It should be noted that adding more batteries to the robot adds more mass thereby requiring more power for locomotion.

Robot	Mass (kg)	Maximum locomotion power (W)
Khepera III [36]	0.69	0.8 (28%)
MarXbot [106]	1	3.5 (33%)
Pioneer DX [104]	9	10.6 (34%)
Auriga-β [101]	286	3000 (87%)
TIM [3]	500	2000 (92%)

Table 3.1: Comparison of various mobile robots' mass and power consumption.

Analysis of previous studies suggest that there is no common approach for creating power and energy consumption models of various components irrespective of the type of mobile robot

and hence a generic modular approach for building power models and predicting the energy consumption of a mobile robot is proposed. This work aims towards the use of robots for mobile robotic applications including radiation inspection applications in hazardous environment and specifically towards ensuring successful completion of tasks from the energy perspective.

3.2   Proposed energy prediction method

Teleoperated robotic system : A general architecture of a teleoperated robot and the components used in the proposed energy prediction method are shown in Figure 3.1. As explained in [101], mobile robots usually have multiple components, such as motors, sensors, and micro-controllers, embedded computers and communication devices. Communication with the robot can be either wired or wireless. Embedded computers are used for high-level computation and micro-controllers for low-level controls. The remote control station (commanding the robot) usually consists of communication devices, computers, information or video display modules, input and control devices such as joystick, keyboard and touch panel.
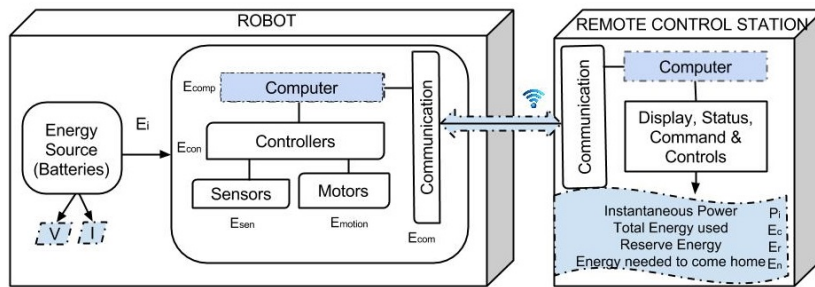
Figure 3.1: General architecture of teleoperated robotic system highlighting the components used in the energy monitoring system.

The time-stamped instantaneous battery voltage and total current used by the robot (instead of measuring current through each component) is used to build the power models. The energy needed by the robot to perform any task (including the on-line estimation of energy required to return to its base station) can be predicted with the help of these power consumption models. Most of the robots provide internal battery voltage information. Some robots are equipped with a battery charging system that provides both voltage and current information at run time.

On-line energy prediction modelling system : Power consumed by the robot depends on the number of active components, whereas the energy consumption depends on the power consumption as well as the amount of time each component is active. A one-time process for generating the power models for various components can be developed by conducting some pre-determined series of operations on the robot (e.g. Figure 3.2) either manually or by programming operations in the robot's embedded computer. When an additional component (hardware) is added to the

robot, the robot's existing power model is updated. This feature makes the energy prediction algorithm modular and expandable for future modifications in the robot.
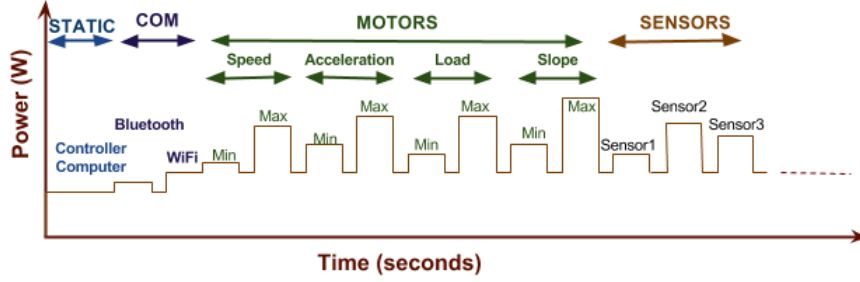
Figure 3.2: Sequence of operations to determine power models of various components in a mobile robot.

The instantaneous power consumption of the mobile robot is the sum of power consumed by static and dynamic power consuming components. Components such as computer, controllers, and communication devices consume steady-state power P_{static} (without many fluctuations). Whereas components such as sensors and motors whose power consumption dynamically varies based on their usage are categorised as dynamic components with power $P_{dynamic}$. The instantaneous power P^i at time instant i is given by:

$$P^i = \sum_{i=1}^{n_1} P^i_{static} + \sum_{i=1}^{n_2} P^i_{dynamic}, \text{ where } n = n_1 + n_2 \tag{3.1}$$

Here, n_1 is the number of static components, n_2 is the number of dynamic components and n is the total number of components in the mobile robot. The energy consumed by a component j is the summation of the power consumed by that component during the time (t_j) the component is active.

$$E_{c_j} = \sum_{i=1}^{t_j} P^i_{c_j} \qquad [\text{J}] \tag{3.2}$$

To obtain the total energy consumed by the robot (E_c) in driving along a path of length p for t_p seconds, integrate all the n components' energy consumption as follows:

$$E_c = E_{static} + E_{dynamic}, \tag{3.3}$$

$$E_c = \int_0^{t_p} \sum_{j=1}^{n} (G^i_{c_j} \cdot P^i_{c_j}) \, \mathrm{d}t, \tag{3.4}$$

where $P_{c_j}^i$ is the maximum power consumed by a component j at time instant i and $G_{c_j}^i$ is the weight function applied to each component based on its type as follows:

$$
G_{c_j}^i = \begin{cases} 1 & \text{when component j is active and static,} \\ \alpha & \text{when component j is active and dynamic,} \\ 0 & \text{when component j is passive.} \end{cases}
$$

The parameter $\alpha \leq 1$ depends on the duty cycle (if it's a motor) or the frequency f (if it's a sensor) of the dynamic component that is active at the instant i. For static components, the maximum power consumed is equal to the average power consumed by them. For instance, the static components such as computers and controllers are always active in a mobile robot, whereas the communication devices need not necessarily be active all the time but can be passive for some duration. The power consumed by a sensor operating at a frequency f can be modelled using a linear equation involving two constants s_1 and s_2 as [104]:

$$
P_{sensors} = s_1 * f + s_2. \tag{3.5}
$$

The motion power depends on various parameters such as the linear velocity υ and angular velocity ω, the linear and angular accelerations $a, \dot{\omega}$, the mass of the robot m and the slope of the surface α.

$$
P_{motion}^i = f(\upsilon, \omega, a, \dot{\omega}, m, \alpha). \tag{3.6}
$$

Most of the mobile robots use multiple DC motors for locomotion with wheels, tracks or modular arrangements. The power model for DC motor with velocity υ and acceleration $\dot{\upsilon}$ at time instant i is given in [108] as follows:

$$
\begin{aligned}
P_{motion}^i = {} & C_1 \cdot {a^i}^2 + C_2 \cdot {\upsilon^i}^2 + C_3 \cdot \upsilon^i + C_4 + C_5 \cdot a^i \\
& + C_6 \cdot a^i \cdot \upsilon^i.
\end{aligned} \tag{3.7}
$$

The parameters $C_1, C_2, \cdots, C_6$ depend on the motor and wheel characteristics such as torque constants, damping force, load inertias, and the nature of the travelling surface. When the robot travels a pre-defined path, the initial and final velocities are zero, and therefore the motion power model can be reduced to:

$$
P_{motion}^i = C_1 \cdot {a^i}^2 + C_2 \cdot {\upsilon^i}^2 + C_3 \cdot \upsilon^i + C_4, \tag{3.8}
$$

$$
E_{motion} = \int_0^{t_p} (C_1 \cdot {a^i}^2 + C_2 \cdot {\upsilon^i}^2 + C_3 \cdot \upsilon^i + C_4) \, dt. \tag{3.9}
$$

The total energy consumed by a robot is given below as a sum of energy consumed by computer, controller, sensors, motors and communication devices.

$$E_c = E_{comp} + E_{con} + \sum_{j=1}^{n_s} E_{sen_j} + \sum_{j=1}^{n_m} E_{motion_j} + E_{com}. \tag{3.10}$$

Once the power model is generated, it can be used to calculate the on-line energy consumption of each component while the robot is performing some task or can be used to predict the energy requirements before the mission based on the nature of the tasks. The list of active components at any instant is determined by the operator (manual teleoperation) or by the program (autonomous). Different tasks or missions exhibit different energy consumption behaviour; nevertheless, the energy characterisation will allow the operator to optimise the energy consumption.

Let E_a be the total energy available in a mobile robot. Since the aim is to predict the energy consumed during/before a mission, the dynamics of the total available energy capacity in a robot (that depends on the battery chemistry) is out of scope of this chapter and treated E_a as constant. The reserve energy available at any instant is given by:

$$E_r^i = E_a - E_c^i. \tag{3.11}$$

Let us assume that the robot is active for t_n seconds during a mission of travelling a path of length d_p with a constant velocity v_p. The time taken by a robot to travel the distance $t_p = \frac{d_p}{v_p}$ (such that $t_p \leq t_n$) is the time during which the motors are active. The energy needed to execute this mission E_n and the reserve energy E_r after the execution of this mission will be:

$$E_n = (P_{static} \cdot t_n + P_{motion}(v^i, a^i) \cdot t_p), \tag{3.12}$$

$$E_r = E_a - E_n. \tag{3.13}$$

3.2.1 Energy prediction algorithm

The energy prediction algorithm for the proposed method is summarised in the algorithm 1. In the algorithm, $x(t)$ is the current position and x_d is the destination position, v(t) is the current velocity and v_{target} is the target velocity, a(t) is the current acceleration, α is the slope of the surface in which the robot is moving, f is the frequency of operation (usually for sensors), $P^i_{predicted}$ is the predicted power for i^{th} component considering all the parameters affecting the power consumption, the Prediction(i) is the power model function depending on the component i, $E^i_{predicted}$ is the predicted energy for i^{th} component, E_c is the energy consumed by the mobile

robot, E_m is the maximum energy stored by the battery in the mobile robot, E_a is the energy available for the rest of the mission execution.

The algorithm works as follows: It first acquires the necessary data from the sensors (such as voltage, current, speed, acceleration, and surface slope) and from internal memory (such as time, component active status, and operational frequency of sensors); then it uses power models of the respective components and the pre-acquired data to compute the energy consumption of individual components in the robot; once the energy consumption is calculated, the algorithm keeps monitoring the robots' activity and compares the remaining energy level with the required energy level for a task completion or for the robot to return back to the control station; based on the current energy levels, decisions are made whether to continue the existing tasks (if the remaining energy is adequate) or to return back to control station if the remaining energy is inadequate or to receive aid from the operator on making complicated decisions.

Algorithm 1 Energy prediction algorithm for mobile robots.

1: **while** $x(t) <= x_d$ **do**
2:      Measure the instantaneous voltage and current
3:      Obtain the (temporal) activity information for each component in the mobile robot
4:      Obtain the speed, acceleration, slope, frequency and related values for each component
5:      Obtain slope α for the current position ($x \in \mathbb{R}^2$)
6:      **for** i in 1 to N **do** % N = number of active components for which power models are available
7:          $P_{motion} = \mathrm{Prediction}(v(t), a(t), \alpha)$
8:          $P_{sensors} = \mathrm{Prediction}(f(t))$
9:          $P_{static} = \mathrm{Prediction}(i)$
10:          $E_{predicted}^i = E_{predicted} + (P_{static} + P_{motion} + P_{sensors}).t$
11:      **end for**
12:      $E_c = \sum_{i=1}^{N} E_{predicted}^i$
13:      $E_a = E_m - E_c$
14: **end while**
15: **if** $E_a <$ Energy required for going back to charging station **then**
16:      Stop executing the task and wait for operator commands
17: **end if**
18: **if** $E_a <$ Energy required for executing a given task **then**
19:      Take necessary backup actions and alarm the operator
20: **end if**

3.3   Experimental evaluation

The proposed energy prediction method has been implemented off-board on two types of mobile robots for experimental evaluation. The first one is a small autonomous commercial mobile robot called Khepera III [61] produced by the K-team corporation and the another is a large mobile robot platform called TIM (developed at CERN). These two mobile robots of different

sizes (in the order of two) are chosen to test the scalability of the proposed method and to make sure that the proposed method can be applied to wide range of mobile robots. The youBot was not available at CERN when these experiments are conducted and reported in the publications [35], [36], and hence only the above mentioned platforms are used in this work.

The experimental setup and the experiments conducted in both of the platforms are different from each other as the size and shape of the platform, the types of environments they are deployed and the nature of the applications they can be used are all dissimilar. In the following subsections, the experimental evaluation and results using these two platforms are discussed separately.

3.3.1 Experiments with Khepera mobile robot
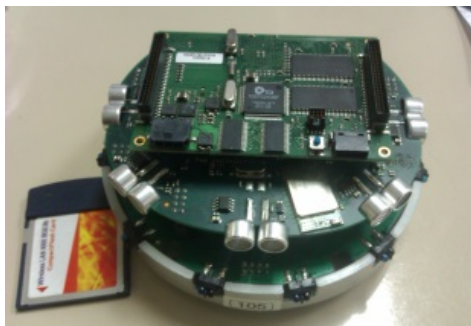
(a) Inner view.

(b) Outer view.

Figure 3.3: Khepera III mobile robot used in the experiments.
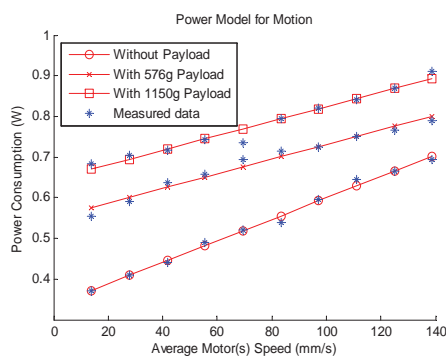
(a) Motion power with respect to the speed of locomotion.
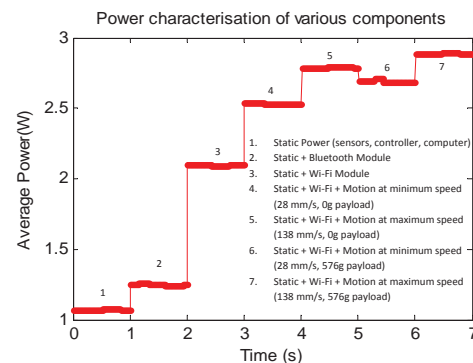
(b) Power characterisation of the Khepera III mobile robot.

Figure 3.4: Measured power models for Khepera mobile robot components.

The Khepera III mobile robot ($127x123x70$ mm^3, Figure 3.3), produced by the K-team Corporation, has an inbuilt smart battery monitoring system providing the current state of the battery (voltage, current, capacity remaining, and temperature) and hence this robot is selected to start with the experiments so that no additional hardware module (e.g. current sensor) is needed. The Khepera III powered by a rechargeable Li-polymer battery pack of 1400 mAh, has 2 DC brushed

servo motors, 11 infra-red sensors and 5 ultrasonic sensors. Korebot II, a mini-computer (extension module) that hosts Bluetooth and Wi-Fi communication modules is added to the Khepera III robot. The voltage and current values are recorded at a sampling frequency of 20 Hz.

As soon as the robot is started, the power consumed by various components is recorded by activating or controlling the components one by one. Programs for deriving the power models from a series of operations (Figure 3.4b) and calculating the energy consumption of each component (by determining the duration for which each component is active) are written in MATLAB and tested with the robot's datasets created during the experiments. Initially the computer is turned on and hence P_{comp} is calculated. Then, the controllers are activated and the power P_{con} is noted. Each other component's power consumption is calculated by subtracting from the previous power value after the activation of the respective components.

Since all sensors data are needed during teleoperation to ensure safety of the robot and surroundings, all the sensing elements are active at maximum frequency throughout the experiments. Motors are the only dynamic components. Hence the static power component is the sum of sensing, controller and computer power. $P_{static} = P_{sen} + P_{comp} + P_{con} + P_{com}$ and $P_{dynamic} = P_{motion}$. The computer consumes an average 0.5 W power. Therefore, the sensing and control power is obtained by subtracting 0.5 W from the static power.

As the Khepera mobile robot is small in size and mass, the power model for locomotion is assumed (and is evident in the experiments) to be linear with respect to the average speed (of both motors) and the only cases considered are constant payload on a flat surface. However for bigger robots, this assumption does not hold true and hence the motion energy model (Equation 3.7 or Equation 3.9) should be used instead. The acceleration effects are negligible when compared to the effect of velocity on power consumed by the motor [104]. Hence, the Equation 3.9 can further be reduced adding the effect of payload mass m_p as:

$$P^i_{motion} = C_v \cdot v^i + C_{m_p} \cdot m_p + C_I, \tag{3.14}$$

where the parameter C_I depends on the robot's mass m_r and its inertia.
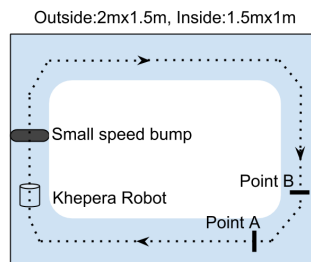
Figure 3.5: Mobile robot path during tasks.

(a) Measured speed, power and energy during $task^A$.

(b) Measured speed, power and energy during $task^B$.
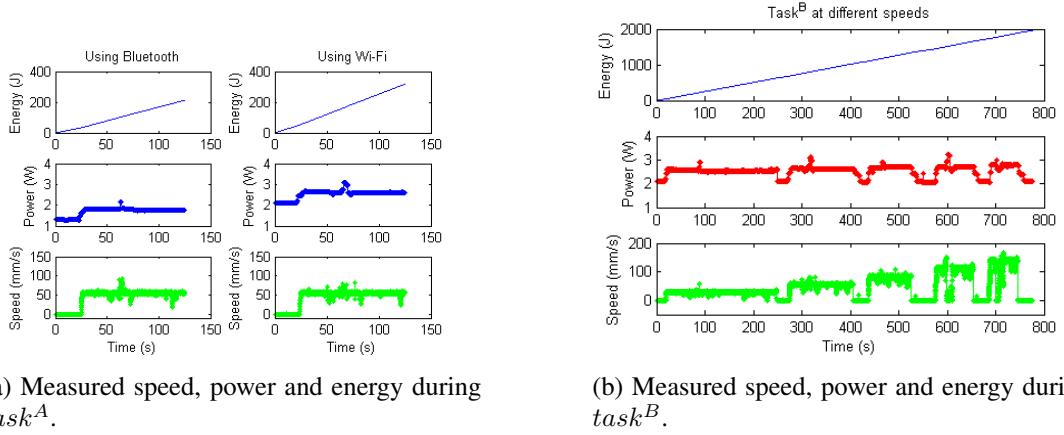
Figure 3.6: Experimental tasks performed and the measured energy values during the operation.

The power consumption of static components is observed to be almost constant (average values are used). The range of speed used in teleoperation experiments is 28 mm/s - 138 mm/s. With the measurement of motion power corresponding to the speed and payload of the robot (Figure 3.4a), a least square fit to the Equation 3.14 can be applied to the measured data arriving at the following equation:

$$P^i_{motion} = 2.4 \cdot v^i + 0.22 \cdot m_p + 0.36. \tag{3.15}$$

The generated power model is used for the energy prediction modelling system. It can be noted that the Wi-Fi module consumes significantly higher power than other components.

To verify the accuracy of the energy prediction models, two different types of tasks with the robot travelling from point A to point B are conducted. For the experiments, the total time for completing the task $t_n = 125$ s and the time for motion is $t_p = 100$ s. The measurements sampling time $dt = 50$ ms.

The first task ($task^A$) is to run the robot with same velocity but with different static power consumers (i.e. the dynamic power consumption remains same in both case). In this scenario, the robot performed the task twice, one using Wi-Fi module ($task^A_{Wi-Fi}$) and again using Bluetooth module ($task^A_{Bt}$). The robot moved at a constant velocity $v = 56$ mm/s. The measured speed, power and energy for $taskA$ (Figure 3.6a) show a minor power change at 70 s due to a small speed bump on the path. The second task ($task^B$) is to circulate the robot in the robot arena (with point A as the origin) at different velocities.

The total energy drawn by the robot can be calculated by using the instantaneous power values (using voltage and current measurements) as follows:

$$E_{ref} = \sum_{i=0}^{t_n} V^i \cdot I^i. \tag{3.16}$$

This energy value (Equation 3.16) is used as the ground truth reference value against which the predicted energy value using the energy models (Equation 3.4) are compared. The predicted energy values E_{pred} for $task^A_{Wi-Fi}$ and $task^A_{Bt}$ are computed using the derived power models and the Equation 3.4, Equation 3.15 and Equation 3.13.
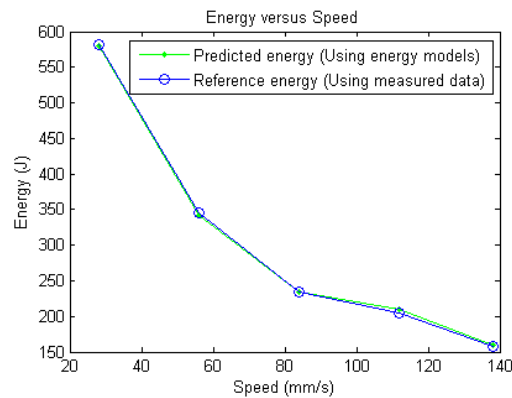
Figure 3.7: Comparison of predicted versus measured energy values with speed for $task^B$.

3.3.2 Experiments with TIM platform
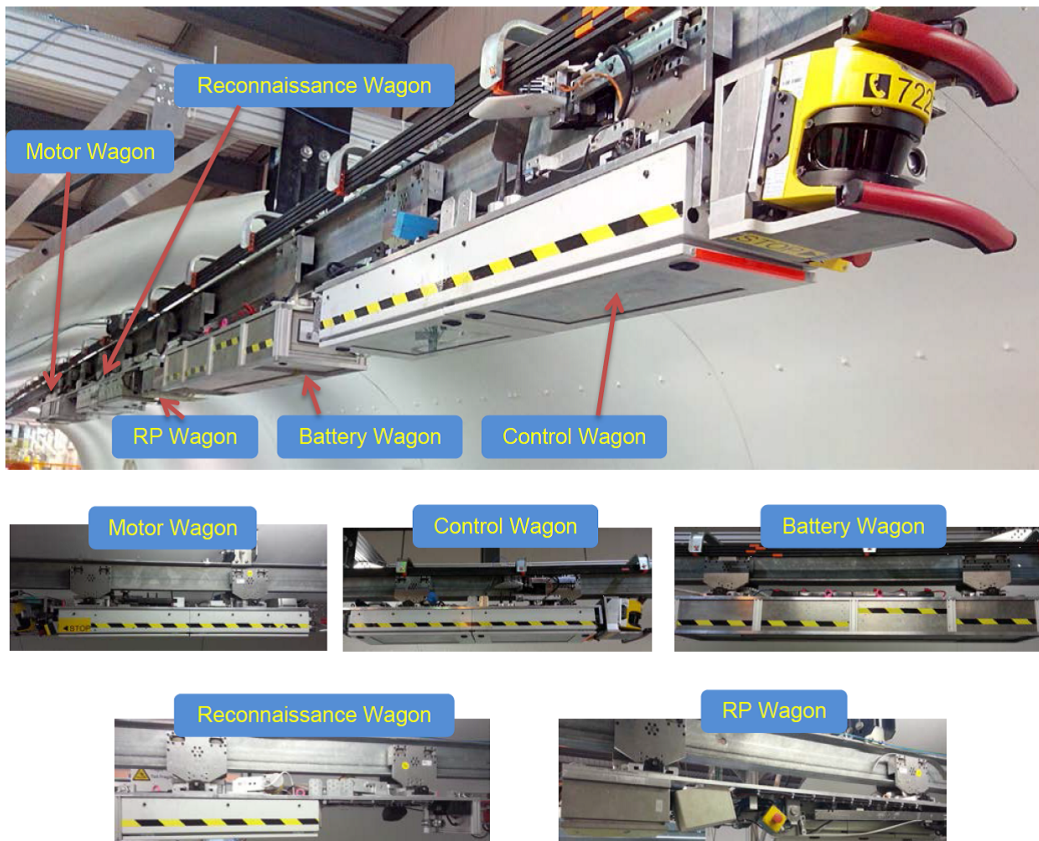
Figure 3.8: The Train Inspection Monorail (TIM) mobile robot (train-like) platform in the LHC mock-up facility at CERN.

A modular robotic platform called "Train Inspection Monorail" (TIM) is a development project at CERN for conducting remote radiation survey and inspections [16]. The TIM platform is specifically designed to conduct radiation measurements and visual inspections over the 27 km circular tunnel of the Large Hadron Collider (LHC). It is mounted on a overhead monorail which initially intended for powering the transport vehicles during the installation of the magnets in the LHC tunnel. The TIM prototype platform is a train-like modular structure consisting of five wagons, has a size of ca. 1000x30x30 cm^3 (LxWxH), and can travel at a maximum realisable speed of up to 6.5 km/h, in slopes up to 1.44 and it weighs around 600 to 700 kg. The TIM prototype platform is battery powered and at the time of testing is installed on a 50 m long monorail test bench (LHC mock-up) facility at CERN. Figure 3.8 shows the structure and design of the TIM platform mounted on the monorail in the LHC mock-up facility.

The energy prediction method proposed in section 3.2 has been modified and adapted to suit the TIM's programming requirements and implemented off-board due to practical reasons, however the method is tested using the data-sets extracted from the real platform. The data-sets from the train are obtained by means of running the train in various possible cases for more than 2 months. For more details on the TIM structure, the programming logic controller (PLC) program structure in TIM, and the experimental trials made, one can refer to [109].

Based on the mechanical design of the train, the locomotion power for the TIM motion is given by the following equation:

$$P_{\text{motion}} = \frac{1}{\eta_{\text{transmission}}} (\frac{9.\text{I}.a(t)}{R^2} + 5.m.(a(t) + g.\sin(\alpha) + \mu.g.\cos(\alpha)) - 2.\mu.\text{Z}) \text{ v}(t) \ [W], \quad (3.17)$$

where I is the motor inertia = 7.2 kg.m^2, a is the acceleration, R is the wheel radius = 50 mm, m is the mass of each wagon = 100 kg, μ is the coefficient for rolling resistance of each wagon = 0.005, g is the acceleration due to gravity = 9.8 $\frac{\text{m}}{\text{s}^2}$, α is the angle of slope in monorail, Z is the upward force acting against the monorail to avoid slipping of the wheels, $\eta_{\text{transmission}}$ is the mechanical transmission efficiency and v is the velocity of the train.

The current and voltage are measured using a Hall effect sensor and a voltage sensor on-board the TIM. The energy prediction system is implemented as an energy manager in the PLC program of the train and its structure is shown in figure 3.9. The effects of energy consumption of the train due to speed, acceleration and slope effects are considered. Figure 3.10 shows the graph of the power and energy consumption with respect to the speed on movement. A polynomial equation is fitted for the corresponding curves and is also shown in the figure. The pattern of power and energy consumption for motion is consistent with the pattern for the Khepera robot which implies that the assumed prediction models are scalable.
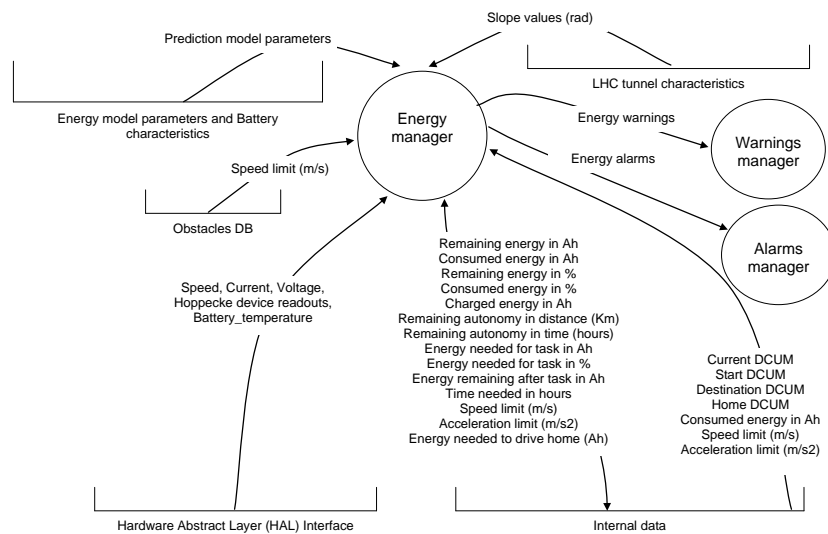
Figure 3.9: Structure of the energy prediction system adapted to the TIM platform.
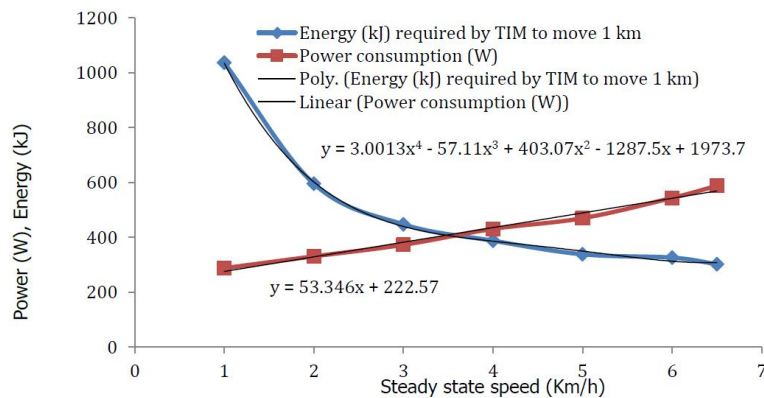
Figure 3.10: Power and energy consumption values w.r.t. the steady-state speed of the TIM mobile platform.

In figure 3.11, the effects of acceleration and deceleration on the robots' power and energy consumptions are shown. The power consumed by the robot is proportional to the speed of locomotion, and is higher when the acceleration is higher as could be observed from this figure where the current drawn at the steady-state speed increases with increase in acceleration. On the contrary, the energy consumed by the robot at the end of the task remains more or less consistent with acceleration (although the energy consumed to achieve the steady-state speed is lower when the acceleration rates are higher). This behaviour could be attributed to the fact that the time taken to complete a given task is inversely proportional to the acceleration and deceleration rates.

The maximum current drawn by the robot while reaching the steady-state speed is proportional to the acceleration rate and therefore, the acceleration rates are limited by the maximum current that can be delivered by the battery at any instant of time (the discharge current and the rate

of discharge can have adverse effects on the performance of a battery and its residual capacity [110]).
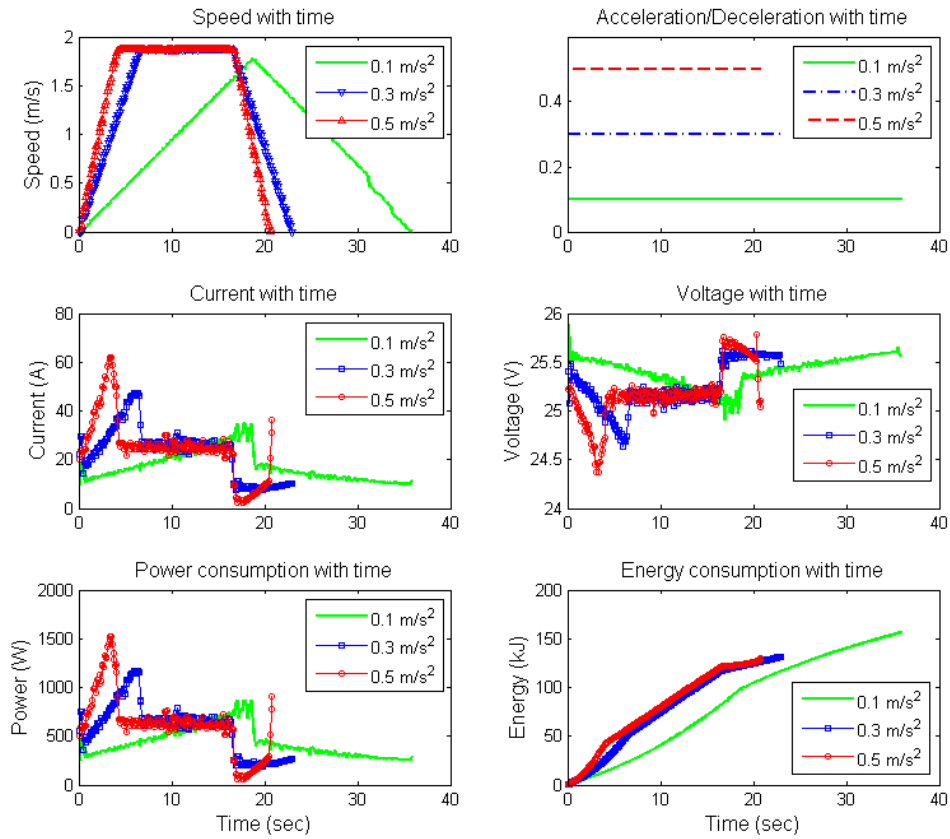
Figure 3.11: Speed, current, voltage, power, and energy values of TIM while travelling a distance of 30m at 6.5 km/h (accelerating and decelerating).

3.4 Results and discussions

The results and outcome of the proposed energy prediction method on Khepera robot and TIM platform are presented in the following subsections separately.

3.4.1 Results from Khepera mobile robot

Figures 3.12 and 3.7 show the comparison of the reference energy values (computed with the measured data) and the predicted energy values (computed with the energy prediction models). The energy prediction error is calculated as:

$$Error(\%) = \frac{E_{ref} - E_{pred}}{E_{ref}} \cdot 100. \tag{3.18}$$
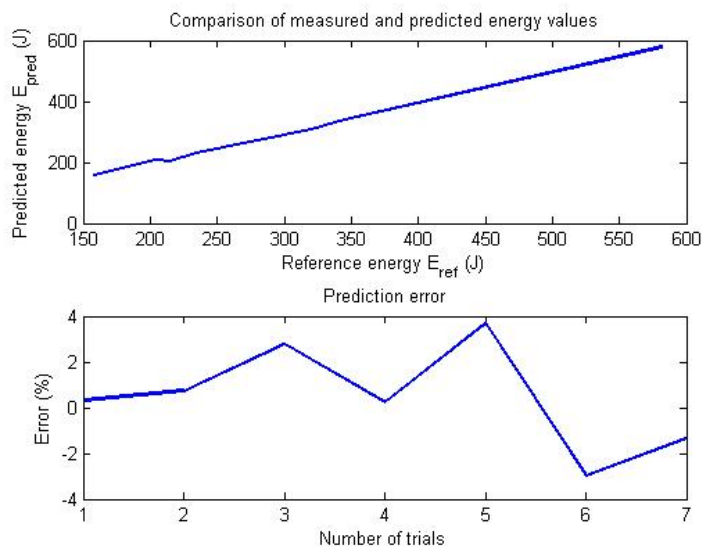
Figure 3.12: Comparison of measured (reference) and predicted energy values in Khepera robot (top). Prediction error of the proposed energy prediction method (bottom).

The mean error of the model-based energy calculation is 1.6% (with a range of -2.8% to +3.8%. This proves that this method is highly accurate for application to energy prediction system to small-scale robots.

Considering the prediction error as 4% (Equation 3.18), measurement error with the current and voltage transducers as 2% (from the transducer specifications), and a standard deviation from the average values as 4% (Equation 3.5), the energy prediction system should have a margin of at least 10% for effective energy prediction and mission panning.

In the future work, effects such as battery's lifetime, proper cycling of charging and discharging the batteries and recovering energy through regenerative braking can be considered for a more accurate energy prediction algorithm.

3.4.2 Results from TIM platform

The energy predicted using the proposed method and the actual consumed energy measured using an industrial Ampere-hour meter device manufactured by Hoppecke GmBH is presented in figure 3.13. The energy consumption (Ah) is converted to the remaining battery percentage (%) by using the equation:

$$\text{Battery percentage} = \frac{\text{Energy}_{\text{available}} - \text{Energy}_{\text{consumed}}}{\text{Energy}_{\text{available}}} \quad [\%]. \tag{3.19}$$

The figure 3.13 also shows the prediction error (in %) calculated on the same basis as given in the equation (3.18). An example of the performance of the power consumption prediction can
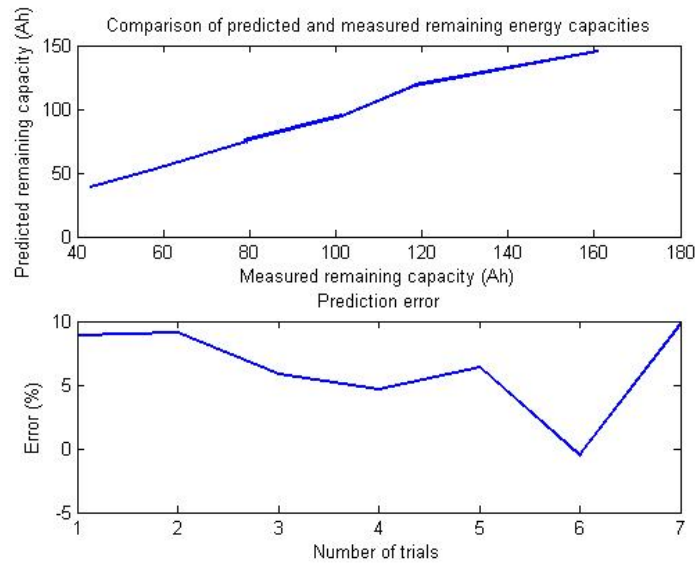
Figure 3.13: Comparison of battery remaining energy percentage calculated using measured energy and predicted energy values in TIM robot (top). Error in energy consumption prediction (bottom).
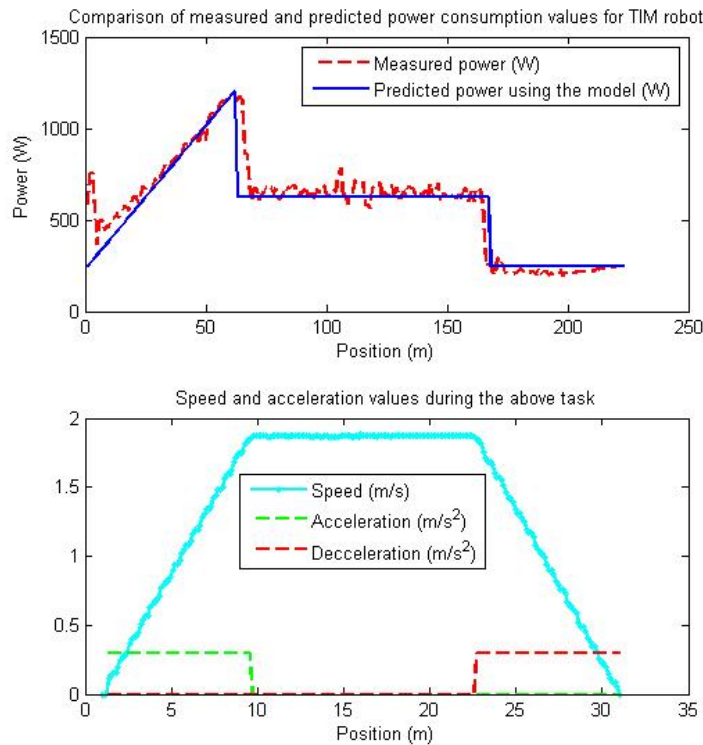
Figure 3.14: Example of predicted and measured power consumption values for TIM while travelling a distance of 30 m (top). Speed and acceleration values during this task (bottom).

be seen in figure 3.14. For instance, the prediction model calculated the energy consumption as 12.73 kJ for a task of TIM making a displacement of 30 m with acceleration of $0.3\,\mathrm{m/s^2}$ and deceleration of $0.3\,\mathrm{m/s^2}$ and with a steady-state speed of 6.5 $\mathrm{km/h}$ (1.86 $\mathrm{m/s}$). For the same task, the

measured energy consumption value 13.16 kJ. This means that the prediction model has around 5% accuracy in this example. This example is shown to provide an intuitive understanding on the performance of the proposed energy prediction method.

Essential results are reported in this thesis and the detailed results and discussions of the energy prediction and management system including the implemented full-scale off-line energy prediction algorithm in the TIM platform are published in the CERN internal report "TIM pre-series energy management system specifications" [109]. The reference [109] also contains information on the maximum slope and acceleration capabilities of the TIM prototype given a specific zone (regions) inside the LHC by considering the power and energy consumption models.

3.5   Energy-efficient strategies for wireless communications

The total energy consumed by a robot depend on the type of wireless communication methods used and the intensity of the tasks. Let us consider an example case with the Khepera mobile robot to demonstrate energy efficiency by choosing different wireless communication methods for a particular task. To travel from point A to point B, the energy saving made by operating the Khepera robot at higher speed ($138 \, \mathrm{mm/s}$) is 73% compared to operating the robot at $28 \, \mathrm{mm/s}$ (based on Figure 3.7). From this study, it can be observed that around 33% of energy can be saved by using the Bluetooth module instead of the Wi-Fi module for communication. However, the Bluetooth wireless standard has more constraints than Wi-Fi (such as less distance range, lower data rate capability). If the robot is operated at maximum speed and does not use any communication device, then the energy savings (computed using energy models) can be up to 83%. Hence, based on the system's needs and requirements, appropriate communication methods have to be selected to minimise energy consumption.

It can be noted from the figure 3.10 that the behaviour of power and energy consumption with respect to locomotion speed of a mobile robot can be different. Therefore, using energy consumption models is a more reliable method (than using power models as in [105], [106]) to plan or manage the energy autonomy of the robot. For instance, if the Khepera robot is operated at maximum speed and does not use any communication device, then the energy savings (computed using energy models) can be up to 83%. Whereas, if only the power models were used for this analysis (e.g. [104]), the savings made in total power consumption would be 30%.

In addition to the advantage of energy savings by using energy prediction models, the tasks to be performed can be well planned to meet the energy and communication demands of the robot with the help of energy simulations. The simulated energy consumption models can be used to optimise and prepare robotic interventions by simulating the energy and communication requirements. For instance, Player/Stage [111] and Gazebo in Robot Operating System (ROS)

[112] are widely used simulator tools [113] in the robotics research community to test robots' performance in a given environment. If the energy models are integrated into such simulators, it will be possible to simulate the energy consumption for specific tasks, situations and surroundings, and using these simulations, the wireless communication strategies can be optimised to suit the task and mission requirements of the intended telerobotic operations.

3.6 Summary

A novel energy prediction method was proposed in this chapter. Literature review suggested that there was no common approach for creating power and energy consumption models of various components of mobile robot and hence a generic modular approach for building power models and predicting the energy consumption of a mobile robot was proposed. The proposed method was designed to be run on-line as well as off-line and could be incorporated in mobile robots as a modular addition. The energy prediction method was implemented in two mobile robots: a small Khepera mobile robot, and a large train-like mobile robot developed in-house at CERN. These two experimental platforms had large differences in size, shape, structure, application capabilities. Several experiments were conducted to verify the performance of the proposed method. The prediction results obtained from the experiments on a small-scale mobile robot (Kehepera III) and a large-scale mobile robot (TIM), shown in the figures 3.13 and 3.12 respectively, demonstrated that the proposed energy prediction algorithm was accurate considering a maximum 10% prediction error. The results had shown that the energy prediction model is indeed suitable to wide variety of mobile robots. The proposed energy prediction method also provided opportunities for discovering various hardware and software defects or faults in the TIM and helped in diagnosing and rectifying such faults and defects [109].

Chapter 4

Communication range prediction methods using RSS models

This chapter deals with the validation of radio signal propagation models and their use in predicting wireless communication range before (off-line) and during (on-line) a robotic mission. As the operational (practical) communication range can be predicted with the help of the radio signal strength (RSS) parameter, RSS prediction techniques will be discussed in this chapter. In the first section, the prediction of the RSS before the mission execution using an extended log-normal shadowing model (ELNSM) will be discussed after analysing the RSS characteristics. This strategy will permit the operators to plan the robotic mission accordingly before deploying the mobile robot in the environment. In the second section, a novel method using Kalman filters and Gaussian process models will be proposed to predict the RSS when the mobile robot is executing its missions assuming an unknown environment.

4.1   Off-line communication range prediction method

Radio signal transmission characteristics are specific to the environment where the mobile robot is deployed. Understanding the radio signal propagation characteristics in the environment where the telerobotic application is sought, is a key part of achieving a reliable wireless communication link between a mobile robot and control station. The radio signal strength (RSS) is a measure of radio signal range. Therefore, using RSS prediction methods, the communication range for a particular setup can be predicted. In this section, the theoretical and experimental characteristics of radio propagation are investigated with respect to time, distance, location and surrounding objects. A case study of a typical telerobotic application in an underground facility at CERN is presented for demonstrating the RSS prediction methodology. Based on experimental analysis of the proposed RSS prediction method, it is shown how a commercial wireless system such as Wi-Fi can be made suitable for a case study application at CERN.

4.1.1   Preliminaries to off-line RSS prediction

For telerobotic applications in radiation environments, the main wireless communication challenges to be considered are that the robot should be able to travel long distances in hostile or tunnel like environments and should be able to transmit large amount of data in very short time. Having a reliable communication link with the robot [114] is essential to avoid the need for personnel access to recover the robot in the event of communication failure.

Wireless communication avoids the cable disconnection problem typical of wired communication, which occurs when a cable is broken as a result of a physical damage during operation. Therefore, wireless communication is preferable to remotely operate mobile robots in such environments.

On the other hand, wireless communications have also found to be unreliable [2], [23]. However, wireless communication offers solutions to some of the fundamental challenges of all tethered communication systems with benefits such as low maintenance, high robustness against failures stemming from physical damage, less manpower needed for managing the tethers and ease of mobility.

Underground tunnels are generally very challenging environments for radio communications [2], [23]. It is observed in [23] that, the behaviour of radio signals is very different in underground mines compared to that in outdoor and line-of-sight (LOS) environments. Hence, there is a need to predict and investigate how radio signals behave in scientific facilities such as at CERN so as to properly design the wireless communication system and ensure reliability. The first step in increasing a wireless network performance is predicting the environment beforehand by understanding the radio signal propagation characteristics specific to that environment.

The contributions of this section are three-fold:

1. Experimental analysis of temporal, spatial and environmental characteristics of radio signal propagation in an underground scientific facility;

2. Prediction of communication range of the mobile robot by the use of the signal strength and the link quality;

3. And a strategy to verify the applicability of an available wireless network setup in a telerobotic application.

This section is organised as follows: firstly, the case study application is explained and the wireless network requirements for this case study application is presented; secondly, the scope of the experiments to be conducted are defined; then, the experimental test-bed is described, the measurement parameters are discussed and the signal propagation characteristics are analysed; lastly, the results of the experimental tests are discussed in relevance to an available wireless network using Wi-Fi technology.

4.1.1.1   Communication quality measurement metrics

Revisiting the background on the communication theory discussed in section 2.3, the communication channel capacity C in a wireless network, according to Shannon's capacity theorem [72], is related to the RSS as shown in the equation below (derived from the equation (2.5)):

$$C = B \log_2(1 + \frac{RSS_{mW}}{P_N}) \qquad [\text{Mbit/s}], \qquad (4.1)$$

where B is the frequency bandwidth of the channel and P_N is the absolute power of the noise in the channel. This indicates that the data rate of the wireless network (which is a measure of the channel capacity C) depends on the received signal strength.

The theory behind the received signal strength is explained in the section 2.2. The RSS is equal to the difference in the transmitted power P_T and the path loss PL_d over a distance d, as given in the equation (4.2),

$$RSS = P_T - PL_d \qquad [\text{dBm}]. \qquad (4.2)$$

The quality of communication links is a function of many variables including location, distance, direction and time [115]. To estimate the distance coverage of radio signal propagation, it is required to analyse the Received Signal Strength Indicator (RSSI) and Link Quality Indicator (LQI) at the receiver end. The latency of the communication network can be measured by using the Round Trip Time (RTT) metric. The definitions of the three metrics to be measured are given below.

RSSI: Measure of the received signal strength. The signal strength mainly depends on the antenna output power and the distance between the transmitter and the receiver. The $RSSI = RSS$ in this work. Therefore, both RSS and $RSSI$ terms are interchangeable.

LQI: Shows the quality of wireless connection. There are several definitions for the LQI and it usually refers to the percentage of packets transmitted successfully.

RTT: Round trip time for a packet to travel from transmitter to the receiver.

Both the $RSSI$ and LQI are non-linear with respect to distance as there are many other factors affecting link quality such as reflections and interference. If there are too many wireless stations in a wireless network, interferences may occur resulting in loss of messages. Reference [66] explains why the RSSI alone is not enough as a measurement parameter because the interference experienced on a link cannot be inferred via $RSSI$ measurements, but can be measured by the LQI. Therefore both $RSSI$ and LQI measurements are needed for link quality assessment and the RTT measurement is needed for latency measurement.

4.1.1.2   Case study application: ISOLDE Vision system for remote handling

ISOLDE (The Isotope Separator On-Line facility at CERN) experimental area is one of the high radiation area at CERN with a radiation dose rate of $100 \ mSv/h$ at $50 \ cm$ from the radioactive target after $1 \ hour$ of decay [28]. Figure 4.1 shows the floor plan of the ISOLDE area.

There are two industrial robots STAUBLI RX 170 used to transfer the used targets [116] from the target irradiation supports (C,D) to the target storage area (G) and pick up new targets from (B), a target interchange point. These robots are preprogrammed and the operator selects the sequence of operations from a dedicated control room (A) outside the ISOLDE facility.

However, in some situations such as robot teaching, the operator has the need to visually monitor the robot's movements. For such real-time monitoring, it is desirable that a reliable wireless video transmission system mounted on a small mobile robotic vehicle such as KUKA youBot [58] is used to transmit the live camera feeds monitoring the industrial robots. In the figure 4.1, the red coloured portions indicate the area where this application is desired.

The communication requirements for this application are mentioned as an "example application" in the table 2.1. It based on HD transmission of two good quality videos so that the operator can observe the environment more in detail including small sparks in the Faraday cages inside the ISOLDE facility. In this chapter, the vision system application at ISOLDE is used as a case study.
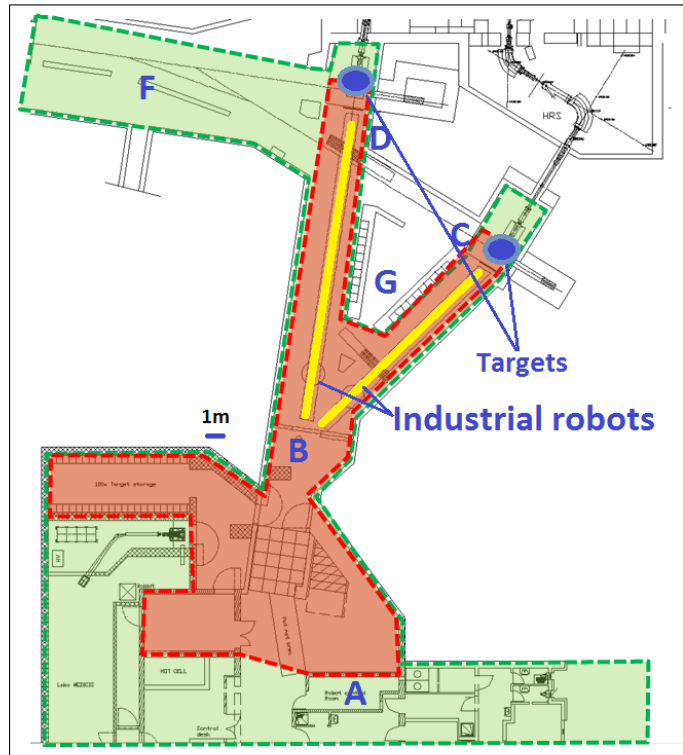
Figure 4.1: ISOLDE experimental facility at CERN.

4.1.2 Experimental analysis of the radio signal parameters

Radio signal parameters in indoor environments (for applications such as localisation [117], [118]) exhibit relatively different behaviours compared to the parameters in unstructured environments (such as underground tunnels and scientific settings), where the non-line-of-sight (NLOS) nature of the radio signal propagation has immense impact in the RSS [2], [23]. Mathieu Boutin et al. [24] analyse the NLOS propagation in tunnels and compare the characteristics of path amplitude and delay spread in a received signal from multiple paths. They suggest that further narrow-band and wide-band measurement campaigns should be also undertaken in galleries with different configurations as the wireless propagation in underground mine tunnels can be a challenge to model accurately in view of the complexity of the environment. Signal propagation simulation tools such as WISE [119] predict the received signal in an indoor RF channel. However, such tools rely on many parameters and are limited to outdoor and LOS situations.

One of the observations by Chou et. al. [120] suggests that for a wireless link, there is a trade-off between the maximum achievable data rate and the packet delivery latency. The latency of radio propagation in scientific facilities is not found in the literature.

The main reasons for conducting experimental analysis of the RSS are:

1. According to [24], using the theories and analysis available in the literature, it is not very simple to quickly predict the signal propagation behaviour in underground environments because the characteristics for each environment are very different;

2. No study is found that analyses the effects of radio signal latency in scientific and tunnel facilities.

Therefore, experiments have been conducted to investigate the spatial, temporal and environmental characteristics of radio signal strength and latency in a scientific facility at CERN.

Figure 4.2: ECN3 tunnel area at CERN showing the location of the radio transmitter (point A in figure 4.4).

Since there is relatively little propagation measurement data available for underground environments, it is important to take into account the impact of various environmental characteristics so that several simulations of link qualities using empirical values can be performed [24]. Conducting experiments at ISOLDE was not allowed during its operation as it is a highly radioactive area [28]. Therefore, experiments are conducted in a tunnel area called ECN3 (shown in the figures 4.2 and 4.3) which was not in operation and hence was available for tests.

Even though the ISOLDE and ECN3 facility are different, using ECN3 as the test facility allowed experimented and analytic techniques to be developed and will provide information on how well results obtained in one facility (ECN3) can be applied to another one (ISOLDE area).

Figure 4.3: ECN3 tunnel area at CERN - view from the tunnel entrance.
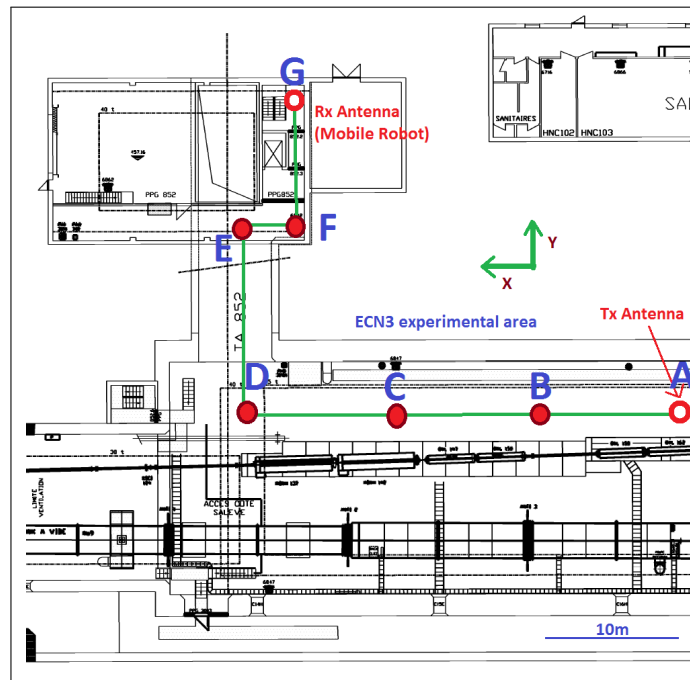
Figure 4.4: Floor plan of the ECN3 tunnel at CERN.

4.1.2.1 Methods and materials

In these experiments one static wireless transmitter (ProSafe Dual Band Wireless-N Access Point WNDAP350 [121]) and five compact Wi-Fi receiver stations are used (Zyxel NWD2105

[122]). The transmitter [121] uses IEEE 802.11n 2.4 GHz standards with maximum transmit power $P_T = 20$dBm, maximum data rate of $144.44 Mbit/s$. The receiver [122] had receive sensitivity threshold R_S of -64dBm at $64^{\text{Mbit}}/\text{s}$ and -82dBm at $11^{\text{Mbit}}/\text{s}$.

The transmitter is fixed at point A in figure 4.4 and the receiver stations are mounted at different positions (and orientations) on a KUKA youBot mobile robot as shown in figure 4.5. The omnidirectional capability in youBot [58] made it the best choice for the experiments because of space and size and space restrictions in the environment. A computer running on Ubuntu operating system on-board the youBot is used for computing.

Figure 4.5: youBot mobile robot used in the tests. Many wireless receivers are mounted on the youBot in different orientations.

The values of $RSSI$ and LQI are obtained by using the $iwconfig$ command in Linux. Each $RSSI$ and LQI measurement is the average of 100 samples of 10 ms interval each. The values of measured $RSSI$ and LQI and the method of measurement depend on the manufacturer of the wireless device. For Zyxel NWD2105, the $RSSI$ is equal to the received power in dBm, $RSSI = RSS$. And the LQI is the percentage of successfully transmitted packets.

$$LQI = \frac{\text{Number of successfully transmitted packets}}{\text{Number of total transmitted packets}} \quad [\%]. \tag{4.3}$$

The $ping$ command provides the RTT values for the respective receivers. The maximum number of bytes able to transfer at a time using $ping$ is 65527 bytes (512 Kilobits). The RTT reading for each receiver is the average of 10 samples. The average of the results from all receivers have been obtained, so that the results are not device dependent.

4.1.2.2 Experiments carried out

The variations of signal strength, link quality and the latency in the wireless channel are investigated for temporal, spatial and environment based characteristics. The three type of experiments conducted are,

1. Temporal characteristics: measurement of time variation of $RSSI$, LQI for around 90 minutes at various distances in the ECN3 tunnel. The RTT variation with the amount of data transmitted is also observed.

2. Spatial characteristics: the mobile robot is moved from one point to another point over a distance of around 50 m through many environmental variations such as LOS and NLOS situations, passing nearby metallic objects. The robot is moving at a speed of $0.2\ m/s$.

3. Environmental characteristics: the mobile robot is moved under a reinforced concrete block and near to large metal objects and the $RSSI$ variations are noted.

Figure 4.4 shows the floor plan of the ECN3 tunnel area and the location of the transmitter and the receiver (youBot) indicating the path the mobile robot used to travel a distance of 37 m in X direction (LOS) and 28 m in Y direction (NLOS). Each experiment is conducted twice and the readings are averaged.

Changes in RSSI and LQI with respect to time, distance and environment variations are detected. The RTT variations are measured with respect to distance and quantity of data transferred. The results of these experiments are described in the following sections.

4.1.2.3 Temporal Characteristics

In [115], the authors say that it is highly possible to conserve the quality of a wireless link within an hour and they observed $RSSI$ variation within 5-6 dBm in a day, however this is in an indoor environment. These measurements shown in figure 4.6, the $RSSI$ variation over a period of 90 minutes at point B in the ECN3 tunnel had a mean of 23.22 dBm and a variance 8.75 dBm.

Figure 4.7 shows the temporal variation of $RSSI$ at different distances from the transmitter. It can be observed that, as the receiver is farther from the transmitter, the frequency of $RSSI$ variations with time got smaller but the magnitude of variation became larger.

The variation of RTT with distance and quantity of data transmitted (at a distance of 40m) can be observed in figure 4.8 and a linear fit for this variation is given by the equation:

$$RTT = 0.0001\text{bit} + 2.3 \qquad [\text{ms}]. \tag{4.4}$$
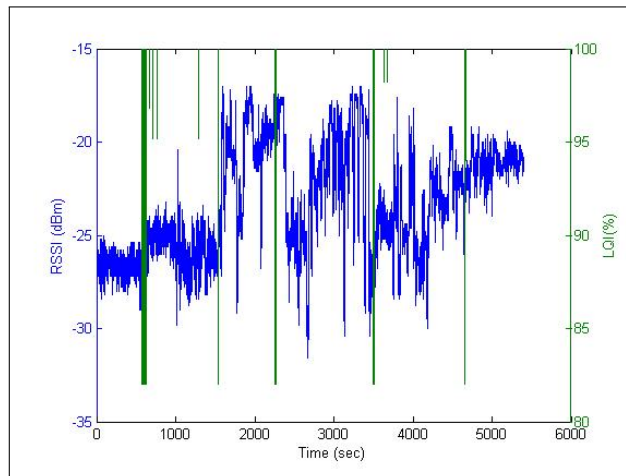
Figure 4.6: RSSI and LQI variations with time.
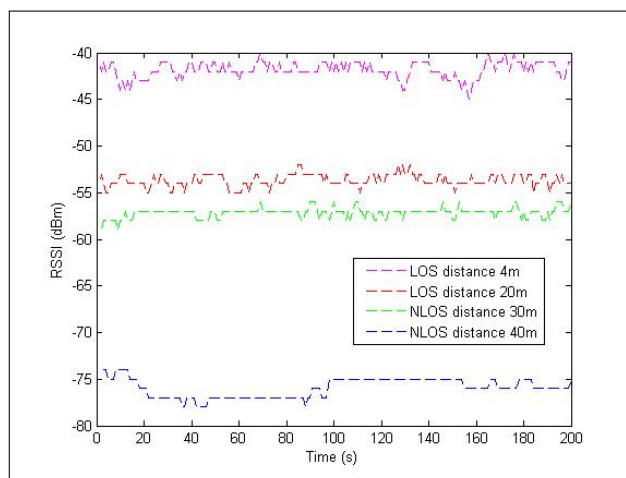
Figure 4.7: RSSI variations with time at various distances.

This result correlates well with the observations in [77] where the RTT is observed as $1s$ for transmission of five good quality video images at $2\mathrm{Mbit}/\mathrm{s}$ each over a distance of $50m$.
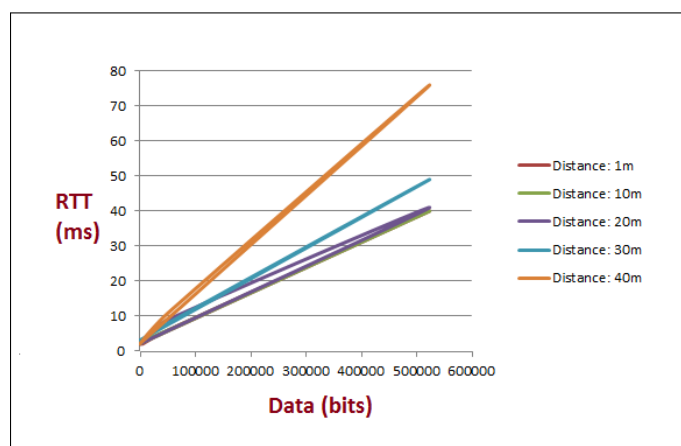
Figure 4.8: RTT variation with quantity of data at various distances.

4.1.2.4 Spatial Characteristics

The received signal power $RSSI$ and the link quality LQI with respect to the distance have been analysed in order to understand the spatial characteristics of the radio signals in underground CERN facilities. It can be observed in figure 4.9 that, the decay of $RSSI$ with distance followed the log-normal distribution as expected [63]. Log-normal fits are applied to the measured data considering the RSS values in LOS and NLOS regions.

The scatter points in the figure 4.9 correspond to the physical location points in figure 4.4. As soon as the robot entered the NLOS region (point D), the decay became more rapid with distance compared to the LOS region. As the receiver further moved into the deep NLOS region (point F to point G), the wireless network became unreliable because the $RSSI$ values reached very near to the sensitivity threshold of the receiver (-82 dBm).

A linear regression (LR) method described in [63] is used to derive the empirical path loss constants. The η value is obtained by equating the derivative of mean square error estimate J_n of the path loss constant to zero, $\frac{dJ(n)}{dn} = 0$. The formula for J_n is:

$$J(n) = \sum_{i=1}^{k}(P_{d_i} - P_{d_0} - 10\eta \log \frac{d_i}{d_0})^2.$$

(4.5)

The σ_x value is calculated by substituting the estimated η value in the following equation:

$$\sigma^2 = \frac{J(n)}{4}.$$

(4.6)

The reference distance used in calculations is $d_0 = 5$m and the received power at the reference distance is $P_{d_0} = -32$ dBm. The path loss constant η and the variance of the Gaussian distribution σ_x calculated using the experimental data from figure 4.9, are shown in Table 4.1. The obtained path loss constants for the LOS, NLOS and deep NLOS regions in the ECN3 corresponds to outdoor region, obstructed factories region and obstructed in building regions respectively in [63].

These empirical values which correspond to the environmental characteristics of the ECN3 tunnel can be useful in predicting the distance range of the wireless network in tunnel areas similar to the ECN3 area. It is assumed that the propagation characteristics of ISOLDE experimental area are similar to the ECN3 tunnel area, therefore the derived log-normal fit can be used in the analysis of the case study application.

Figure 4.10 shows the behaviour of LQI versus distance. When the robot entered the deep NLOS region (point F), the link became unstable with very poor connectivity and the LQI decreased linearly with distance d. The linear-fit equation for LQI variation with distance more

Location	Path loss exponent, η	Variance σ_x
LOS (Point A to D)	2.54	1.77
NLOS (Point D to E)	3.02	1.52
Deep NLOS (Point F to G)	4.36	2.72

Table 4.1: Empirical values of path Loss constants found in experiments.

than $38m$ is:

$$LQI = -1.57d + 160 \qquad [\%]. \tag{4.7}$$

According to [123], the Packet Reception Ratio PRR which is equivalent to LQI, should be at least 85% to consider the link as being of a good quality. Applying the threshold of 85% LQI for a good connection, the distance range for good quality wireless link in the ECN3 tunnel is 48 m from the point A.
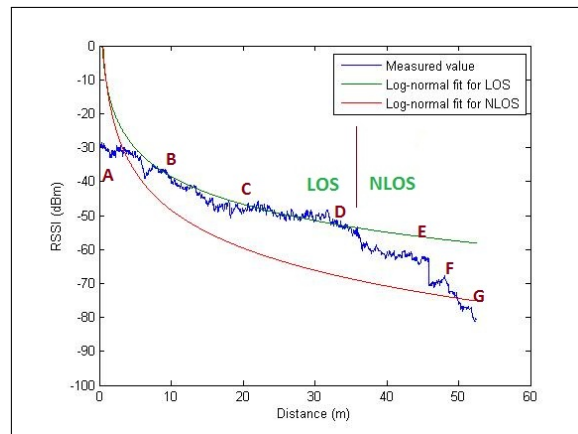
Figure 4.9: RSSI versus distance in the ECN3 tunnel.
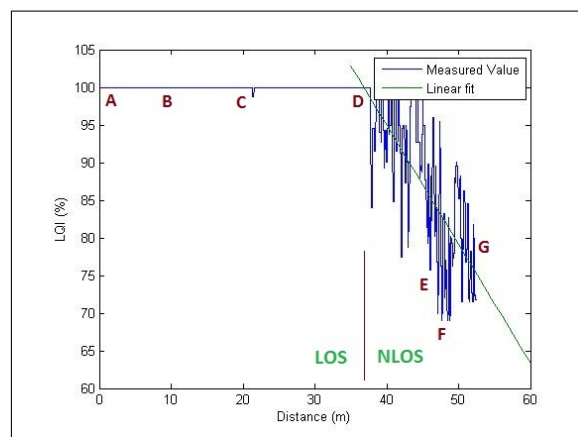
Figure 4.10: LQI versus distance in the ECN3 tunnel.

4.1.2.5 Environmental Characteristics

Radio signals suffer significant attenuation near some metallic surfaces due to reflections [23]. According to [63], the expected path loss for radio waves obstructed by a 4 m metal object is $10 - 12$ dBm. To analyse the characteristics of metallic reflections and obstructions, the robot is made to pass a meter wide metallic obstruction as shown in figure 4.11. Figure 4.12 show the observed changes in $RSSI$ caused by the reflections and obstructions due to metal objects. The end-to-end variance in $RSSI$ is 8.2 dBm which is consistent with the values in the literature [63].
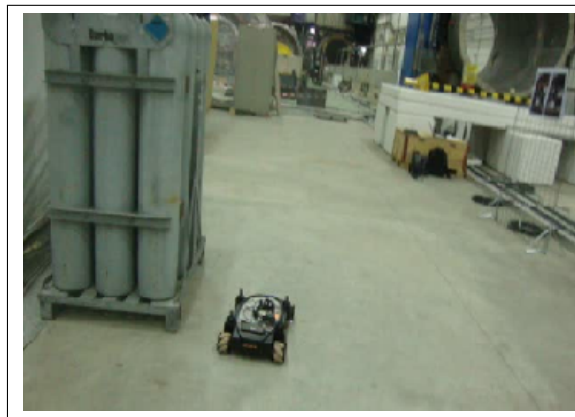
Figure 4.11: Metallic objects found in the test environment.
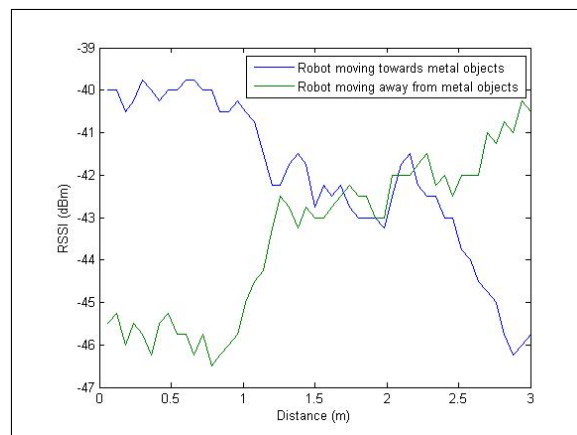
Figure 4.12: RSSI variation because of metallic objects.

Obstructions by reinforced concrete walls can also deteriorate the radio signal strength as the radio waves find it difficult to penetrate through walls and reinforced concrete materials. The expected path loss because of obstruction by a 0.6 m square reinforced concrete pillar is $12 - 14$ dBm [63]. Figure 4.13 shows an half meter thick concrete block used for the experiments. The mobile robot is driven between two concrete blocks and the changes in $RSSI$ due to the obstruction by these blocks are noted as shown in figure 4.14. The $RSSI$ variance observed is 17.2 dBm which compares to the $13 - 20$ dBm path loss due to a concrete block wall in [63].

Figure 4.13: Thick reinforced concrete block used for tests.
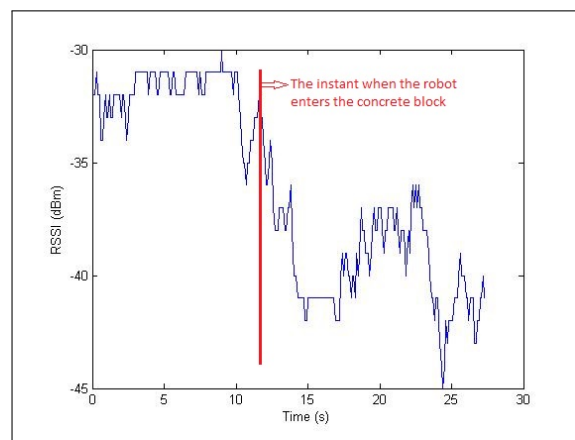
Figure 4.14: RSSI variation because of concrete block.

4.1.3 Prediction of communication range and communication qualities

In this section, the communication range achievable of the Wi-Fi system used in the experimental analysis, is predicted and using this prediction, the question of whether an available Wi-Fi system can be suitable for the case study application at ISOLDE is discussed. As defined in [124], "If the estimated received power is sufficiently large (relative to the receiver sensitivity), the link budget is said to be sufficient for sending data under ideal conditions". The amount by which the received power exceeds receiver sensitivity is called the link margin and is calculated as follows:

$$\text{Linkmargin} \quad = \quad RSS - R_S. \tag{4.8}$$

The wireless communication range and link quality can be improved by one or more of the following approaches [124]:

- Increase the "transmit power P_T" of the transmitter;

- Have enough link margin considering the path loss of the environment;

- Relocating or repositioning the antennas.

Among these possibilities, Reference [124] recommends that adequate link margin is factored into the link budget to overcome the multipath fading when designing a wireless system.

4.1.3.1 Communication range prediction

Let us assume that, for the case study application, the transmitter antenna is located at a point which ensures LOS connectivity to all the points where the receiver robot can be placed. A link margin of 18dBm is required to ensure 99% link availability (as a percentage of time) in LOS conditions [124].

For ISOLDE area, a link margin that corresponds to inevitable $RSSI$ fluctuations due to temporal variations and objects within the LOS has to be considered. This means that, for the receiver used in tests with sensitivity threshold $R_S = -82$ dBm, a strong wireless connection 99% of time with an $RSSI$ stronger than -64 dBm is maintained in LOS situations.

The variation of LQI with respect to $RSSI$ in the ECN3 tunnel is shown in figure 4.15. A linear fit for LQI with respect to $RSSI$ is applied for $RSSI$ values less than -40dBm.

$$LQI = 0.8\text{RSSI} + 140 \qquad [\%]. \qquad (4.9)$$

It is evident from figure 4.15 that, to achieve a completely stable and reliable connection where $LQI = 100\%$, the $RSSI$ should be greater than -57dBm in a 95% confidence interval. This $RSSI$ value corresponds to a distance of $35m$ in figure 4.9.

To satisfy the distance requirement of the case study application, an $RSSI$ value of -57 dBm is required at 40 m distance. In figure 4.9, at 40 m, the $RSSI$ value is -60 dBm. Therefore, the need of having an additional 3 dBm in the link budget can be solved by increasing the transmitter power from 20 dBm to 23 dBm, the legal limit of maximum transmitter power (equivalent to 200 mW) in Europe for the 2.4 GHz unlicensed frequency band. Therefore, using a more powerful transmitter or a receiver with better sensitivity threshold, according to theory, can be used to solve the problem of meeting the requirement of maximum communication distance reachable by the experimented Wi-Fi system in the ISOLDE vision system application.

4.1.3.2 Data rate and Latency prediction

For the ISOLDE application, a data rate of 5120 $^{\text{Kbit}}/_{\text{s}}$ is required to transmit two HD quality video images. This means that, within one second, 5120 Kilobits should have been transmitted.
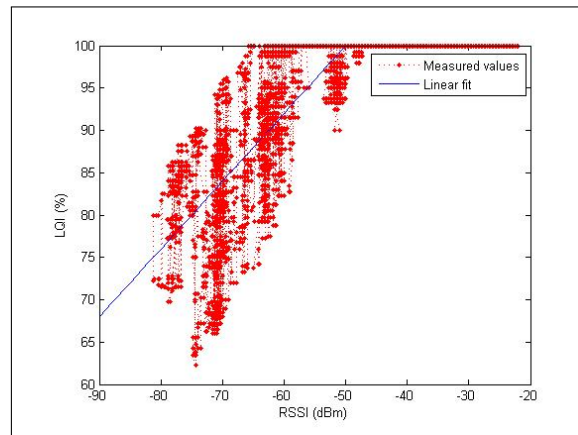
Figure 4.15: LQI variations with RSSI.

Applying the data requirement at 40 m distance in equation (4.4), RTT value is obtained as $514ms$, which can lead to two inferences.

1. $5120 Kilobits$ of data can be transmitted within one second. Therefore, this system will satisfy the data rate requirement,

2. Since the $RTT = 2 * Latency$, the system latency is $257ms$ at 5120 Kbit/s. Therefore, a latency requirement of $200ms$ is not achieved.

However, transmitting multiple packets with less amount of data in each packet, the latency requirement can be met. Assuming that data are sent at 4 Mbps, the system latency will be 200 ms which meets the latency requirements for the case study application but not the data rate requirement. Therefore, there is a trade-off between the latency and data rate requirement in a wireless application.

Table 4.2 summarises the requirement and the observed possibilities for the case study application at ISOLDE.

	Distance	**Data rate**	**Latency**
Needed	40 m	5 Mbit/s	200 ms
Achievable with present system	35 m	5 Mbit/s	257 ms
Present system + more transmit power	40 m	5 Mbit/s	257 ms
Present system + less data rate	40 m	4 Mbit/s	200 ms

Table 4.2: ISOLDE case study application: needs and calculated requirements.

4.2   On-line communication range prediction method

Mobile robots used for sensing, inspection, search & rescue or exploration tasks need wireless connectivity as its heartbeat. Two-dimensional spatio-temporal prediction of the radio signal strength (RSS) in a wireless mobile robot network is essential in communication autonomy computations, wireless positioning (localisation), and in providing communication-aware intelligence features.

In this section, a method to predict the radio signal range during a mission execution is presented. This "on-line" distance autonomy prediction is realised by predicting the RSS in locations ahead of the robots travel path. This method capacitate the mobile robot to predict the communication black spots (localised regions where a stable communication link cannot be maintained) in advance and plan its motion accordingly. Towards this objective of "on-line" RSS prediction, a state-of-the-art solution to quickly predict the future two-dimensional spatial and temporal RSS values in an unknown complex environment such as underground tunnels where the fading effects are significant, is described.

4.2.1   Preliminaries to on-line RSS prediction

Wireless communication in hostile environments (such as in scientific research facilities, indoor or industrial settings) where the effects of reflection, multipath fading and shadowing are significant, present important connectivity issues [2], [125], [126]. A commonly used model for radio signal propagation as a function of distance and time is the extended Log-Normal Shadowing Model (ELNSM) as shown in the equation (2.3). The path loss fading is a slow process (large-scale), whereas the fading due to shadowing and multipath effects are relatively medium-scale and fast processes respectively. While the path loss fading is deterministic, the shadowing and multipath fading are non-deterministic variables.

This model takes in account factors listed above but it requires the setting of many parameters including the number of walls, floors, obstacles on the way of radio waves for modelling the shadowing effects. The approach proposed in this section is to filter the RSS and predict the future RSS samples by applying a localised learning (fitting) and location-independent modelling instead of trying to achieve a global location-specific model [127]. This RSS prediction could be useful for communication-aware intelligence algorithms such as throughput threshold detection, efficient motion planning, communication autonomy estimation. The ultimate objective of this work is to predict the communication autonomy in time and distance so that the robot will not lose its connection and had to be rescued from the site of deployment.

Predicting the wireless signal strength in temporal and spatial domain has been deeply investigated in [64], [127]–[130]. Characterisation and learning of the wireless channel parameters

and their applications in motion planning for mobile robot networks are extensively studied in [131], [132]. In [128], the authors used tri-weight kernel based RSS smoothing and prediction of RSS using a linear fitting model. They have shown comparable improvement against the auto-regressive (AR) prediction model. Temporal RSS prediction has been analysed in [129] where the authors proposed Kalman filter (KF) based smoothing and prediction of future samples using a normalised cross correlation based filter. Fink, Beikirch, Voss, *et al.* [64] proposed a Gaussian processes based model to estimate the future RSS samples in unknown environment. Inspired by this probabilistic approach, a RSS prediction method that uses KF based smoothing and covariance estimation is proposed taking benefit from a Radial Basis Function kernel function for modelling the shadow fading as a first order Markov-Gaussian process [127] and an adaptive log-fit model for modelling the path loss fading.

4.2.2   Fast on-line RSS prediction using Kalman filters

The main focus in this section is to provide a solution for on-line RSS prediction that is reasonably accurate and computationally efficient. As it is well known that the Kalman Filters are fast, efficient and useful in reliable on-line estimation and prediction [127], [129], a Discrete Kalman Filter (DKF) is adopted in this work. The advantages of Gaussian process kernels are also leveraged by employing a Laplacian kernel (a Radial Basis Function (RBF) kernel) for estimating the prediction variances in spatial domain as this kernel is less sensitive to its correlation parameter which in a dynamic environment has huge variation. The objective is an on-line and adaptive solution using empirical model parameters as the environment (and its parameters) is assumed to be unknown. The only assumption is that the robot can localise itself. Since the proposed algorithm deals with empirical fitting, the proposal is departed from Gaussian process model [64] because the computing cost of the covariance matrix inverse ($[K - \sigma^2 I]^{-1}$) is expensive ($O(n^3)$) if it's updated in every iteration.

A moving average filter with a sliding window of N depending on the frequency of the wireless channel (such that the sampled distance $> 10\lambda$ [128]) is used to mitigate the multipath effects (RSS^{mp}). $N = N_{min} + \frac{\nu 10\lambda}{f_s}$ where f_s is the sampling frequency and ν the velocity of robot. The attenuation in the RSS due to path loss (RSS^{pl}) is modelled with an empirical log-fit (adaptive to the error) by minimising the linear least squares error (for fitting parameters α and β). A variogram modelling is followed as described in [127] for spatial correlation of RSS due to shadow fading (RSS^{sh}) as a Laplacian (exponential RBF) kernel function $k(x, y) = exp(-\frac{\|x-y\|}{\tau_s})$ where τ_s is the correlation distance. An empirical variogram ($\tilde{\gamma}(\lambda)$) is equated to the analytic variogram ($\gamma(\lambda)$) using eqn. (4.12) to obtain the parameters (c_m, c_v, and

τ_s), where λ is the lag distance.

$$\gamma(\lambda = c_m \left[1 - e^{\left(-\frac{\|\lambda\|}{\tau_s}\right)}\right] + c_v, \tag{4.10}$$

$$\tilde{\gamma}(\lambda) = \frac{1}{2N} \sum_{k=1}^{N} \left[R\tilde{S}S_{k+\lambda}^{sh} - R\tilde{S}S_k^{sh} \right]^2, \tag{4.11}$$

$$\gamma(\lambda) = \tilde{\gamma}(\lambda). \tag{4.12}$$

The DKF implementation is described as follows with the following system dynamics:

$$x_k = A_k x_{k-1} + B_k u_k + G\omega_{k-1}; \qquad z_k = Hx_k + \epsilon_k, \tag{4.13}$$

where x_k is the state vector, u_k is the control input vector (in this case, it's the distance from the Access point), ω is the process noise vector $\sim \mathcal{N}(0, c_\omega)$, z_k is the measurement vector, ϵ is the measurement noise vector $\sim \mathcal{N}(0, c_v)$, The matrices A, B, G and H are the respective covariance Jacobian.

$$x_k = \begin{bmatrix} RSS_k^{pl} \\ RSS_k^{sh} \end{bmatrix}, u_k = \begin{bmatrix} \log(d_k) \\ 1 \end{bmatrix}, z_k = \begin{bmatrix} RSS_k \end{bmatrix}. \tag{4.14}$$

$$A = \begin{bmatrix} 0 & 0 \\ 0 & e^{\left(-\frac{T_s}{\tau_s}\right)} \end{bmatrix}, B = \begin{bmatrix} \alpha & \beta \\ 0 & 0 \end{bmatrix}, G = \begin{bmatrix} 0 \\ 1 \end{bmatrix}, H = \begin{bmatrix} 1 & 1 \end{bmatrix}. \tag{4.15}$$

The T_s is the sampling interval. N is the number of training samples. Initialisation, time and measurement updates of the proposed DKF described in (4.13),(4.14),(4.15) are follows:

$$\hat{X}_0 = \begin{bmatrix} RSS_0 \\ 0 \end{bmatrix}, C_0 = \begin{bmatrix} 1 & 1 \\ 0 & -1 \end{bmatrix} \begin{bmatrix} c_v & 0 \\ 0 & c_m \end{bmatrix} \begin{bmatrix} 1 & 0 \\ 1 & -1 \end{bmatrix}, \tag{4.16}$$

$$\alpha = \frac{\sum_{i=1}^{N} (z_i \log d_i) - N\bar{z}\overline{\log d_i}}{\sum_{i=1}^{N} (\log d_i)^2 - N\overline{\log d_i}^2}, \qquad \beta = \bar{x} - \alpha\bar{u}, \tag{4.17}$$

$$c_v = c_v + \frac{1}{N} \sum_{i=1}^{N} (\hat{x}_i - (\alpha u_i + \beta)), \tag{4.18}$$

$$c_\omega = [1 - e^{\left(\frac{-2T_s}{\tau_s}\right)}]c_m, \tag{4.19}$$

$$x_k^- = A_k \hat{X}_{k-1} + B_k u_{k-1}, \tag{4.20}$$

$$C_k^- = A_k C_{k-1} A_k^T + Gc_\omega G^T, \tag{4.21}$$

$$K_k = C_k^- H^T (HC_k^- H^T + c_v)^{-1}, \tag{4.22}$$

$$\hat{x}_k = x_k^- + K_k[z_k - Hx_k^-], \tag{4.23}$$

$$C_k = [1 - K_k H]C_k^- [1 - K_k H]^T + K_k c_v K_k^T. \tag{4.24}$$

4.2.3   RSS filtering and prediction algorithm

The process steps in the algorithm developed for the prediction of RSS while the mobile robot is performing some movement is provided in the algorithm 2.

Algorithm 2 On-line RSS prediction algorithm for mobile robots in unknown environments.

1: Measure RSS M times (at the same location $x = (x_1, x_2) \in \mathbb{R}^2$ with distance $d = \sqrt{x_1^2 + x_2^2}$)
2: Apply temporal moving average filter. $RSS = \sum_{i=1}^{M} RSS_i$
3: Obtain the previous N filtered RSS samples. RSS_i where i=1..N
4: Initialise the parameters as in equations (4.14) and (4.15).
5: Fit the RSS values for path loss using the linear fitting. $RSS^{pl} = \alpha \log(d) + \beta$
6: Measure parameters α and β
7: Remove the RSS^{pl} from the measured RSS values for further processing. $RSS^{sh} = RSS - RSS^{pl}$
8: Compute the experimental variogram parameters $\tau_s, C_m c_v$ by fitting the equation (4.12)
9: Update the parameter $c_w = (1 - \exp(\frac{-\|2*Ts\|}{\tau_s}))c_m$;
10: Update the mode as in equation (4.13)
11: Perform time and measurement updates as in equations (4.24)
12: p-step ahead prediction: $RSS^{pl}_{k+p} = \hat{X}_{k+p}$; $RSS^{sh}_{k+p} = c_m(1 - \exp(\frac{-\|k\|}{\tau_s})) + c_v$

The algorithm provides a functional flow of the algorithm implemented using the Matlab software and proceeds as follows: Measure the RSS samples ; perform temporal and spatial filtering; determine RSS model and variogram parameters; perform time and measurement updates of the DKF using the updated model parameters; and predict the future RSS samples for a given location.

4.2.4   Experimental evaluation of the on-line RSS prediction algorithm

The algorithm is implemented off-board the youBot mobile robot and is tested with RSS samples measured with a youBot mobile robot in an underground scientific facility (having huge magnets and metal objects) and inside a building (that exhibits an industrial setting characteristics) under both LOS and NLOS. For these initial experiments, the filtering and prediction algorithm is not embedded in the robot but done off-line. The results are presented in figure 4.16.

A Normalised Mean Square Error (NMSE) of RSS prediction at 22.2 m ahead (437 samples) as 0.89 E-4 is obtained. The resulted NMSE is significantly better than the results in [128]. The Mean Absolute Error (MAS) for 20 m ahead prediction is 4.1 dBm and for less than 20m-ahead prediction is less than 2 dBm which is up to twice better than the previous studies [128], [129]. The whole algorithm took less than 0.05 s per iteration ($N = 50$) in an Intel i7 2.9 GHz CPU with 4GB RAM. The RSS is sampled at 10 Hz. This shows that the algorithm can perform filtering and prediction before the next RSS is sampled.
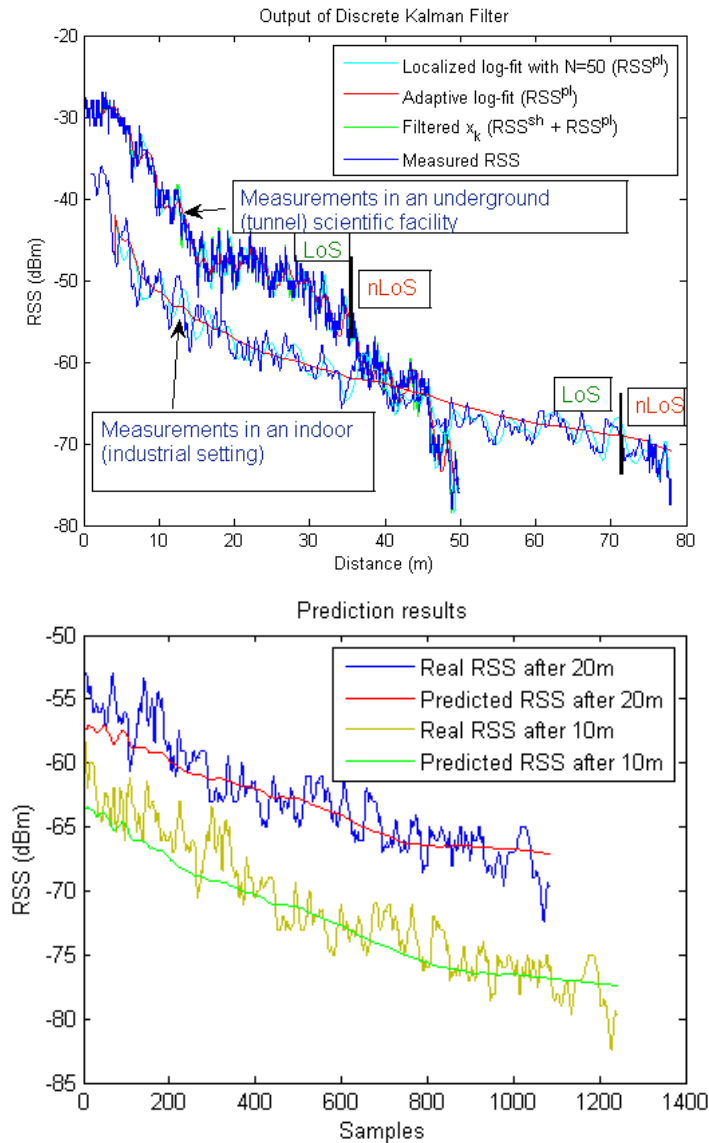
Figure 4.16: Results of the RSS filtering and prediction algorithm using DKF.

In figure 4.17, the shadowing part of the RSS RSS^{sh} is presented as a variance bound over the mean path loss RSS value RSS^{pl}. The figure shows four plots: the black line is the measured value at 5m ahead, the green line is the filtered value with DKF, the red line is the predicted RSS mean value RSS^{pl}, the green shaded region is the predicted shadowing variance RSS^{sh} applied over the predicted mean. It can be clearly observed that the actual measured values lies mostly within the predicted mean and variance region, except in case of the transition from LOS to NLOS around sample number 80. This is because of the change in the RSS pattern as the environment evolves or changes, so it is acceptable and inevitable in a RSS prediction scheme. It is interesting to note that the error in prediction lies within $\pm 5\,\mathrm{dBm}$, which is fairly reasonable given the state-of-the-art methods such as in [64] show the prediction error of more than $\pm 20\,\mathrm{dBm}$.

Once the RSS is predicted at a given location ahead of the robot's path, the distance autonomy can effortlessly be estimated by applying a RSS threshold over which the link quality is sufficient for maintaining the communication quality.
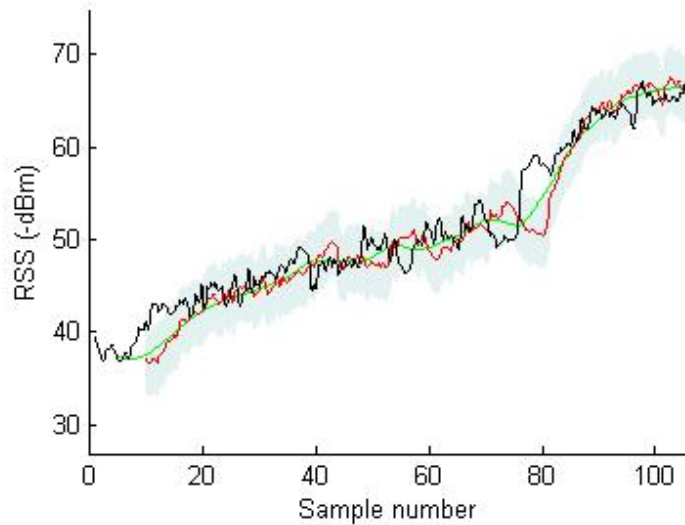
Figure 4.17: Results for 5m-ahead RSS prediction. Black line is the measured value at 5m-ahead. Green line is the filtered value with DKF. Red line is the predicted RSS mean value RSS^{pl}. Shaded region is the predicted shadowing variance RSS^{sh} applied over the predicted mean.

4.3   Summary

In this chapter, two RSS prediction schemes were presented that dealt with off-line and on-line communication range prediction abilities. Both the proposed methods were demonstrated using experimental analysis and the results were discussed following an explanation of the developed algorithms.

In the first section, the off-line prediction method was presented which used the radio signal parameters such as the radio signal strength indicator (RSSI), link quality indicator (LQI), and the latency in data transmission. The off-line prediction method exploited the temporal, spatial and environmental characteristics of the radio signal propagation especially in scientific and tunnel facilities. The outcome of the experiment to verify an available Wi-Fi system to suit the ISOLDE case study application requirements was that the data rate requirement could be met however, the distance requirement could be met only under LOS conditions, whereas the latency requirement could be met only for low-quality video transmissions. An interesting finding was that there should be a trade-off between the latency and data rate requirements, otherwise, powerful wireless transmitters and receivers (with better receive sensitivity and transmit power but within the legal limits) will be needed.

In the second section, a fast on-line RSS prediction method was presented. The on-line RSS prediction scheme used the extended log-normal shadowing radio signal propagation model (defined in section 2.2) for modelling the path loss in the RSS, an exponential kernel for modelling the shadowing fading part of the RSS, and a discrete Kalman filter (DKF) that integrated both the path loss and shadowing models while simultaneously using their covariances for modelling the multipath fading effects. The method took advantage of the DKF and RBF kernel function for modelling Gaussian process. A mean prediction accuracy of more than 90% in predicting the RSS up to 20m in advance was achieved and the results outperformed the state-of-the-art methods. The main limitation of the proposed method was that it can predict the RSS only in the direction of travel. However, the future plan will be to overcome this limitation and implement a two-dimensional RSS prediction mechanism with multi-sensor RSS sampling techniques.

Chapter 5

Communication quality optimisation methods using spatial sampling

Improving the radio signal strength (RSS) at the mobile robot will optimise wireless communication quality and the network throughput (and goodput). This chapter will present the use of spatial sampling methods to receive the best RSS by exploiting the mobility of the robot. Firstly, the proposed method to optimise the RSS at the receiver will be presented together with related works, experimental evaluation, and the results of the conducted experiments. Having experimentally verified the spatial sampling methods for RSS improvement in the first section, the second section will describe a case study application of the RSS spatial sampling methods in superior haptic teleoperation features where the operator can navigate a mobile robot in low-wireless signal environment using the RSS haptic feedback.

5.1   Robot position optimisation using RSS spatial sampling

Having reliable wireless communication in a network of mobile robots is an ongoing challenge, especially when the mobile robots are given tasks in hostile or harmful environments such as radiation environments in scientific facilities, tunnels with large metallic components and complicated geometries as found at CERN. In this section, a decentralised method for improving the received signal strength and wireless network throughput by optimising the mobile robot position using implicit spatial diversity concepts and spatial gradient search algorithms is presented. The effectiveness of the proposed algorithms is experimentally demonstrated with a KUKA youBot omnidirectional mobile robot. The performance of the algorithms is compared under various scenarios in an underground scientific facility at CERN.

CERN has around 50 km of underground scientific facilities, where mobile robots could help in the operation of the particle accelerator facilities, e.g. in conducting remote inspections and radiation surveys in different areas [16], [18], [35], [133]. The main challenges to be recalled here are not only that the robot should be able to go over long distances (longer than 200 m [18]) and operate for relatively long periods, but also the underground tunnel environment, the possible presence of electromagnetic fields, ionising radiations, the fact that the robots shall in no way disrupt the operation of the accelerators, and should be able to avoid wireless communication failures, radio interferences, multipath and deep fading effects [134].

Using umbilical cables rather than wireless system in such applications has some drawbacks and the reasons why wireless communication is preferred over wired communication has already been discussed in section 4.1.1. Wireless communication in underground mine tunnels had been investigated in [2], [23] and the authors highlight the necessity of placing mobile robot nodes as the wireless network did not perform well under non-line-of-sight (NLOS) condition.

The wireless system should be able to tolerate interferences and multipath effects [134]. Given the dynamic changes in the wireless signal behaviour arising from movement of objects and changes in the environment, optimising the mobile robot's position will optimise the wireless network performance of the mobile robot while performing the assigned tasks such as search, inspection or survey.

In hostile environment where the robot is going to be deployed, it has to be taken into account that several components of the wireless devices may fail or get damaged. This can for instance happen due to radiation effects as discussed in the section 1.2. Hence, there is also a need for redundancy features in the communication devices in order to avoid communication failures and enable recovery in the event of failure.

Referring back to equation (4.1), the wireless network capacity has a strong correlation with the received radio signal strength. The higher the received RSS, the higher is the wireless network capacity (and eventually the goodput): an improvement of $1\,\mathrm{dBm}$ in RSS will trigger an improvement of approximately $1\,\mathrm{Mb/s}$ in the network capacity when the RSS is above -86 dBm [135].

Hence, in an attempt to improve the radio signal strength, a decentralised method is proposed for wireless mobile robot positioning using a gradient search algorithm to optimise communication link qualities at the mobile robot using the concept of spatial diversity (receiving radio signals with multiple receivers at different positions). This method also integrates redundancy features as will be discussed later. The main objective behind this work is thus to navigate the mobile robot to a position where the received signal strength is a local maximum or at least above the minimum threshold.

The main contributions in this section are the following:

1. A methodology for using simultaneous spatial and temporal measurements is proposed to find the best RSS thereby enhancing the capacity and redundancy in the wireless network;

2. Experimental results of the proposed variants are provided with performance metrics such as improvement in signal strength, time taken, distance travelled by the robot;

3. The objective of this research is also to investigate the time-independent methods for RSS measurements (RSS sampled at the same time) compared to time-dependent methods (RSS sampled at different times) used for localisation or motion planning.

The work described in this section is a step towards adding autonomy (or intelligence) for mobile robots that can optimise their position in order to achieve optimised wireless communication performance. The research work made in this chapter will act as the base for relay robots in the next chapter (Chapter 6).

5.1.1 Related works

Spatial sampling methods and robot mobility have been used to improve and optimise wireless communication qualities by previous researches [136]–[140]. In [136], the authors suggest motion planning techniques in a group of mobile robots to increase the robustness in wireless networking. They propose a global search based method adopting a stochastic model for mobility planning for a group of robots. In [137], a team of mobile robots including ground and aerial robots used wireless tethering concepts for collectively achieving a task of exploring the environment. The authors follow a decentralised approach and present an antenna diversity method

for positioning the mobile robot using a gradient search technique, i.e., multiple antennas are connected to a receiver and are used to sample the RSS at all the antennas to obtain the direction of the highest RSS [141].

Gradient-based methods have proved a promising method for improving wireless connectivity of mobile nodes [38], [138], [141], [142]. Radio source seeking techniques are studied using RSS gradient [138] and angle of arrival methods [140]. The use of directional antennas and pattern based search algorithms is presented in [139] for improving the RSS. However, these methods are time-dependent and could suffer from temporal fluctuations in the RSS. At the time of working on this research, none of the previous research in RSS-based mobile robot position optimisation utilised multiple receivers and time-independent methods for optimising wireless communication qualities.

In this work, the concepts used in [141] and [139] are leveraged. The main difference is that instead of using multiple antennas connected to the same receiver, multiple receivers are used as shown in figure 5.1. In this way, the need to switch between different antennas connected to a same receiver can be avoided. The proposed approach is to use the RSS gradient information to position the mobile robot to obtain a relatively better RSS (local maxima), thereby increasing the communication range and coverage area.

A key advantage with the proposed method is that it does not require prior knowledge of the environment which is essential in hostile unknown or unstructured environments. The novelty in the proposed solution is indicated below.

- The proposed algorithms are fully 2D, in contrast to the greedy algorithms used in [139], [141] which approximate the 2D physical reality by doing sequential 1D computations that combine to 2D. By doing so, there are more opportunities to experiment with, for instance, different finite difference stencils, and can demonstrate that the time dependence of the Wi-Fi field cannot always be neglected.

- Multiple receivers distributed spatially are installed on the mobile robot instead of multiple antennas for measuring the RSS and estimating the RSS gradient at the centre of the robot.

- Because low-cost transceivers with high receive sensitivity are used, there exists an advantage of redundancy and fault-tolerance. When the connectivity is lost with one receiver either due to fault in the device or due to environmental influence, other receivers can replace the failed receiver. Furthermore, the history of the RSS at all the receivers can help in navigating the robot towards the region where the connection is available in order to recover the robot from communication failure situations. This redundancy feature could be very useful in a rescue scenario and is also not explored in the literature of mobile robots.

5.1.2 Proposed RSS spatial sampling methods

A method on improving the received RSS with the help of spatial diversity without explicitly implementing antenna diversity (using multiple receivers instead of multiple antennas) is attempted in this work. A key aspect of the proposed method is that the robot position is unknown and the mobility of the robot is exploited.

As described in the section 2.2, the RSS varies randomly because the signal propagates through a multipath fading channel (radio signals from the transmitter arriving at the receiver through multiple paths and the signal strength fades with distance travelled). In particular, all walls, ceilings, and other objects that affect the propagation of radio waves will directly influence the signal strength and the directions from which radio signals are received. The path loss in the received signal strength can be modelled with a log-normal distribution [63] as shown in the equation (2.3).

It's already mentioned in section 2.3 that the best channel is already chosen based on the traffic conditions, to avoid adjacent and co-channel interference and hence the channel optimisation is assumed to be already attained in this work.

5.1.2.1 Algorithm

To enable the mobile robot move to an optimal position for receiving better RSS, a gradient ascent algorithm is used. Gradient ascent, or the method of steepest ascent, is an iterative optimisation algorithm, with steps proportional to the gradient of the optimisation function at the current point [143].

With the robot moving on a two-dimensional surface $S \in \mathbb{R}^2$ and the current position of the mobile robot as (x^i, y^i), the RSS values at each receiver k as R_k^i where $k = 1, 2...N$, and
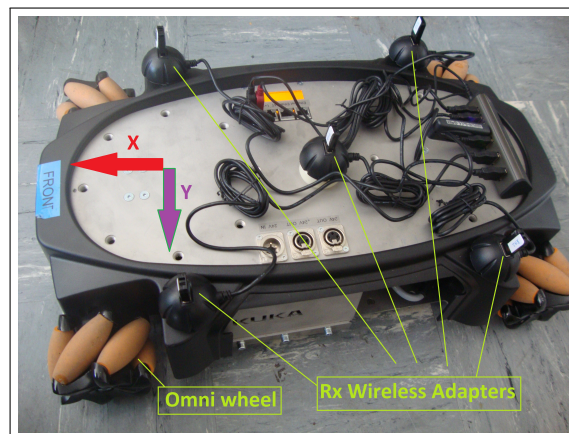
Figure 5.1: youBot mobile robot with spatially distributed multiple wireless receivers on-board.

$N \leq 5$ as the number of receivers used (based on the arrangements of sensors), the algorithm can be expressed as follows:

Algorithm 3 Wireless signal gradient ascent algorithm.

1: Measure the RSS at central receiver $R^i_{meas} = R^i_1$
2: **while** $(R^i_{meas} < R^i_{threshold})$ **do**
3:     Compute the gradient in ∇R^i as $\vec{\nabla} R^i = (\nabla R^i_x, \nabla R^i_y)$
4:     $x^{i+1} = x^i + \alpha_x \cdot \nabla R^i_x$
5:     $y^{i+1} = y^i + \alpha_y \cdot \nabla R^i_y$
6:     Move the robot to position (x^{i+1}, y^{i+1})
7: **end while**

The α_x and α_y are pre-defined step size parameters that depend on the spacing of sensors in x and y dimensions ($\alpha_x \propto \Delta_x$, $\alpha_y \propto \Delta_y$). In this proposed algorithm, the aim is not to reach the global optimum but the local optimum, because within a reasonable range around the robot's local optimum, the wireless communication quality is sufficient. The stop criterion is defined as a threshold RSS level, depending on the experimental setup (see section 5.1.3).

Since a local gradient-estimation-based optimisation algorithm is used, circular symmetry issues (uniform radiation around the source) with gradient search algorithms is avoided as the radio signals normally suffers from huge multipath effects in hostile environments because of thick concrete walls in the tunnel and large metallic objects.

5.1.2.2   Approach

The concept of spatial diversity by using multiple receivers at the robot is used for sampling the RSS. Diversity helps in dealing with the multipath fading effects. In antenna diversity [141] and beam steering/forming techniques [140], multiple antennas are used with one signal receiver to trap the radio signals in one or several antennas at a time forming a beam pattern. However, the difference in the proposed method compared to antenna diversity techniques is that multiple receivers each connected to single antenna are used instead of multiple connected to a single receiver to form spatial diversity, therefore minimising signal processing loads at the physical or the data link layers in the network stack of OSI reference model.

Two variants of architectures to implement the proposed algorithm 3 are experimented. The first variant is to use multiple transceivers on the robot and measure the RSS values at different positions at the same time. In the second variant, only one receiver is used and the robot moves locally in a pre-determined structure to measure the RSS values at different positions. While the first variant is termed as time-independent as the RSS is sampled across all the receivers simultaneously, the second variant is termed as "time-dependent" as the RSS is sampled at different time instants.

5.1.3 Experimental setup
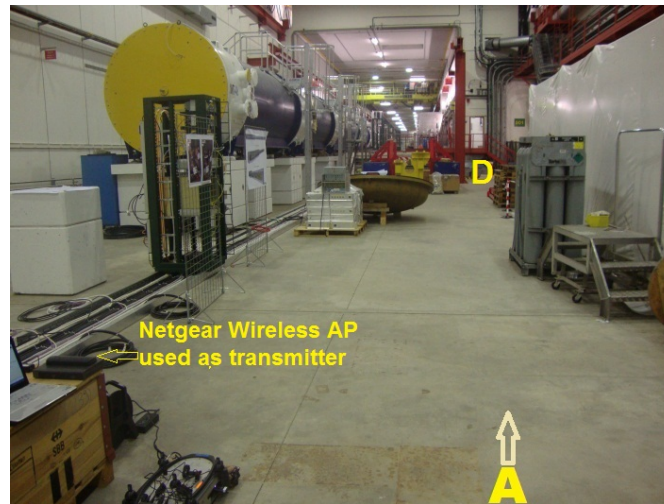
Figure 5.2: View of the ECN3 tunnel showing the radio transmitter (Netgear wireless AP) location and the landmark points (A,D) on the path taken by the mobile robot during the experiments.

(a) ECN3 layout and measured RSS values.

(b) $RSSI$ with distance along the robot path.
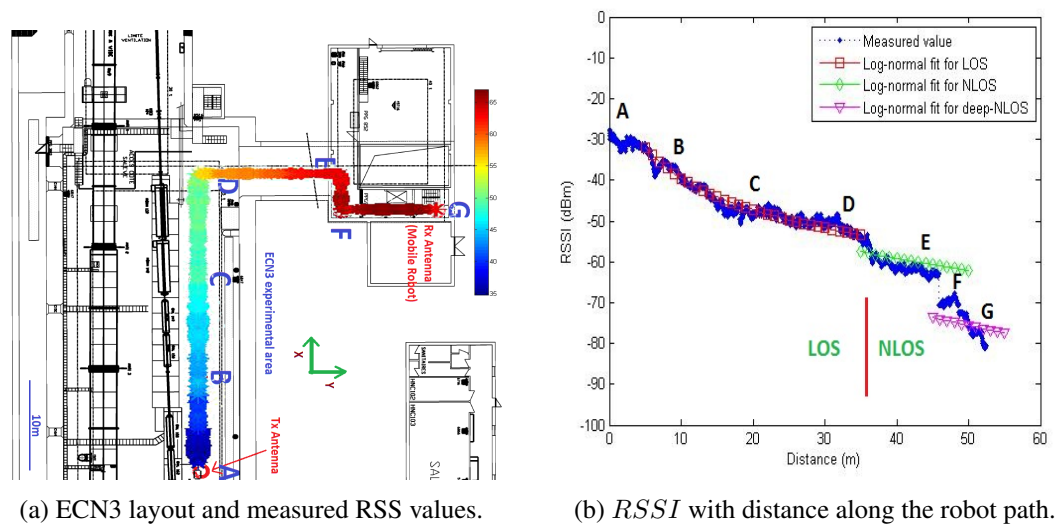
Figure 5.3: RSS measurements in ECN3 tunnel facility at CERN.

For executing the experiments, the KUKA youBot [58] is used as the mobile robot. Since the youBot has omnidirectional wheels (which permit any combination of longitudinal, transversal and rotational movement of the robot), navigation is efficient given the space restrictions in the underground scientific facility. The control equations for the youBot located in inertial frame of reference pose (X, Y, Θ), are given as follows:

$$\begin{bmatrix} X_t \\ Y_t \\ \Theta_t \end{bmatrix} = \begin{bmatrix} X_{t-1} \\ Y_{t-1} \\ \Theta_{t-1} \end{bmatrix} + \begin{bmatrix} \pm\vartheta_X & 0 & 0 \\ 0 & \pm\vartheta_Y & 0 \\ 0 & 0 & \pm\omega \end{bmatrix} \begin{bmatrix} \tau_\vartheta \\ \tau_\vartheta \\ \tau_\omega \end{bmatrix}, \tag{5.1}$$

where ϑ_x, ϑ_y, and ω are the longitudinal, transversal and rotational velocities respectively. τ_ϑ and τ_ω are time constants which determine the displacements $\delta x, \delta y$, and $\delta \theta$ in X, Y, and Θ directions.

$$\tau_\vartheta = \frac{\sqrt{(\delta X)^2 + (\delta Y)^2}}{\vartheta} \text{ and } \tau_\omega = \frac{\delta \Theta}{\omega}. \tag{5.2}$$

The value of $\vartheta_X = \vartheta_Y = \vartheta$ is fixed at $0.1\,\mathrm{m/s}$ and the rotational DoF Θ is not used as the youBot can be controlled independently in each DoF (holonomic platform).

A static wireless transmitter (ProSafe Dual Band Wireless-N Access Point WNDAP350 [121]), only used for control data (not involved in the algorithm) and five compact Wi-Fi receiver stations (Zyxel NWD2105 [122]) are used in the experiments. The transmitter [121] uses the IEEE 802.11n $2.4\,\mathrm{GHz}$ standard with a maximum transmit power $P_T = 20\mathrm{dBm}$, and a maximum data rate of $144.44\,\mathrm{Mb/s}$. The receiver [122] has a receive sensitivity threshold R_S of $64\,\mathrm{dBm}$ at $64\,\mathrm{Mb/s}$ and $-82\mathrm{dBm}$ at $11\,\mathrm{Mb/s}$. The transmitter is fixed at a position $(X, Y) = (0, 0)$ and the receiver stations are mounted at different positions on the youBot as shown in Figure 5.1.

The experiments are conducted in a tunnel facility known as ECN3 at CERN, shown in Figures 5.2 and 5.3a. Each receiver is set to channel 3 in the $2.4\,\mathrm{GHz}$ spectrum and all the receivers have same characteristics. The RSS values are obtained with the received signal strength indicator ($RSSI$) using the `iwlist scan` command or the `iwconfig` command in Linux which is computationally less expensive than `iwlist`. The Zyxel NWD2105 receiver uses the RALink 2850 wireless driver and the $RSSI$ measurement is equal to the received signal power in dBm, $RSSI = RSS = R$. Each $RSSI$ sample is measured at a $100\,\mathrm{Hz}$ sampling rate for $1\,\mathrm{s}$, and then averaged to diminish the statistical temporal fluctuations:

$$\overline{RSSI} = \frac{1}{100} \cdot \sum_{i=1}^{100} RSSI_i. \tag{5.3}$$

A preliminary experiment to understand the variation in $RSSI$ in an underground tunnel facility is conducted in [18] (Refer section 4.1.2). In this experiments, the mobile robot (youBot) is driven along a path defined by points A to G, as shown in figure 5.3a, selected to accommodate LOS and NLOS conditions. Figure 5.3a shows the path taken by the robot and measured RSS values along the robot path. The colour of the RSS values indicated the mean RSS value (μ) among the five receivers and the width indicates the standard deviation (σ). It can be observed evidently from this figure that the variation (σ) of RSS among the receivers decreases when the robot is moving away from transmitter. The log-normal fits can be obtained for n and σ_x from the equation (2.3) under LOS and NLOS conditions in the ECN3 tunnel (figure 5.3b). It can also be observed that the $RSSI$ values decay faster in NLOS than in LOS condition.

Note on power consumption: The Zyxel NWD2105 receivers each consume around 1.5 W at peak transmit power. Therefore, when using 5 receivers, the total communication power is around 7.5 W, compared to 100 W for computing and motion power in the youBot. It should also be noted that, not all the receivers need to be active at the same time and the receivers in idle state normally consume less than half of the peak transmit power.

Note on cost of receivers: The cost of each wireless receivers is around €10 and hence are less expensive than a customised hardware design using directional antennas on a single receiver.

5.1.3.1 Algorithmical setup

The proposed algorithm (Algorithm 3) has been implemented using the following two different approaches.

1. Static stencils (time-independent sampling): using up to five receivers on the youBot at the same instant for computing 2D RSS gradients.

2. Dynamic stencils (time-dependent sampling): using only the central receiver, the youBot is made to move dynamically to create a stencil pattern.
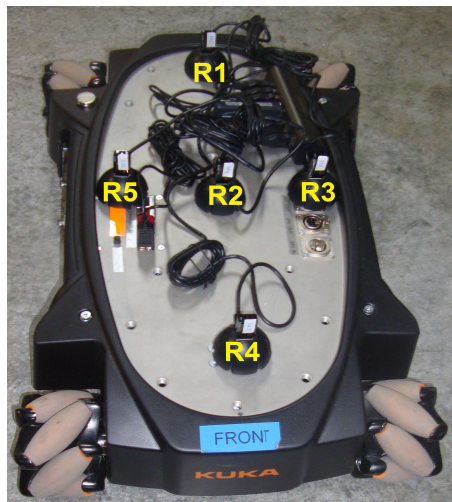
(a) Diamond configuration.

(b) Rectangular configuration.

Figure 5.4: Spatial arrangement (configuration) of wireless receivers on youBot.

The dynamic stencil approach has the disadvantage that the temporal changes in the sampled RSS values need to be negligible, while the static stencil method necessitates more wireless receivers and is thus more prone to configuration errors. Different first order numerical stencils are used for the 2D gradient computation. A brief mathematical basis of gradient estimation formulas and the corresponding arrangement of sensor nodes is presented in table 5.1.
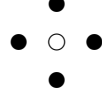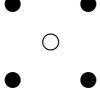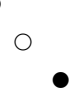
Hardware configuration	Description	Formula	Stencil	Representation
Diamond configuration	Classical 2D five-point stencil, first-order central differences [5$_p$CL]	$\begin{bmatrix} \dfrac{R^i_{j+1,k} - R^i_{j-1,k}}{2\Delta_x} \\[2ex] \dfrac{R^i_{j,k+1} - R^i_{j,k-1}}{2\Delta_y} \end{bmatrix}$	● ● ○ ● ●	5$_p$CL
Rectangular configuration	Averaged 2D five-point stencil, first-order central differences [5$_p$C-Static, 5$_p$D-Dynamic]	$\begin{bmatrix} \dfrac{1}{2}\left(\dfrac{R^i_{j+1,k-1} - R^i_{j-1,k-1}}{2\Delta_x} + \dfrac{R^i_{j+1,k+1} - R^i_{j-1,k+1}}{2\Delta_x} \right) \\[3ex] \dfrac{1}{2}\left(\dfrac{R^i_{j-1,k+1} - R^i_{j-1,k-1}}{2\Delta_y} + \dfrac{R^i_{j+1,k+1} - R^i_{j-1,k+1}}{2\Delta_y} \right) \end{bmatrix}$	● ○ ● ● ●	5$_p$C, 5$_p$D
Diamond configuration	2D three-point stencil, first-order backward differences [3$_p$BD]	$\begin{bmatrix} \dfrac{R^i_{j,k} - R^i_{j-1,k}}{\Delta_x} \\[2ex] \dfrac{R^i_{j,k} - R^i_{j,k-1}}{\Delta_y} \end{bmatrix}$	○ ● ●	3$_p$BD
Diamond configuration	2D three-point stencil, first-order forward differences [3$_p$FD]	$\begin{bmatrix} \dfrac{R^i_{j+1,k} - R^i_{j,k}}{\Delta_x} \\[2ex] \dfrac{R^i_{j,k+1} - R^i_{j,k}}{\Delta_y} \end{bmatrix}$	● ● ○	3$_p$FD
Rectangular configuration	1D two-point stencil, first-order differences [2$_p$]	$\begin{bmatrix} \dfrac{R^i_{j+1,k+1} - R^i_{j-1,k-1}}{2\Delta_x} \\[2ex] \dfrac{R^i_{j+1,k+1} - R^i_{j-1,k-1}}{2\Delta_y} \end{bmatrix}$	● ○ ●	2$_p$

Table 5.1: Gradient estimation formulas and corresponding configuration of receivers.

The two different hardware arrangement of wireless receivers (diamond and rectangular configurations) are shown in figure 5.4. Using these two configurations, five different stencils (arrangements) could be formed as indicated in the table 5.1. All the receivers are placed in the same orientation so that the antenna orientation effects are negligible.

It is mentioned in [144] that, there should be a minimum spacing of $0.38\lambda_c$ (where, λ_c is the wavelength of the wireless signal) between two RSS spatial samples to obtain independent uncorrelated measurements. Therefore the receivers are spaced at least 10cm (which is $0.8\lambda_c$ at 2.4 GHz), $\Delta_x \geq 10\,\text{cm}$ and $\Delta_y \geq 10\,\text{cm}$, to obtain independent uncorrelated spatial samples so that the interference between various receivers are negligible. It also means that the effects of channel noise and inter-receiver interferences are negligible between each RSS spatial sample as each sample is measured at more than $\frac{\lambda_c}{2}$ spacing.

For the Diamond configuration (Fig. 5.4a), $\Delta_x = 10\,\text{cm}$ and $\Delta_y = 20\,\text{cm}$, and for the Rectangular configuration (Fig.5.4b), $\Delta_x = 16\,\text{cm}$ and $\Delta_y = 20\,\text{cm}$.

5.1.4   Results and discussion

All the five different configurations mentioned in table 5.1 (5_pCL, 5_pC, 3_pBD, 3_pFD and 2_p) for the static stencils approach and an averaged 2D first order central difference configuration (5_pD) for the dynamic stencil approach are considered in the experimental evaluation. Ten trials are performed for each algorithm with the mobile robot being at various distances from the transmitter under both LOS and NLOS conditions.

The results of all six experimental configurations are presented in Figure 5.5. It can readily be observed that the central difference method using 5 receivers (5_pC) performed better than other methods in terms of performance in the time taken to reach the optimised position and improvement in the RSS values. One of the possible explanations for this observation is the fact that there is an inherent averaging of the spatial $RSSI$ measurements in the 5_pC algorithm. The $RSSI$ gain (G) is defined as the improvement in $RSSI$ value at the new position compared to the $RSSI$ value at the previous position as follows:

$$G = RSSI_{(X^{i+1}, Y^{i+1})} - RSSI_{(X^i, Y^i)}. \tag{5.4}$$

And the unit $RSSI$ gain (G = 1 dBm) is expressed as the improvement of 1 dBm in $RSSI$. The results are normalised in terms of unit $RSSI$ gain so that the spatial and temporal performances of various algorithms can be fairly compared. The spatial performance of the algorithm is measured as a quantity of distance (D) the robot moves to achieve unit $RSSI$ gain and the temporal performance of the algorithm is measured as the time taken (τ) by the algorithm moving the
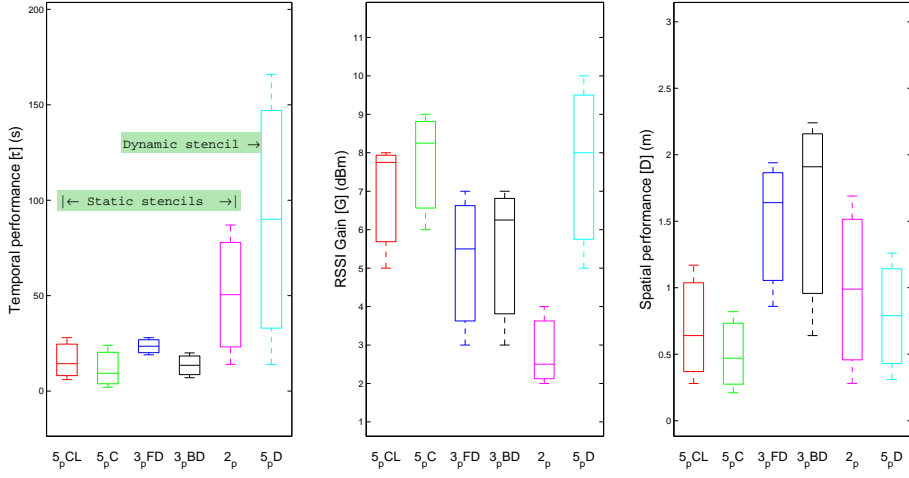
Figure 5.5: Performance results of various algorithms.

robot to achieve unit $RSSI$ gain:

$$D_{1\,\text{dBm}} = \sum_1^S \frac{D}{G}, \ \tau_{1\,\text{dBm}} = \sum_1^S \frac{\tau}{G}, \tag{5.5}$$

$$D_{1\,\text{dBm}} = \frac{\sum_1^S D}{\sum_1^S G}, \ \tau_{1\,\text{dBm}} = \frac{\sum_1^S \tau}{\sum_1^S G}, \tag{5.6}$$

where S is the number of iterations. Table 5.2 summarises the time taken by the algorithm and the rectilinear (Manhattan) distance moved by the robot from its current position to achieve unit $RSSI$ gain. Comparing the central difference method in static (5_pC) and dynamic (5_pD)

	5_pCL	5_pC	3_pBD	3_pFD	2_p	5_pD
Mean $RSSI$ gain $\bar{G}$ (dBm)	7.75	8.25	5.5	6.25	2.5	8
Spatial performance $D_{1\,\text{dBm}}$ (m)	0.21	0.18	0.92	0.89	0.39	0.79
Temporal performance $\tau_{1\,\text{dBm}}$ (s)	4.77	3.73	20.25	25.5	20.2	90

Table 5.2: Comparison of temporal and spatial performance of various gradient algorithms.

mode, the former has better performance which demonstrates that the time dependence of signal strength measurements degrades the performance of the gradient search algorithm. This then also suggests that the static stencil approach is better than previous time-dependent approaches [137], [138].

One of the advantages obtained with static stencil (using multiple receivers at the same time) is the selection diversity gain in $RSSI$. That is, the strongest signal could be selected among the multiple receivers. When there are N receivers (which receive independent and Rayleigh distributed radio signals), the expected diversity gain in $RSSI$ expressed as a power ratio [145]

has been shown to be:

$$G_{Selection\,Diversity} = \sum_{k=1}^{N} \frac{1}{k}. \tag{5.7}$$

Since five independent receivers are used for each gradient estimate, a RSSI gain of at least 2.28 dBm should be expected according to the equation 5.7 and a minimum gain of 5.5 dBm is observed in the experimental trials (for 5_pC, 5_pCL and 5_pD algorithms).

According to [144], the probability of obtaining a gain of G (compared to the local average) in $RSSI$ is:

$$\text{Prob(G)} = 1 - \left|1 - e^{-10^{(G/10)}}\right|^5. \tag{5.8}$$

This means that, when the average RSS is -70 dBm (in the NLOS region, shown in figure 5.3b), a gain of at least 5 dBm at 80% probability can be achieved with 5 independent samples (using 5 receivers), which is in fact proven in the experimental results. Therefore, a first conclusion is that it is indeed possible to improve the wireless communication performance even in the NLOS region.

The results show that the central difference methods (5_pC and 5_pCL) can be used for computing gradients in RSS using the spatial diversity concept which could then be used to move the robot to the local strongest signal location to improve the communication performance. The algorithms using 5 receivers demonstrated better performance than the algorithms using 3 or 2 receivers which shows the importance of having multiple receivers on-board the robot for achieving better performance compared to single receiver. Also, it is found that the static stencil 5_pC (time-independent sampling) methods work better than dynamic stencil 5_pD (time-dependent sampling) methods in terms of time and energy performances. This proves the time dependency of RSS measurements even though the spatial samples are uncorrelated.

Another advantage of using multiple receivers on-board the robot is that it reduces the chances of failure in wireless communication or local interference (signal blocking due to deep fading) to one of the receivers without blocking the reception on the entire system. Hence there is an inherent advantage of redundancy and fault-tolerant mechanisms in the proposed approach. In addition to device redundancy, there is also a possibility of algorithmic redundancy. For instance, the diamond configuration arrangement with 5 receivers can also be used for 3_pFD and 3_pBD in addition to 5_pCL algorithm. On top of the advantages mentioned earlier, the algorithms are acting in the application layer (and not in the physical layer) and hence this gives flexibility in designing improved wireless communication system without complex design changes in the hardware.

5.2   Application of the spatial sampling methods to haptic teleoperation

Wireless teleoperation of mobile robots for maintenance, inspection and rescue missions is often performed in environments with low-wireless connectivity, caused by signal losses from the environment and distance from the wireless transmitters. Various studies from the literature have addressed these problems with time-delay robust control systems and multi-hop wireless networks. However, such approaches do not solve the issue of how to present wireless data to the operator in order to avoid losing control of the robot. Despite the fact that teleoperation for maintenance often already involves haptic devices, no studies look at the possibility of using this existing feedback to aid operators in navigating within areas of variable wireless connectivity. Therefore, a method is proposed to incorporate haptic information into the velocity control of an omnidirectional robot to augment the operator's perception of wireless signal strength in the remote environment. In this section, the radio signal strength (RSS) from multiple receivers are mapped to the force feedback of a 6 Degree of Freedom (DoF) haptic master device and evaluate the proposed approach using experimental data and randomly generated wireless maps. This approach, even though overloads the operator with radio signal strength haptic feedback, is influential and pivotal in the development of methods for superior teleoperation of wireless mobile robots in environments with low-wireless signals.

5.2.1   Proposed haptic wireless teleoperation method

The issues of low-wireless connectivity in teleoperation of mobile robots become increasingly important in large, unstructured environments, such as in maintenance of large scientific facilities and rescue situations [1], [2]. Several previous studies have aimed to solve the problems of high latency and areas of wireless coverage loss by increasing autonomy [146], [147]. While this autonomy can be advantageous in some robotic applications, there is still a demand for teleoperation.

Unknown and unpredictable environments and operating conditions mean that operators must maintain some control over the robot in order to avoid disaster, as human operators are inherently more versatile than autonomous systems [148], [149]. One well established way of utilising this human versatility is through haptic teleoperation [150]–[153]. However, enabling teleoperation comes at the cost of higher bandwidth to provide continuous feedback to the user, which can be difficult in areas of low-wireless signal. One effective way to boost wireless coverage is to implement ad-hoc wireless systems utilising multiple mobile wireless transmitters [154].

As the resulting wireless coverage is unknown, human operators must then be supplied with information on the wireless system to avoid driving the robot into an area of low coverage. As

teleoperation interfaces often already include haptic devices it may be advantageous to extend this to give the user a perception of the wireless signal. It appears on analysing literature on this research that previous studies have not looked at the possibility of extending this information on wireless connectivity to the existing haptic feedback available to the human operators to allow them to move more naturally in these environments with unknown wireless connectivity.

(a) z-restricted haptic plane.   (b) Simulated youBot in Rviz.
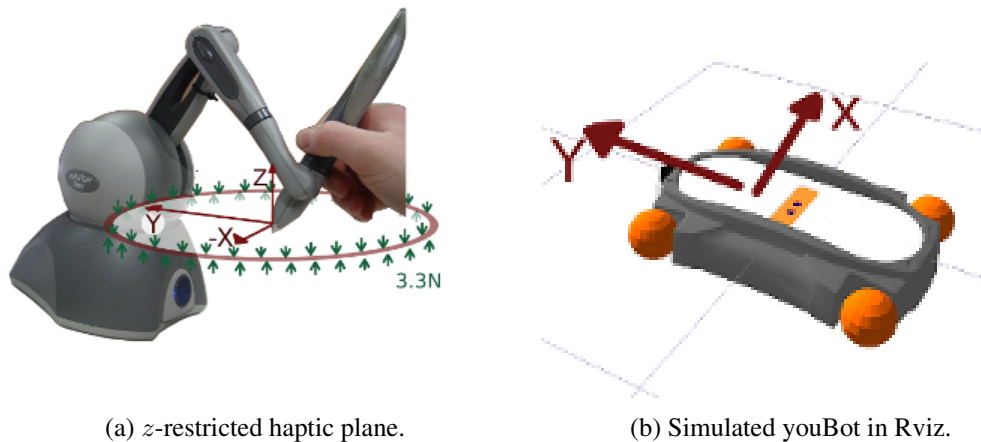
Figure 5.6: Haptic operation of youBot mobile robot with a 6 DoF PHANToM OMNI slave with 3 DoF haptic feedback in (x, y, z) direction.

This section proposes the use of haptic feedback to give the operator of a teleoperated mobile robot a perception of the wireless signal in the remote environment to allow them to intuitively travel in areas of high wireless signal.

Maintenance tasks often involve haptic feedback to the operator, to improve telemanipulation [155]. Utilising this existing feedback to allow the operator to perceive the received wireless signal strength (RSS) through haptic feedback is the objective in this work. The motivation behind this work is that this approach will be useful to allow the operator to make better decisions when driving a mobile robot. For example, if the operator feel that the mobile robot is entering an area with lower wireless signal they may choose to activate an autonomous mode, gracefully degrade the video feedback or take a different route.

This is useful when the mobile robot has to be operated in a very low radio signal region and the properties of the wireless network and the environment may not be fully known previously, due to the unknown reflection and absorption by the environment. It is important to note that the proposed method is not designed to remove control from the operator, as automatic systems do. Instead, the proposal allows the operator to make better decisions of the robotic intervention with the man-in-the-loop control model.

Although four sensors are used in this study for RSS spatial sampling, the proposed algorithm can be extended to as many or as few sensors are available, making it very flexible - the more wireless receivers, the better the feedback to the operator. However, even only two sensors

are available, in a left-right configuration, this will provide the operator enough feedback to naturally steer the mobile robot towards the area with better signal.

The next subsection describes the methodology for wireless communication modelling and the haptic control architecture for the master-slave system. Finally, section 5.2.3 describes the experimental setup in a simulated remote environment and Section 4 describes the results.

5.2.2 Haptic control architecture for RSS feedback

This study uses a mobile robot and haptic master and a randomly generated environment of wireless signals, implemented in the RViz and Gazebo simulator of Robot Operating System (ROS) framework [112]. This simulated environment both allowed a larger complex environments and the possibility to create multiple, unknown wireless environments to ensure that the operator is only relying on haptic feedback for their perception of the wireless signal. For these reasons the simulated environment is preferable over the limited available physical environment.

The hardware used is a KUKA youBot [58] as the slave robot and a PHANToM OMNI haptic pen [156] with 6 DoF as a master device, shown in Figure 5.6.

5.2.2.1 Wireless communication model

In a typical wireless network, when the connectivity worsens because of movement of the wireless receiver and/or the transmitter or change in antenna orientation, for instance, the data rate is automatically adjusted downward to maintain the reliability in connection. However, when the radio signal power is not enough to maintain the link quality, there is a possibility of losing the communication link for some time depending on conditions such as interferences and obstructions.
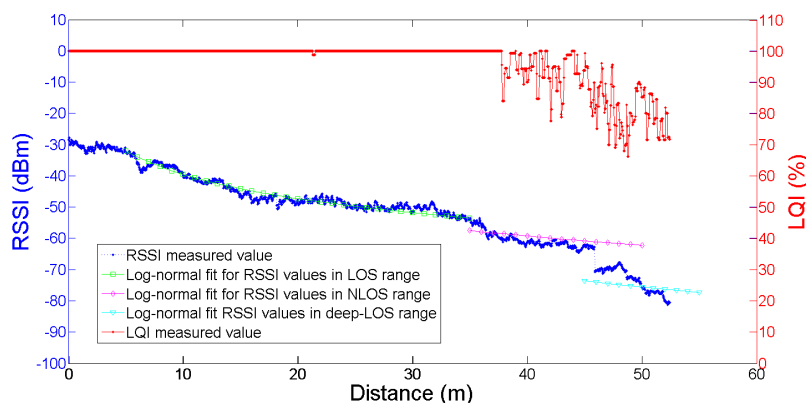
Figure 5.7: Experiments conducted in the ECN3 tunnel at CERN for determining the radio propagation parameters: RSSI and LQI values versus distance.

Background on the radio signal strength, wireless network capacity and path loss in radio signal propagation are provided in the sections 2.2 and 2.3. Prior to this work, an experiment is conducted to empirically determine the environmental parameters n and σ_x specific to complex environments in chapter 4.1. A wireless access point is used as a transmitter and is stationed at a point. Several wireless adapters are mounted on the youBot mobile robot and are used as receivers. The details of wireless transmitter/receivers used in this study are shown in Table 5.3.

	Access Point	Wireless Transceivers
Make and Model	ProSafe, WNDAP350	ZyXEL, NWD2105
Protocol	IEEE 802.11n	IEEE 802.11n
Frequency (f)	2.4 GHz	2.4 GHz
Transmit Power (P_t)	20 dBm	15.5 dBm
Receive Sensitivity (R_t)	-	-64 dBm
Antenna Gain (G)	3 dBi	0 dBi

Table 5.3: Wireless transceiver details used in this study.

Figure 5.1 shows the youBot with five wireless receivers arranged in a diamond-like configuration where the receivers are placed one on each side and one at the centre. The mobile robot is autonomously driven in the ECN3 underground tunnel scientific facility at CERN shown in figure 5.2. The values of the RSS and the quality of link is recorded using the $RSSI$ (Received Signal Strength Indicator) and LQI (Link Quality Indicator) metrics [66], [115].

Up to 35 m distance from the static transmitter, the robot travelled in line-of-sight (LOS) condition. After that, the robot is moving in non-line-of-sight (NLOS) condition until 45 m. Then the robot is moved in a deep NLOS condition. The resultant average of $RSSI$ and LQI of the five receivers with respect to distance are shown in figure 5.7. From the $RSSI$ values, the calculated values are $n = 3.02$ and $\sigma_x = 1.52$dBm for NLOS conditions using the log-normal fit in the equation 2.3.

5.2.2.2 Velocity control on fixed haptic plane

As the youBot can only move in the xy plane in figure 5.6b, the 3 dimensional workspace is restricted in the z-axis by a hard haptic plane of 3.3 N, as shown in Figure 5.6a, which is the maximum executable force of the PHANToM OMNI. The x and y components of the radial distance from the centre of the workspace are used to control the translational velocity $\dot{v}$ of the mobile robot. Torsional velocity of youBot is not considered in this study.

The position of the OMNI tip is used to control the velocity of the youBot using the relationship shown in equation 5.9.

$$
\begin{bmatrix} \dot{x} \\ \dot{y} \\ \dot{\theta} \end{bmatrix} = \begin{bmatrix} \alpha_x & 0 & 0 \\ 0 & \alpha_y & 0 \\ 0 & 0 & 0 \end{bmatrix} \begin{bmatrix} c_x - p_x \\ c_y - p_y \\ c_z - p_z \end{bmatrix} , \tag{5.9}
$$

where $\vec{c}$ is the centre of the haptic workspace and $\vec{p}$ is the position of the tip of haptic device relative to this centre. α_x and α_y.

Figure 5.8: PHANToM OMNI slave controller is used to control the youBot simulated using ROS.

5.2.2.3   Wireless signal to force mapping

The received radio signal strength RSS (measured by using the $RSSI$ metric) is converted into a haptic feedback profile which can be perceived by the operator at the tip of the OMNI device in all the directions on xy plane. Before using the $RSSI$ values, it is first filtered using an averaging function of $\overline{RSSI} = \frac{1}{100} \cdot \sum_{i=1}^{100} RSSI_i$ with 100 samples at a sampling rate of 100 Hz.

The position of the wireless receivers x, y is converted to polar coordinates r, θ. The $RSSI$ values from four outer receivers on the youBot represents the signal strength in four directions $0°, 90°, 180°, 270°$ from the centre of the robot in xy plane as the receivers are configured in such manner (figure 5.6b). A spline cubic smoothing polynomial function is used to interpolate the $RSSI$ values in all the directions between 0 to 2π radians.

The use of four wireless receivers on the robot is useful for calculating the two-dimensional feedback to the operator in perceiving the signal strength in all the directions. The higher the

number of wireless receivers, the better the resolution of interpolation, with a minimum of 2 sensors as previously discussed. In fact, even with only one wireless receiver, haptic feedback to the operator is possible with vibration which occurs when the robot enters low-wireless signal region. However, such feedback cannot let the operator determine the direction to move the robot in order to avoid the low signal region.

To translate arbitrary $RSSI$ signal values into a force which is intuitive to the user, it is required to choose signal levels which correspond to normal operating signal levels for teleoperation of the robot. The conversion of $RSSI$ to force vector for haptic force feedback is made using equation 5.10.

$$\vec{F} = \begin{bmatrix} \beta_x \left| \cos \theta_p \right| & 0 & 0 \\ 0 & \beta_y \left| \sin \theta_p \right| & 0 \\ 0 & 0 & \beta_z \end{bmatrix} \begin{bmatrix} \Theta_x \\ \Theta_y \\ \Theta_z \end{bmatrix}, \tag{5.10}$$

where,

$$\begin{aligned} \vec{\Theta} &= \vec{c} - \vec{p}, \\ \theta_p &= atan2(\frac{p_x}{|\vec{p}|}, \frac{-p_y}{|\vec{p}|}), \\ F_i &: \mathbb{R}\left\{0 > F_i > 3.3N\right\}, \ i = x, y, z, \\ \beta_x &= \beta_y. \end{aligned}$$

θ_p is the heading of the tip of the haptic device relative to the centre of the haptic plane described. A spring force is applied to the tip of the master device towards the centre of the plane and is calculated instantaneously at each polar coordinate.

The factor $\beta_z = 0.2$ is used to give a haptic plane lying on c_z, described by the spring equation:

$$F_z = 0.2(c_z - p_z), \tag{5.11}$$

giving a maximum force of $3.3N$ at:

$$(c_z - p_z) = \frac{3.3}{0.2} = 16.5mm. \tag{5.12}$$

The value of β_z has been chosen to eliminate the noise which occurs at higher gains in feedback. The values for β_x and β_y are derived empirically, represented by the following function:

$$\beta_x = \beta_y = \begin{cases} F_{max} & \text{when } P_r \leq -55\text{dBm,} \\ \Upsilon_{P_r} \cdot P_r & \text{when } -55\text{dBm} < P_r \leq -42\text{dBm,} \\ F_{min} & \text{when } P_r > -42\text{dBm.} \end{cases} \qquad (5.13)$$

According to [123], the Packet Reception Ratio PRR which is equivalent to LQI, should be at least 85% to consider the link as being of a good quality. Applying the threshold of 85% LQI in figure 5.7, for a good connection, the $RSSI$ value should be greater than -55 dBm. Therefore, a minimum $RSSI$ value of -55 dBm is required to operate the youBot, and thus the highest force is applied below this signal.

Table 5.4 shows the signals which are chosen and the corresponding force levels which are applied. These are chosen to give a natural force profile that would allow the operator to perceive the direction of better wireless signal region and move within areas of good signal with ease, naturally guiding them towards areas with higher RSSI and only restricting them from areas where the signal is too low to operate the robot ($-55\,\text{dBm}$). As the aim of this system is not to remove the control from the operator, operating to these low $RSSI$ level areas is still possible, but gave sluggish control.

	Signal Strength (RSSI)	Centring Force (per mm)
Minimum Signal	-55dBm	0.1500 N
Low Signal	-53dBm	0.0340 N
Preferred Signal	-50dBm	0.0195 N
Good Signal	-47dBm	0.0123 N
Great Signal	-42dBm	0.0050 N
Best Signal	-20dBm	0.0050 N

Table 5.4: The signal levels used in this study and the force exerted by the haptic master towards the centre of its workspace, corresponding to a speed command of zero to the mobile robot in all directions.
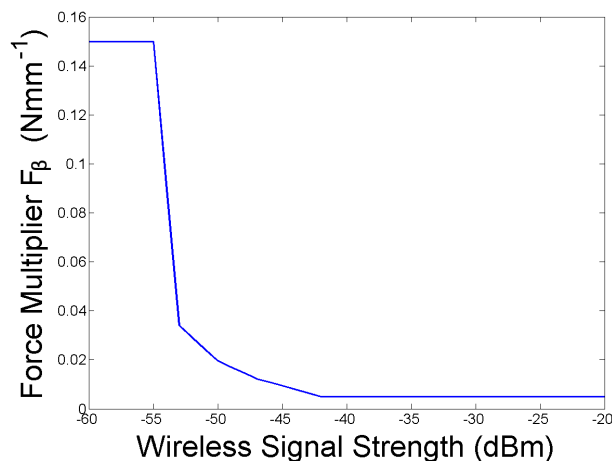
Figure 5.9: The force multiplier derived for the usable range of $RSSI$ signal values.

Figure 5.9 shows the force profile with respect to $RSSI$ values. The applied force to the operator is piecewise linear with the received signal strength, P_r with the linearity factor Υ_{P_r} depends on the $RSSI$ which is necessary for various levels of reliability of the wireless communication with the robot, as shown in Table 5.4.
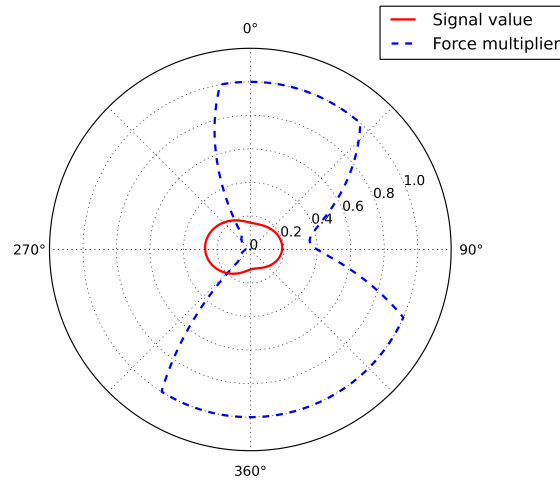
Figure 5.10: The RSSI and resultant force profiles scaled to between $[0, 1]$ with 0.0 being minimum RSSI (-55 dBm) and minimum force (0.005 N) and 1.0 being maximum RSSI (-20 dBm) and maximum force (0.15 N).

The force values and the $RSSI$ values are scaled between $[0, 1]$ and figure 5.10 shows the measured $RSSI$ at one position of the robot and the applied force vector to the operator in each direction. Figure 5.10 is displayed in real-time while the operator is driving the robot. Therefore the operator can visualise the wireless signal levels in different directions and can move the robot in the direction of better signal strength.

5.2.3 Experimental Setup

Since real environments are unavailable to use at the time of this study, the wireless environments are simulated using equation 2.3 with the propagation parameters obtained empirically ($n = 3.02$ and $\sigma_x = 1.52$dBm). Also that the youBot mobile robot is simulated on the virtual environment controlled by a real haptic master device. Using simulated wireless environment maps is advantageous as it both allowed the creation of unknown landscapes of wireless signal, as would be the case in a real situation, and allowed a larger working area than is available in the physical space.

Also, it is important to note that in real environments the wireless signal would be less radial, with reflections and distortions of the signal by various surfaces and materials in the environment. However, the mapping of a perfect simulation of such properties is beyond the scope of this chapter, which is to demonstrate the effectiveness of the haptic feedback.

5.2.3.1   Simulated environment

A virtual rescue environment is created in the Gazebo simulator. A fixed course of obstacles is placed to add some realism to the scenario as shown in Figures 5.11 and 5.13a. Two types of teleoperaion modes will be used for each simulation experiment: one using haptic feedback; and another without haptic feedback.
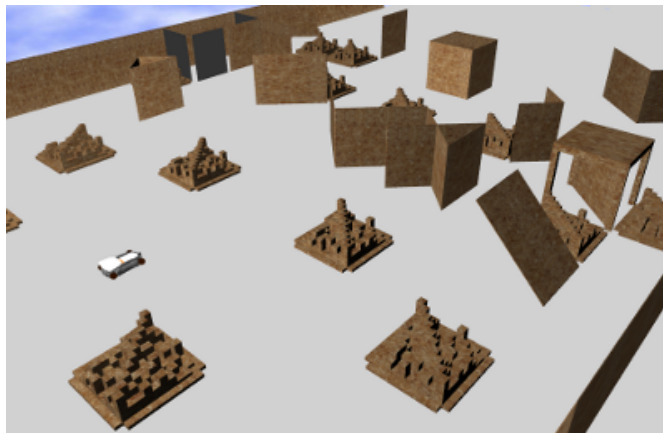
Figure 5.11: Gazebo simulation of a rescue scenario.

In each experiment, the operator is instructed to drive the mobile robot in an unknown wireless environment from a pre-defined start point to an end point. One of the operator is adept with the haptic device but not an expert on wireless distribution. A subjective evaluation is made with multiple trials and multiple operators with and without haptic force feedback. While driving the robot, the operator saw two windows on-screen. The operator view of the youBot located in the simulated environment in gazebo is shown in figure 5.11. In another window (only when haptic feedback is used), the force and signal profile at the centre of the robot as in figure 5.10 is displayed so that the operator can decide the change in direction of the robot to avoid bad radio signal regions.

5.2.3.2   Map Generation

A selection of 6 manually generated maps of wireless coverage are chosen at random using a MATLAB script. The path loss equation (equation 2.3) is used for creating random maps of wireless signal coverage. To make the map more realistic, additive white Gaussian noises (AWGN) are added in both the time and space dimension with zero mean ($\mu = 0$) and standard deviation $\sigma = 2\,\mathrm{dBm}$ as shown in figure 5.12. In this way, both the temporal and spatial fluctuations in $RSSI$ are simulated. In addition, randomly generated black spots (where $RSSI = 0$) are placed on the map in difference sizes and at different places to simulate the loss of wireless communication at certain places.
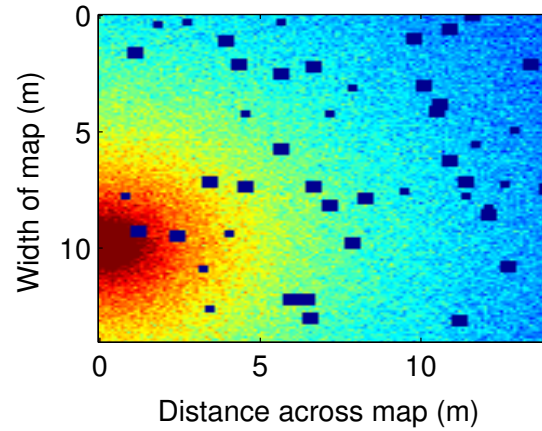
Figure 5.12: Plot of the wireless map with randomly placed black spots and transmitter.

Figure 5.13 shows the Rviz visualisation of the wireless map and its corresponding environment. The spatial resolution of the map is set to $0.1\,\mathrm{m}$ which is greater than $0.38\lambda_c = 12.5\,\mathrm{cm}$ at $2.4\,\mathrm{GHz}$. Therefore, uncorrelated and independent $RSSI$ samples are obtained at each point in space [144].
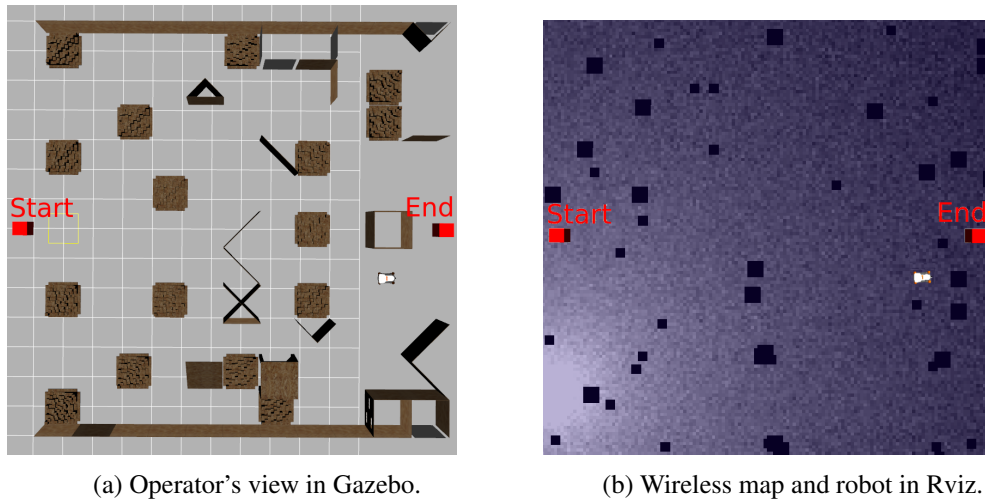
(a) Operator's view in Gazebo.

(b) Wireless map and robot in Rviz.

Figure 5.13: Views of the test setup in both Gazebo and RViz.

Since the wireless environmental properties are considered unknown to the operator, the wireless signal map is hidden from the operator during the experiments.

5.2.4 Results and Discussion

5.2.4.1 Reaching the goal

30 automatically generated maps are created, each with three randomly placed wireless transmitters. To avoid the situation where transmitters are all placed in the same location, the width

	With Haptic Feedback		Without Haptic Feedback	
Trial Number	Distance (m)	Success?	Distance (m)	Success?
1	12.9	Y	5.7	N
2	12.9	Y	8	N
3	12.9	Y	13.5	Y
4	12.9	Y	8.1	N
5	13	Y	7.4	N
6	12.9	Y	8	N
7	12.9	Y	7.9	N
8	13	Y	13.5	Y
9	12.9	Y	8.5	N
10	12.9	Y	5.7	N

Table 5.5: Distance travelled and success of each trial with and without haptic feedback enabled.

is sectioned into thirds. The goal of the operator is to start the robot at $(0, 0)$ and reach the goal at $(13, -2)$ and the trajectory is recorded. Figure 5.14 shows one such map.
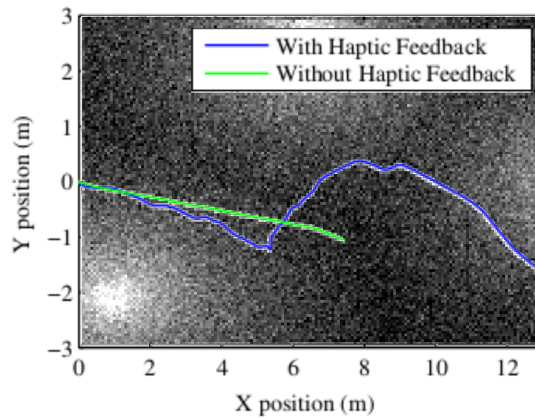
Figure 5.14: The path of the robot along with the $RSSI$ map is shown with and without haptic feedback enabled.

The results for all 10 trials are shown in Table 5.5. It can be seen that with force feedback, the operator can achieve the goal in contrast to having no haptic feedback where the operator enters into bad signal coverage and loses communication link. In Figure 5.15, the distance travelled by the operator in different trail is shown. The success ratio with haptic feedback is observed to be five times better than the success ratio without haptic feedback. This demonstrates the use of haptic feedback to perceive wireless signal strength.

5.2.4.2   Avoiding black spots

To further test the effectiveness of the proposed method, the operator is instructed to drive the robot with and without haptic feedback from start point $(1, 7)$ to end point $(14, 7)$ across multiple black spots that are randomly generated. The trajectory along with the number of black spots
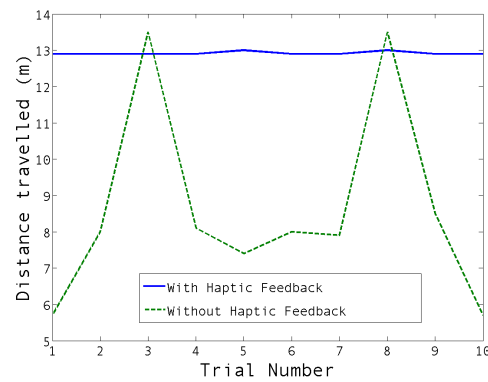
Figure 5.15: Completed distances along the test track for test runs.

across the way and the $RSSI$ values are recorded during the test. When haptic feedback is used, the operator is able to avoid all the black spots except in one place where the robot entered a black spot but is able to return back to operation because of effective haptic feedback. When the haptic feedback is not used, the operator drove the robot through 3 black spots, which, in a real world situation, means that the robot would have lost the communication with the operator whenever the robot had passed through the black spots.
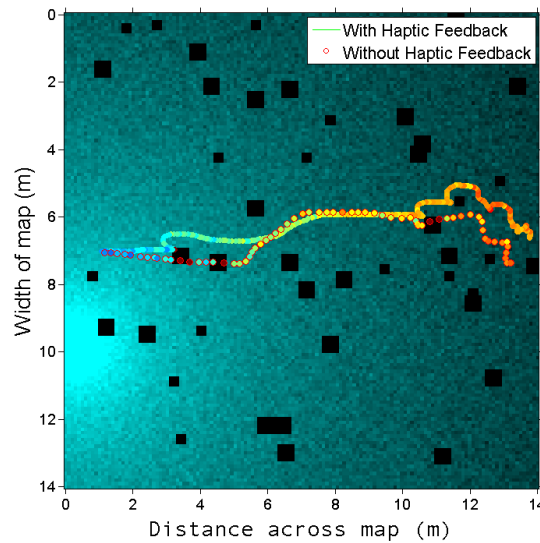
Figure 5.16: Map of RSSI values overlaid with paths for a trial with and without haptic feedback. With feedback the robot completes the track (13m) in all trials, while without haptic the robots loses communication at an average of 8m.

Figures 5.16 shows the path taken by the operator with and without haptic feedback and the corresponding RSSI is shown in 5.17. It can be observed that, with haptic feedback, the operator avoided the area where the wireless signal level falls below the minimum required (-55 dBm) to operate the robot.
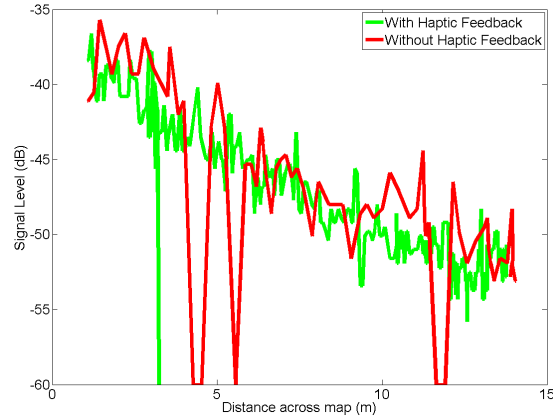
Figure 5.17: The $RSSI$ values recorded over distance.

5.3 Summary

Radiation environments and rescue scenarios often exhibit environmental properties which are complicated for radio signal propagation. In the first section of this chapter, a decentralised, time-independent, spatial diversity based, radio signal strength (RSS) improvement methods were proposed by making use of multiple receivers on a mobile robot to improve network reliability and optimise wireless communication qualities in hostile environments such as underground scientific facilities where the reflections, interferences and multipath effects of radio signals make wireless communication unreliable. The mobile robot's position was optimised using gradient ascent algorithms to receive the best RSS subject to local maxima. The performance of the proposed algorithm was experimentally evaluated in the ECN3 tunnel facility at CERN. The results had shown that the proposed time-independent spatial sampling methods were more efficient than the state-of-the-art spatial sampling methods available in the literature (N.B. None of the previous researches used time-independent RSS-based spatial sampling methods).

In the second section, the spatial sampling methods were applied to a haptic teleoperation application. The idea was to provide radio signal strength feedback to the operators (through haptics) in order to aid them in navigating the mobile robot smoothly in low-wireless signal regions and avoid communication loss. An important interpretation of the literature review was that, none of the previous studies had looked at the possibility of providing RSS haptic feedback to operators so as to allow them to move more naturally in low-wireless signal environments. This application study was experimentally tested for performance and feasibility using a quasi-simulated real-time experimental setup. The outcome of this study suggested that the proposed approach was indeed applicable to haptic teleoperation and could enhance the communication and teleoperation capabilities.

Chapter 6

Communication quality enhancement methods using relay robots

This chapter will examine the application of autonomous relay robots in enhancing wireless communication qualities. The first section will introduce the relay robot concept that can be used for wireless tethering. The second section will review the literature work related to this research. The third section will present a preliminary yet efficient algorithm for autonomously positioning the relay robots in between two mobile robots. In the fourth section, a robust relay robot mobility controller that balances the RSS to optimally place the relay robot between two mobile robots depending on the radio signal strength will be presented. This fourth section forms a vital part of this thesis by fully exploiting the concept of autonomous relay robots that can position themselves in an optimal location to enhance wireless communication range and qualities in telerobotic applications.

6.1   Introduction to autonomous relay robots

Wireless communication in underground mine tunnels has been investigated in [23] and the authors highlight the necessity of placing repeater nodes as the wireless network did not perform well under non-line-of-sight (NLOS) condition. It has already been mentioned in section 5.1 that the use of wired communication in hostile environments has not proven reliable, with fibre-optic cables susceptible to tangling, breakage, and being run over by the robot [1], whereas wireless communication offers benefits over wired communication systems such as low maintenance, higher robustness against failures stemming from physical damage, less manpower needed for managing the tethers and ease of mobility. However, wireless communications in hostile environments have been reported to be unreliable as well [2], [23].

To remedy this unreliability and more specifically to improve the wireless communication performance in non-line-of-sight (NLOS) conditions and in underground tunnels, the concept of wireless tethering using intermediate relay robot nodes (forming a network of mobile robotic nodes) has been suggested by many researchers [23], [131], [134]. Especially as the main objective in this thesis is the application of mobile robots in complicated and hostile indoor or outdoor environments, wireless tethering [134], [157], [158] could prove useful when the direct communication link between two wireless robot nodes cannot be reliably achieved due to factors such as multipath fading effects [134], non-line-of-sight (NLOS) characteristics or the environment itself (such as the underground tunnel facilities [23]).

Therefore, the use of a mobile robot serving the purpose of wireless tethering (relaying) of radio signals between two wireless robot nodes (which are termed as a server robot and a client robot as will be later explained) is considered in this chapter. The wireless tethering serves as the basis for mobile ad-hoc networks (MANETs) that have been widely studied and demonstrated [157], [158].

Tethering of radio signals can either be achieved by a static wireless node or by a dynamic (mobile) robot node (a mobile relay robot for instance). A commonly used networked wireless nodes model is the Server-Relay-Client (SRC) framework which has been introduced in section 2.6.

Figure 6.1 shows the systematic view of the wireless tethering system using a mobile relay robot at the centre. The server robot node could be a static command station and the client robot node could be static (for some time) or dynamic (robotic) in nature which is used for performing some tasks such as inspection or manipulation. The human operator interacts with the server node to command some control operation on the client node. Establishing and balancing the communication quality between two nodes (server and client) is the main job of a wireless relay robot. A relay robot node is usually autonomous (to ease the operator overload) and strives to position itself such that the communication quality between the server and client nodes are reliable and more importantly, always available.
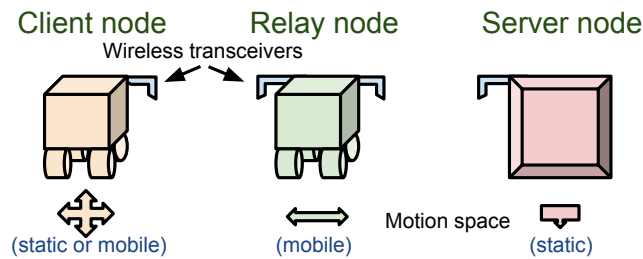
Figure 6.1: Server-Relay-Client (SRC) robots system: conceptual view of this study.

Distributed relay robot nodes can be rapidly deployed in hostile environments. Figures 6.2 and 6.3 show examples of using relay nodes for multi-hop wireless connectivity from an operator command station to the client/task node in line-of-sight (LOS) and non-line-of-sight (NLOS) conditions respectively. If relay nodes are autonomous with decentralised operations, it can permit the human operator to concentrate on controlling only the client node. An important intelligence feature necessary for the relay robot node is to locally optimise its position such that the communication quality between the server and client nodes is sufficient and more importantly, always available. The main idea here is that the operator should only be concerned with teleoperating the main robot while the chain of relay robot nodes follows automatically. This work is a step towards intelligent decentralised relay nodes that can improve connectivity in wireless tethering applications by using the node mobility [138], [141], [159]–[161].
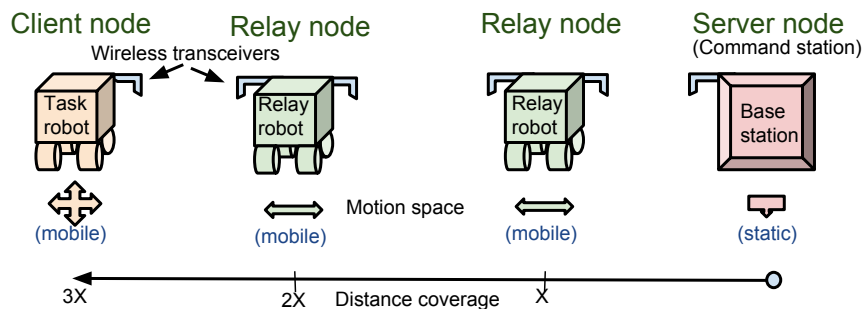
Figure 6.2: An example architectural view of SRC networked robot nodes system in line-of-sight (LOS) environments.

The wireless link quality and the network throughput have a strong correlation with the received signal strength (RSS) [38], [135] and the Signal to Noise Ratio (SNR) [141], [159]. One way to improve the throughput of the network is to improve as well as balance the RSS (at the relay node) from the server and client nodes. As the RSS is proportional to the logarithmic distance between two wireless nodes in LOS conditions, The RSS at each side of the relay node can be balanced by optimising its position using the mobility of the relay node. The RSS changes dynamically arising from the movement of objects and small-scale fading effects. Therefore, continuously optimising the relay node's position will optimise the wireless network performance [38], [136].
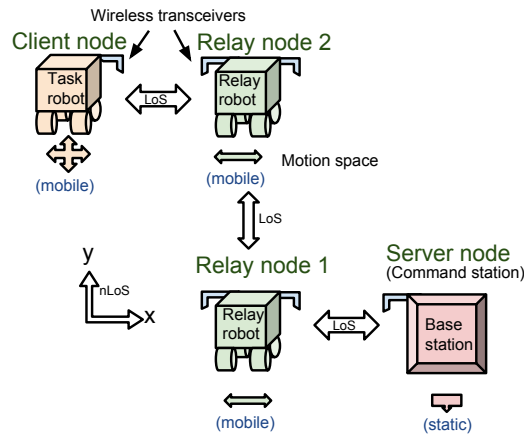
Figure 6.3: An example architectural view of SRC networked robot nodes system in non-line-of-sight (NLOS) environments.

In addition to the need for relay nodes, there is also a need for redundancy features in order to improve reliability, avoid communication failure due to unforeseen reasons and enable recovery in the event of failure in the wireless network. Enhancing reliability by applying redundancy feature (at device level) has been widely studied. In this work, redundant wireless transceivers are used on the relay robot node which means the relay robot carries minimum two similar wireless transceivers (instead of one) for tethering wireless signals form the server node to the client node.

6.2   State of the art in wireless relay robots

Many researchers have attempted to enhance the wireless connectivity in a network of mobile robots using various techniques [136]–[139], [141], [161]–[163]. The use of mobile relay nodes in tackling serious communication issues are usually addressed with solutions such as self-configuration, self-healing and wireless tethering as explained in DARPA Landroids [162] program. The use of relay robot nodes are also encouraged in [158]–[160].

In NLOS environments, mobile robot platoons can be used as wireless relays to form a wireless network from the operator base station to the main robot performing search or rescue missions. MANETs using a team of autonomous mobile robots for robotic wireless tethering have been demonstrated in [134], [157], [158].

The role of RSS has been significant in most of the research in wireless communication performance optimisation. Research has been done on using the RSS for wireless tethering in multi-robot networks and wireless localisation [138]–[140], [161]. A data driven probabilistic

model is used in [161] for localisation and wireless tethering algorithms using the RSS information. In [164], the RSS, mapped to the distance between the relay robots, is used for wireless tethering in multi-hop robot networks.

The authors in [141] used aerial robots as relay nodes and used antenna diversity for autonomously positioning the relay node using a gradient search technique, i.e., sampling the RSS from multiple antennas (in different directions) that are connected to a receiver and obtain the direction of the highest RSS. Reference [165] also studies the use of antenna spatial diversity in building wireless coverage maps and using it in optimal deployment of relay robots in a mobile robot network. As they are time-dependent or off-line methods, temporal fluctuations in RSS might influence and degrade the algorithm performance [38].

Most of the research solutions possess drawbacks such as the use of customised hardware with changes at the physical layer in the network stack of the wireless router (for instance, using wireless transceivers with multiple directional antennas). The dependency on customised hardware re-design could be overcome by using algorithms acting in the application layer of the OSI reference model so that they can easily be integrated and shared. As already mentioned in section 5.1.1, none of the previous research in RSS-based tethering of nodes utilised multiple receivers (for redundancy and spatial RSS sensing) and time-independent methods for improving the RSS [38].

It has been shown in [166] that using multiple sensors improves redundancy and reduces data loss rate. It is worth noting that their application is in a static biomedical data collection system and all the redundant devices are spread widely whereas in the proposed method, all the redundant sensors are placed in one moving node. Nevertheless, the redundancy advantage can still be proven, as shown in [165] that the use of multi-antenna (in this case, multi-sensor) spatial RSS sampling could improve the wireless network capacity by selecting the receiver with higher RSS.

6.3   Relay robots positioning using decentralised mobility control

Wireless relay robots can be used to bridge wireless communication between two wireless nodes or two robots (performing inspection or exploration missions) for extended coverage range especially in complicated environments (such as the underground facilities at CERN). In this section, a simple but effective radio signal strength (RSS) based reactive motion controller for wireless relay robots is presented. This approach is inspired by the concept of the Braitenberg vehicle controller [167]. The proposed method aims at efficiently balancing the RSS between two wireless nodes by optimising its position. Experimental verifications of the proposed method is

conducted using a youBot mobile robot platform as a relay agent and two stand-alone Raspberry Pi computers as server or client stations.

Reactive motion controllers are generally used for obstacle avoidance [168], [169], radio source seeking applications [140] and motion planning applications [136]. Though these methods perform well in terms of the error performance, they either need prior modelling/information in order to achieve the assigned control job (using distance range basis [158] or radio propagation model [157]) or they are not targeted towards wireless tethering application.

In this section, the design and use of a RSS-based reactive motion control (that is novel and has not been reported in the literature) for wireless relay robot positioning inspired by the concept of Braitenberg vehicle controller [167] is presented. The mobile relay robot measures the RSS received from both the client and server sides and optimises its position where both the RSS of client and server nodes balances. A single transceiver in the relay node can suffice to this purpose, however, to enhance reliability, two identical transceivers (bridged internally) communicating with one of the client or server nodes are used. The proposed method applies only to the relay robots (used for wireless tethering) and not to the client robot which performs the actual command (tasks/inspections). The main objective of this study is to provide a simple RSS-based reactive motion controller for relay robot and to demonstrate that it works with the help of basic experimental evaluation. While the proposed method is inspired by the Braitenberg vehicle controller concept, it has been significantly optimised to take into account the kinematics of the vehicle and the application context.

6.3.1   Braitenberg vehicle controller concept

Before introducing the proposed reactive motion controller, a short introduction to Braitenberg vehicle controller for radio (wireless signal) source seeking tasks is provided here. Figure 6.4 shows a single 3-wheeled differential drive robot having two antennas (sensors) pointed in opposite direction. The output of the sensors are directly connected to the motors of opposite side (the higher the sensed RSS, the higher the wheel velocity) so that the robot will steer towards the direction of higher RSS due to the differential drive control (one wheel rotates faster than another creating angular motion). This mechanism is also similar to a biologically-inspired approach such as the ant's foraging behaviour using two antennas to track its path.

6.3.2   Proposed reactive motion controller for RSS balancing

Knowing that the Braitenberg vehicle concept uses identical sensors to measure a single radio source, it can be extended to multiple sources (nodes) by using multiple identical sensors that measures the RSS from each source. It is important to note that the Braitenberg vehicle concept
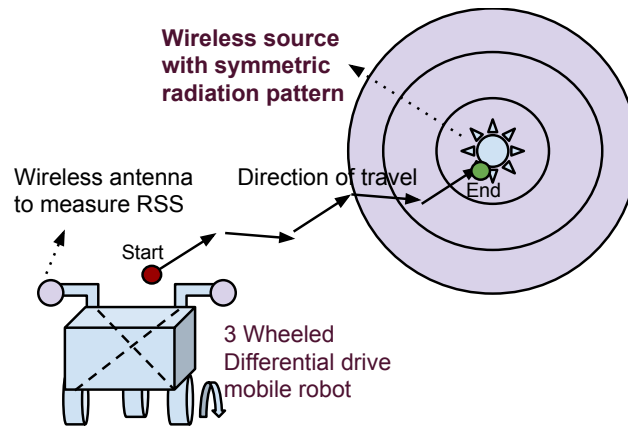
Figure 6.4: Conceptual example of radio source seeking robot using a "Braitenberg vehicle controller".

is designed for two wheeled differential steered robot so that the simple mechanical (kinematic) design of the robot can be augmented with an intelligent control action at the hardware level. To extend this concept to different radio signal sources and to position in 2D space, four sensors are needed one in each side of the robot (Front, Back, Left and Right) but then the motion control will become complicated. As the objective and scope of this section is proving the concept of the proposed method, experiments are conducted for only a 1D position optimisation method. However, in the next section, this controller is extended to a 2D space and will be enhanced with controllers that are gradient based [18] and connectivity threshold based wireless tethering [134].

In figure 6.5, a conceptual design of the proposed method with a wireless relay node between two wireless nodes is presented. The relay robot is configured with source avoiding mechanism by associating the sensors (wireless transceivers) information on each side of the robot to their respective side direction of motion, hence steering towards the node with the weaker RSS and the relay robot stops when the RSS from both the sides are balanced.
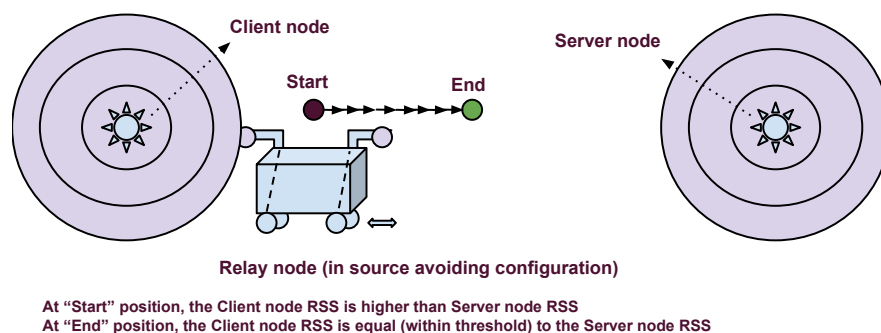
Figure 6.5: A wireless relay robot balancing the RSS between two wireless nodes: Inspired by the Braitenberg's thought experiment on vehicle control.

6.3.2.1 Algorithm

The proposed concept in Figure 6.5 is implemented using the following algorithm:

Algorithm 4 RSS-based reactive 1D motion control algorithm for a relay robot.

1: Measure the RSS from both client and server nodes at instant i when relay robot is in position x^i, y^i
2: The RSS of front and back transceivers in relay node $\mathbf{R_f^i} = \mathbf{RSS_{client}^i}$, $\mathbf{R_b^i} = \mathbf{RSS_{server}^i}$
3: **while** ($|\mathbf{R_f^i} - \mathbf{R_b^i}| < \mathbf{R_{threshold}}$) **do**
4:     $\mathbf{x^{i+1}} = \mathbf{x^i}$
5:     $\mathbf{y^{i+1}} = \mathbf{y^i} + \mathbf{Stepsize^i} \cdot \mathbf{sign}(\mathbf{R_f^i} - \mathbf{R_b^i})$
6:     Move the robot to position $(\mathbf{x^{i+1}}, \mathbf{y^{i+1}})$
7: **end while**

Here, R_f is the RSS value at the wireless transceiver placed on the front of the robot and R_b being the RSS measured by the transceiver placed at the back of the robot. The term $sign(\mathbf{R_f^i} - \mathbf{R_b^i})$ gives the sign of the difference between RSS from the client and server nodes. The step size is either kept constant (in some cases) or kept dynamically changing in each iteration proportional to the difference in the RSS values.

$$\text{Step size} = \alpha \cdot (\mathbf{R_f^i} - \mathbf{R_b^i})$$

where the value of α is set at 0.1. The $R_{threshold}$ has been set to $2\,\text{dBm}$ to reduce temporal variations and to attain stable control action when the relay robot reached the optimal position.

6.3.3 Experimental evaluation

For the experimental study, the KUKA youBot omnidirectional mobile platform as the relay robot and two Raspberry Pi computers as Client/Server nodes (Fig. 6.6) are used. YouBot can be controlled independently in each degree of freedom (holonomic platform), it can move in any direction thanks to the special Swedish wheel design [59]. The computer in youBot as well as the Raspberry Pi computers are running on Linux operating system. The wireless transceivers used in all the nodes is a low cost Zyxel NWD2105 USB Wi-Fi adapter (running on the Ralink 3070 driver) that can be configured either as "Station" mode to act as RSS sensor or as "Soft AP" mode to act as radio signal source.

As mentioned already in section 6.3.2, the algorithm implemented in the relay robot is for motion control in one dimension (forward-backward or the y direction). Figure 6.7 shows the youBot in the LHC mock-up facility. The initial distance between server relay had been always fixed at 5 m and the client to relay distance had been varied from 10 m to 30 m. The evaluation metrics used here are the distance travelled by the relay robot towards client robot and the number of iterations
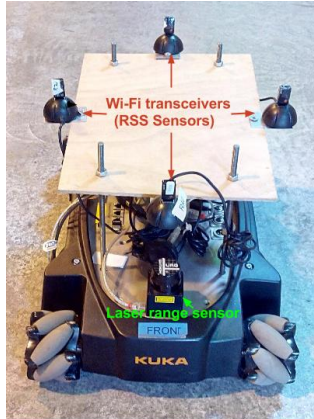
(a) Multiple spatially distributed RSS sensors mounted on the relay robot node.
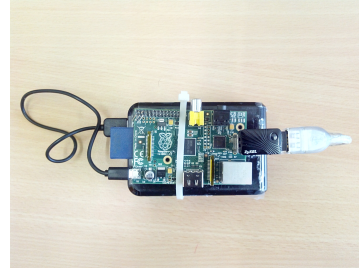
(b) Raspberry Pi computer (connected to a battery) used as client or server node.

Figure 6.6: Raspberry pi and youBot being used as client/server and relay nodes respectively.

Figure 6.7: The LHC mock-up facility at CERN used for the experiments.

taken by the algorithm to arrive at the position where the RSS is balanced. It is assumed that the algorithm performs better when it uses less iterations and travels short distances to reach the optimal position.

The RSS is measured by using the RSSI (Received Signal Strength indicator) metric provided by the *iwlist* command in Linux. The algorithm is implemented as a bash shell script and the actual motion on the youBot is achieved using a C++ program called through the shell script. The measured RSSI values represent the signal level in dBm (and has a negative sign) which means that higher the RSSI value, lower the signal strength. The velocity of youBot is set

at 0.8 ᵐ/ₛ. The RSSI is first filtered using a temporal moving average filter to mitigate sudden changes in the measured values due to fading effects.

(a) Balancing of the RSS from client and server nodes at the relay robot.

(b) Effect of the step size on the performance.

(c) Effect of Client to relay node separation distance.

(d) Effect of client node velocity.
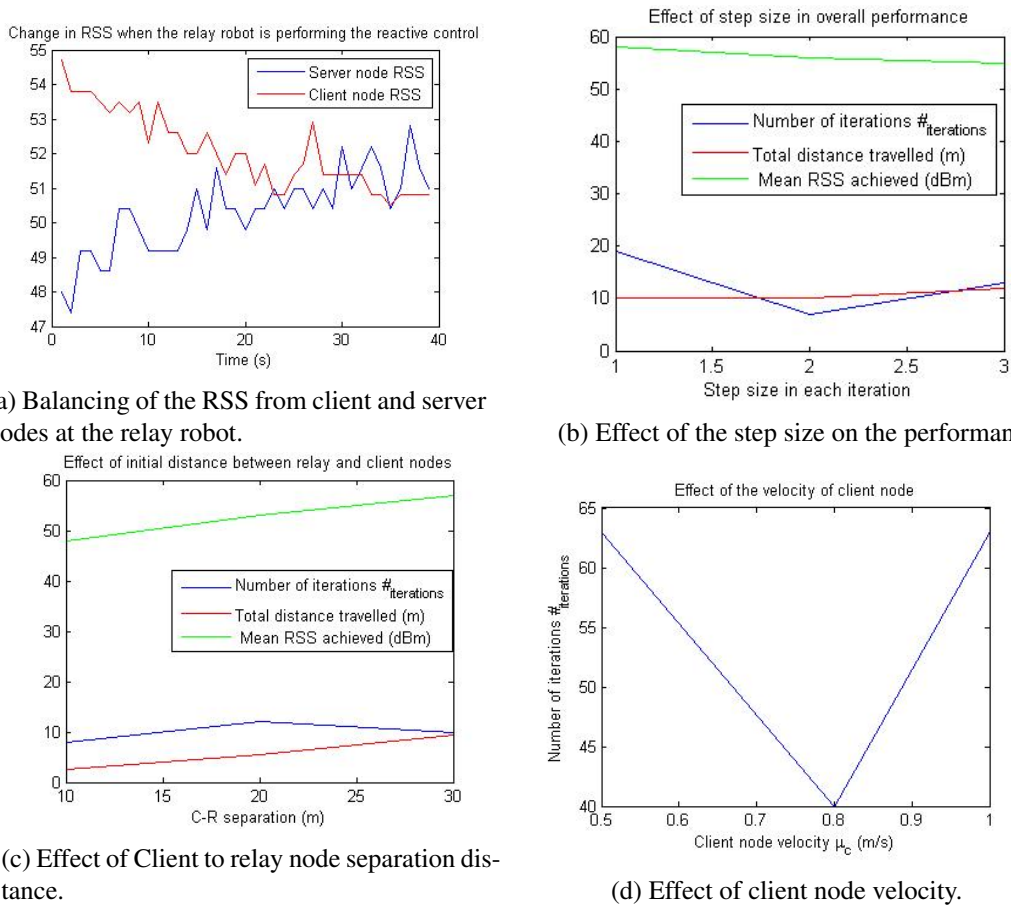
Figure 6.8: Experimental performance of the algorithm 4 and effects of step size, velocity and separation distances on the performance.

An example of RSS balancing action is shown in figure 6.8a. It can be observed in the figure 6.8b that, even though the mean RSS achieved in both the nodes is lower (which means higher signal strength) when the step size in increased, the step size should be properly calibrated in order to achieve the optimised position in less number of iterations and with distance travelled. The step size is kept the same for all the iterations. Figure 6.8c shows the effect of the initial distance between the client and relay robot on the algorithm performance in terms if number of iterations. It is clear from this figure that, the number of iterations is not monotonically decreasing with the client-relay node (C-R) separation because of the dynamic step size adjustment.

In one case, the client node has been moved manually with a steady velocity (by steadily travelling a fixed distance in a fixed time). The effect of client velocity on the algorithm performance can be observed in figure 6.8d. When the client velocity is more or less equal to the relay robot velocity, the algorithm performed better. This section is concluded with this idea of balancing the RSS in one dimension. In the next section, an algorithm is developed for two-dimensional RSS balancing by optimally positioning the relay robots with robustness to noise.

6.4 Relay robots positioning using multi-sensor spatial sampling method

Reliability of wireless communication in a network of mobile wireless robot nodes depends on the received signal strength (RSS) values in each wireless link. When the robot nodes are deployed in hostile environments with ionising radiations (such as in some scientific facilities), there exists the possibility of some electronic components to fail randomly (due to radiation effects), which causes problems in wireless connectivity. The objective of this work is to maximise robot mission capabilities by maximizing the wireless network capacity and reduce the risk of communication failure. Thus in this work, the multi-node wireless tethering structure called as "Server-Relay-Client" framework that uses (multiple) relay nodes in between a server and a client node is considered and a robust stochastic optimisation algorithm using multi-sensor based RSS sampling method at the relay nodes to efficiently improve and balance the RSS between the source and client nodes in order to improve the network capacity and also to provide redundant networking abilities is proposed. Special preprocessing techniques such as exponential moving average and spatial averaging filters on the RSS data has been used for smoothing. The receiver spatial diversity concept is utilised and a position controller is employed on the relay node using a stochastic gradient ascent method for self-positioning the relay node to achieve the RSS balancing task. The effectiveness of the proposed solution is validated by extensive simulations and field experiments in CERN facilities. The youBot mobile robot platform is used in the filed trials as the relay node, and two stand-alone Raspberry Pi computers as the client and server nodes.

In the previous chapter, several methods [38] for optimising the node position to receive the best RSS relative to one radio signal source (transmitter) are studied. The work in the current chapter extends the spatial sampling methods in the previous chapter and propose a decentralised method for wireless relay node positioning using a spatially spread multi-sensor RSS sensing technique to optimise the wireless signal strength at the relay node using the receiver spatial diversity concept (receiving radio signals with multiple receivers at different positions). In this way, redundancy is also added to the network so as to avoid wireless device failures due to single event effects (SEE) induced by ionising radiation in the environment. In this section, an adaptive and robust "stochastic optimisation" (SO) algorithm for the RSS relative to both client and server nodes is proposed and apply it to the relay node for RSS balancing. The proposed algorithm is made robust to measurement noise by special preprocessing techniques.

The main objective in this work is to navigate the relay node to a position (between two nodes) where the RSS is at a local maximum or at least above the minimum threshold needed to maintain a strong connectivity. The main contributions in this section are the following:

1. A decentralised stochastic optimisation algorithm (robust to measurement noise) employing gradient ascent method that can be applied in the relay node using multi-sensor spatial RSS sampling to find the optimal position of the relay node between two nodes is proposed;

2. The proposed method is validated using simulation and field experiments and considered performance metrics such as the temporal and spatial performance of the relay node, accuracy and success rate in reaching the optimal position. The proposed algorithm is compared with the state-of-the-art (SoA) methods at relevant places in this section.

The problem formulation in defined in section 6.4.1 and the proposed solution along with its implementation details is described in sections 6.4.2 and 6.4.3. Then this theory is evaluated by conducting simulations presented in section 6.4.4, and is supported with experimental verification in the section 6.4.5.

6.4.1   Problem formulation

The problem to be solved in this section can be formulated as follows; the RSS field (and the environmental model) is assumed to be unknown a priori. The RSS can be measured by the node using the spatially distributed wireless receivers (which act as the sensors). A single-relay SRC framework is used. Both server and client nodes are assumed to be mobile (dynamically changes their position) and the relay node has no control over other nodes' movement. The server, relay and client nodes are placed at positions $p_s, p_r, p_c \in \mathbb{R}^2$ respectively. The algorithm is implemented in the relay node, which can provide its position information as one of the inputs to the algorithm. Assuming the relay node has fully controllable dynamics, the objectives are:

Problem 1: Find an optimisation objective function which should be maximised by optimising p_r such that the network capacity (goodput) of the end-to-end server-client link is optimal;

Problem 2: Find a robust stochastic optimisation algorithm to optimise the network goodput, is robust to environmental changes, and maximises the objective function that solves Problem 1;

Problem 3: Find an RSS sensing method and RSS preprocessing techniques to increase the robustness of the algorithm that solves Problem 2;

Problem 4: Find a suitable dynamics controller for the relay node that supports the solution of Problem 3 and also ensures that the relay node can reach the objective smoothly.

The robustness of the proposed algorithm is verified under sensory and environmental noise for objective maximisation. In this regard, simulations and experimental evaluations are conducted for a number of trials considering various environmental conditions are conducted.

6.4.2 Proposed solution

In this research, the concepts used in [139], [141], [159], [165] are used while intending to remove the hurdles and drawbacks observed in these research works. The novelties in the proposed method are presented below which also show the solution departs from the state-of-the-art methods.

1. The proposed method does not require prior knowledge or model of the radio environment. Special preprocessing techniques such as exponential moving average filters are used to deal with the measurement noise and stochastic nature of the RSS and mitigate fading effects.

2. Multiple receivers are distributed spatially on-board the relay node instead of using multiple antennas connected to the same receiver. Therefore, the need to switch between different antennas connected to a same receiver can be avoided and it also makes the algorithm applicable directly at the application layer.

3. RSS is measured instead of SNR as the noise signal power is not measurable in many commercial wireless devices. Hence the approach is to use the RSS gradient information (instead of SNR gradient) and propose a suitable robust stochastic optimisation algorithm to optimise the relay node position to receive relatively better RSS (local maxima), thereby increasing the communication range and coverage area.

4. The proposed algorithm is evaluated with simulations and field experiments using a position controller that can work even when the RSS gradient measurements are noisy and the RSS field in the environment is unknown with NLOS conditions.

In a network of nodes, a relay node can use either a Relay-and-Retransmit (RR) scheme or a Flow-Pipe (FP) scheme for data transport [159]. While the former scheme is based on packet switching, the latter scheme has the functionality of a radio-repeater. The total network goodput (application-level throughput) G_t of a robotic network having n nodes (first is the server node and n_{th} is the client node, and $n-2$ relay nodes) is given by the following equations [170]:

For the RR scheme:

$$G_t = \frac{1}{\displaystyle\sum_{i\in[1,n-1]}^{j=i+1} \frac{1}{G_{ij}(RSS_{ij})}} = \frac{1}{\displaystyle\sum_{i=2}^{n}\left(\frac{1}{\alpha_T\alpha_G Blog_2(1+10^{\frac{RSS_{dBm}-PN_{dBm}}{10}})}\right)}, \qquad (6.1)$$

and for the FP scheme:

$$G_t = \min_{\substack{i\in[1,n-1]\\ j=i+1}}\{G_{ij}(RSS_{ij})\} = \min_{\substack{i\in[1,n-1]\\ j=i+1}}(\alpha_T\alpha_G Blog_2(1+10^{\frac{RSS_{dBm}-PN_{dBm}}{10}}), \qquad (6.2)$$

where $RSS_{dBm}(i, j)$ represents the signal strength of node j measured at node i. $G(r, s)$ and $G(r, c)$ are the goodput of the relay-server and relay-client links respectively.
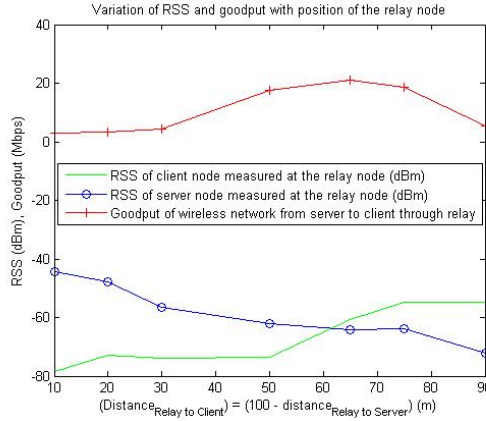
Figure 6.9: RSS and goodput measured by relay node at various positions and instants in NLOS condition.

In this work, it is assumed that the relay node uses the FP scheme for relaying the data from server to client (as it is more efficient case compared to the RR scheme). Therefore, the equation (6.2), for a single-relay SRC becomes:

$$G_t = \begin{cases} \left[\frac{1}{G(r,s)} + \frac{1}{G(r,c)} \right]^{-1} & \text{for the RR scheme,} \\ \min(G(r,s), G(r,c)) & \text{for the FP scheme.} \end{cases} \tag{6.3}$$

The figure 6.9 indicates how the measured goodput changes as the relay node moves with respect to server and client in a single-relay SRC framework using the FP scheme. The goodput is maximal when the RSS from server and client become close to each other, which supports the target of this work, i.e. the RSS balancing between the server and the client node is beneficial for improving the total network throughput. The goodput indirectly depends on the position of the relay node because the goodput depends on the RSS which in turn depends on the position and the radio environment.

In the further sections, solutions are proposed for each of the problems defined in section 6.4.1.

6.4.2.1   Objective function

Let the measured RSS at the relay node from the client node be RSS_c and from the server node be RSS_s. A way to solve Problem 1 is to find a function that maximises both the RSS_c and RSS_s at the same time so that the total goodput is maximised. figure 6.9 shows the RSS readings as the relay node travels between the server and client nodes. The reason for non-symmetrical RSS values between two nodes is that the environment has NLOS conditions and hence has

different propagation constants. It can be observed from figure 6.9 that the goodput is maximal when RSS_c and RSS_s become equal. However, it is also worth noting that this figure 6.9 shows a one dimensional RSS measurement, if extrapolated to a 2D scenario, there are multiple possible positions where $RSS_c = RSS_s$, as will be shown later in section 6.4.4. Hence it is important to consider a function that maximises the value of RSS_c and RSS_s together while maintaining them equal at the same time. The objective can be formulated as follows:

$$G^* = \max(G_t) \text{ such that } \underset{p_r}{\arg\max} \, RSS_c = \underset{p_r}{\arg\max} \, RSS_s \text{ and } \max RSS_c = \max RSS_s,$$

(6.4)

where G^* and G_t are the optimal and total goodput respectively and the p_r is the argument to be used in the optimisation. This can be directly translated to an optimisation problem that equalises and maximises the RSS on the both sides as shown below.

$$p_r^* = \underset{p_r \in \mathbb{R}^2}{\arg\max} \, f(p_r) = \underset{p_r}{\arg\max} \, f(RSS_c(p_r), RSS_s(p_r)),$$

(6.5)

$$\text{s.t. } G^* = G_t(RSS_c(p_r^*), RSS_s(p_r^*)) \text{ and } \max RSS_c(p_r^*) = \max RSS_s(p_r^*).$$

(6.6)

Here $p_r = (x_r \in \mathbb{R}, y_r \in \mathbb{R})$ is the position of the relay node and is the argument that is optimised for maximizing an objective function $f(p_r) : \mathbb{R}^n \rightarrow \mathbb{R}$. In the previous work [38], the objective function used is $f(p_r) = RSS_s(p_r)$ as used only one signal source is used. But in the present work, the relay node has to balance between two signal sources, and hence a simple solution can be to use $f(p_r) = RSS_c(p_r) + RSS_s(p_r)$ as the objective function, however this does not satisfy the constraint $RSS_c(p_r) = RSS_s(p_r)$ and so there will be two optima, one at the server node position $p_r^* = p_s$ and another at the client node position $p_r^* = p_c$ instead of the optimum position between these two, which will be apparent in the later sections. Therefore a different objective function that satisfies all the constraints has to be chosen. For example, in [159], $f(p_r) = min\{SNR_c, SNR_s\}$ has been used as the objective function and a least-squares gradient estimation (LSGE) method is adopted for determining the gradient of the objective function and deal with its non-smooth nature. However, as the algorithm rely purely on the spatial gradient approximation (using measurements), determining the gradients for solving a non-smooth objective function has many practical difficulties [171]. Therefore, the non-smooth objective function used in [159] is approximated to a smooth valued function. Also, as the direct SNR measurements are not available, RSS measurements are used instead. Hence a smooth objective function in equation (6.7) using a smoothing approximation proposed in [172] to approximate the non-smooth min function is used in this work.

$$f(p_r) = -\log(\exp(-RSS_c(p_r, p_c)) + \exp(-RSS_s(p_r, p_s))) \text{ s.t. } p_r \in \{p_{min}, p_{max}\} \in \mathbb{R}^2.$$

(6.7)

6.4.2.2   Optimisation method

optimisation methods using only an approximated gradient (of the objective function) information typically use stochastic optimisation algorithms [143], [159]. Gradient-based methods offers advantages such as the convergence and stability of the gradient-based optimisation methods as mentioned in [159]. The gradients of the objective function are estimated using the RSS measurements and is used to determine the future direction recursively to maximise the objective function. The stochastic gradient ascent (SGA) algorithm iteratively updates the parameters according to the following equations:

$$
\begin{aligned}
x_r^{i+1} &= x_r^i + \gamma^i g_x(p_r^i), \\
y_r^{i+1} &= y_r^i + \gamma^i g_y(p_r^i), \\
\text{where } g_{x_r}(p_r^i) &= \nabla_x f(RSS_c(p_r^i, p_c), RSS_s^i(p_r^i, p_s)), \\
\text{and } g_{y_r}(p_r^i) &= \nabla_y f(RSS_c(p_r^i, p_c), RSS_s^i(p_r^i, p_s)), \\
\text{and } RSS_c(p_r^i) &= RSS_c^{pl}(\|p_r^i - p_c\|) + \Phi_c^{sh}(p_r^i, p_c) + \Omega_c^{mp}(p_r^i, p_c, t), \\
\text{and } RSS_s(p_r^i) &= RSS_s^{pl}(\|p_r^i - p_s\|) + \Phi_s^{sh}(p_r^i, p_s) + \Omega_s^{mp}(p_r^i, p_s, t).
\end{aligned}
\tag{6.8}
$$

Here $\gamma^i \in \mathbb{R}_+$ is the learning rate (also called "step size") which should always be a positive value to ensure convergence. The selection of this learning rate is crucial to obtain fast convergence [173] and should satisfy the conditions $\sum_i \gamma_i = \infty$ and $\sum_i \gamma_i^2 < \infty$. The choice of γ will be discussed in the next subsection. The multi-variate gradients $[g_x(p_r), g_y(p_r)] = [\nabla_x f, \nabla_y f]$ of the objective function is determined in the following way:

$$
g_x = \nabla_x f = \frac{\partial f}{\partial x} = \nabla_{RSS} f \cdot \nabla_x RSS = \frac{\partial f}{\partial (RSS_c)} \cdot \frac{\partial (RSS_c)}{\partial x} + \frac{\partial f}{\partial (RSS_s)} \cdot \frac{\partial (RSS_s)}{\partial x},
\tag{6.9}
$$

$$
g_y = \nabla_y f = \frac{\partial f}{\partial y} = \nabla_{RSS} f \cdot \nabla_y RSS = \frac{\partial f}{\partial (RSS_c)} \cdot \frac{\partial (RSS_c)}{\partial y} + \frac{\partial f}{\partial (RSS_s)} \cdot \frac{\partial (RSS_s)}{\partial y},
\tag{6.10}
$$

$$
\text{where } \frac{\partial f}{\partial (RSS_c)} = \frac{e^{RSS_s}}{e^{RSS_c} + e^{RSS_s}} \text{ and } \frac{\partial f}{\partial (RSS_s)} = \frac{e^{RSS_c}}{e^{RSS_c} + e^{RSS_s}}.
\tag{6.11}
$$

Here the position of the relay node (x_r, y_r) has been replaced with (x, y) for notational simplicity. The above method is called the stochastic gradient ascent method because the objective function has both deterministic and stochastic parts as it's a function of RSS (section 2.2) and therefore the stochastic gradient is $\nabla f(p_r^i) = g(p_r^i) + \epsilon_i$. The ϵ_i is the noise in the gradient at position p_r^i. The RSS gradients $[\nabla_x RSS, \nabla_y RSS]$ are approximated by measurements at a single position of the relay node. Thus the proposed method attempts to increase robustness and achieve fast convergence by using the concept of stochastic gradient ascent [174].

The convergence of gradient ascent method requires that the objective function $f(p_r)$ is concave and the gradient $g(p_r)$ is locally Lipschitz continuous [143]. We can show that the chosen objective function $f(p_r)$ is concave as the function $log(exp(|x|) + exp(|y|))$ is convex and hence the negation is concave. It can also be shown that the gradient function $[\nabla_x f, \nabla_y f]$ is locally Lipschitz continuous by showing that, there exists a positive constant $L \geq 0$ such that $\|\nabla f(p_r^{i+1}) - \nabla f(p_r^i)\| \leq L\|p_r^{i+1} - p_r^i\| \ \forall \ p_r^i, p_r^{i+1} \in \mathbb{R}^2$ as $\nabla_{RSS} f$ is an exponential function which is continuously differentiable in a finite set of parameters $RSS \in [RSS_{min}, RSS_{max}]$ and hence locally Lipschitz continuous. Though global optimum can be reached if $f(x)$ is strictly concave, the stochastic nature of the RSS is not in favour of this phenomenon and hence the objective function has multiple local optima. With careful preprocessing techniques (discussed in section 6.4.3.1) the local optima issue can be mitigated.

The key factor driving the choice of a stochastic optimisation method (as a solution to Problem 2) is that the environmental factors affecting the RSS are not known a priori and hence an optimisation method that is both adaptable (to environmental changes) and robust (to noise) is needed. Stochastic optimisation methods can work with noisy gradient measurements, which is a vital requirement because the RSS measurements usually contain random variations which can be treated as the measurement noise in the optimisation problem. The stochastic optimisation algorithm is devised to increase robustness and guarantee local optimum at each iteration.

6.4.2.3   Multi-sensor sampling

The intention is to provide a sampling method that is both simple to implement in different hardware platforms and reliable to guarantee performance. Therefore multiple wireless devices are installed to act as sensors and enhance reliability and redundancy in wireless networking. The concept of multi-sensor spatial diversity is implicitly utilised for measuring gradients instead of methods such as least squares gradient estimation (LSGE) method [138], [159], search based methods [175] and multi-antenna spatial diversity techniques [139], [160], [165]. Four sensors are distributed spatially around the centre of the relay node to measure the RSS_c and RSS_s at appropriate spatial locations (as shown in the figure 6.6a) that help us to determine the RSS gradients. Finite differences methods such as "Forward Finite Difference (FFD)" and "Central Finite Difference (CFD)" methods are typically used to estimate the gradient using measurements spatially distributed about a central point [173]. The RSS gradients of the client node $[\nabla_x RSS_c, \nabla_y RSS_c]$ and of the server node $[\nabla_x RSS_s, \nabla_y RSS_s]$ are obtained using the

derivative approximations with the CFD algorithm as shown below:

$$\nabla_x RSS_c = \frac{\partial RSS_c}{\partial x} \doteq \frac{RSS_c(x + \Delta x, y) - RSS_c(x - \Delta x, y)}{2\Delta x}, \tag{6.12}$$

$$\nabla_y RSS_c = \frac{\partial RSS_c}{\partial y} \doteq \frac{RSS_c(x, y + \Delta y) - RSS_c(x, y - \Delta y)}{2\Delta y}, \tag{6.13}$$

$$\nabla_x RSS_s = \frac{\partial RSS_s}{\partial x} \doteq \frac{RSS_s(x + \Delta x, y) - RSS_s(x - \Delta x, y)}{2\Delta x}, \tag{6.14}$$

$$\nabla_y RSS_s = \frac{\partial RSS_s}{\partial y} \doteq \frac{RSS_s(x, y + \Delta y) - RSS_s(x, y - \Delta y)}{2\Delta y}. \tag{6.15}$$

Here, Δx and Δy are the spatial separations of the RSS sensors along x and y axis respectively on the relay node and depends on the physical constraints of the relay node. The authors in [173] show that the CFD method gives a much lower deterministic error than FFD method and in the CFD scheme, the stochastic error in gradient estimation is four times better than the FFD scheme. This fact is already proven experimentally in the section 5.1 in which is has been shown that the CFD algorithm has better performance than the FFD algorithm. Hence the proposal is to use CFD algorithm as a solution to Problem 3. Based on the gradient estimation method shown in equation (6.11), the optimisation method in equation (6.8) becomes,

$$
\begin{aligned}
x_r^{i+1} &= x_r^i + \gamma_c^i \left(\nabla_{RSS_c} f \cdot \|\nabla_x RSS_c\| \right) + \gamma_s^i \left(\nabla_{RSS_s} f \cdot \|\nabla_x RSS_s\| \right), \\
y_r^{i+1} &= y_r^i + \gamma_c^i \left(\nabla_{RSS_c} f \cdot \|\nabla_y RSS_c\| \right) + \gamma_s^i \left(\nabla_{RSS_s} f \cdot \|\nabla_y RSS_s\| \right).
\end{aligned}
\tag{6.16}
$$

As gradient measurements are used mainly for determining the next direction of movement, the gradient measurements are normalised as unit vectors along x and y coordinates using the l^2 norm to minimise errors due to noise in the gradient measurements.

$$
\begin{aligned}
\|\nabla_x RSS_c\| &= \frac{\nabla_x RSS_c}{\sqrt{(\nabla_x RSS_c)^2 + (\nabla_y RSS_c)^2}}, \|\nabla_y RSS_c\| = \frac{\nabla_y RSS_c}{\sqrt{(\nabla_x RSS_c)^2 + (\nabla_y RSS_c)^2}}, \\
\|\nabla_x RSS_s\| &= \frac{\nabla_x RSS_s}{\sqrt{(\nabla_x RSS_s)^2 + (\nabla_y RSS_s)^2}}, \|\nabla_y RSS_s\| = \frac{\nabla_y RSS_s}{\sqrt{(\nabla_x RSS_s)^2 + (\nabla_y RSS_s)^2}}.
\end{aligned}
\tag{6.17}
$$

The learning rate γ is optimised to be high at initial iterations and low at the end of convergence [175]. A natural choice for the learning rate that exhibits such behaviour is $\gamma_c^i = \frac{\kappa}{RSS_c^2}$ and $\gamma_s^i = \frac{\kappa}{RSS_s^2}$ to enable the accelerated convergence when the relay node is farther from the optimum (lower RSS) and decelerated convergence and stabilisation when the optimum (higher RSS) has almost been reached. The values of κ are selected empirically. This learning rate selection will make sure the convergence to a local minimum as the learning rate asymptotically satisfies $\sum\limits_{n=1}^{\infty} \gamma_k \to \infty$ and $\gamma_k \to 0$ as $n \to \infty$ where n is the number of iterations.

6.4.2.4 Controller design

A closed-loop incremental position controller as shown in figure 6.10 is devised as the solution for the Problem 4. The robust stochastic optimisation algorithm consists of the following sub-modules: Multi-sensor RSS sensing, temporal and spatial smoothing, gradient estimation using CFD method, gradient normalisation, and SGA algorithm. The motion dynamics is controlled using a position controller acting on the relay node. The radio environment variables are unknown (hidden) to the algorithm as indicated in the figure 6.10. The spatial and temporal smoothing of RSS are discussed in section 6.4.3.1. The controller is stopped on meeting both of the following two conditions:

- The absolute value of the difference in average values of the RSS from server and client nodes is less than the RSS Threshold, $|\widetilde{RSS_c} - \widetilde{RSS_s}| < RSS_{\text{threshold}}$;

- The l^2 norm of the gradient is less than the gradient threshold (when it becomes close to zero), $\|g\| < g_{\text{threshold}}$.

In addition to the algorithmic parameters such as $\Delta x, \Delta y, \kappa$ and stop criterion parameters such as $RSS_{\text{threshold}}, g_{\text{threshold}}$, the inputs to the algorithm are relay node position $p_r^i = (x_r^i, y_r^i)$ and four RSS measurements each for server and client sides. The next subsection presents the implemented algorithm.

6.4.3 Algorithm

Assuming that the relay node moves on a 2D surface (X, Y) with the current position of the relay node as (x^i, y^i), the RSS values at four receivers on the relay node from server node as $RSS_s^i(x \pm \Delta x, y \pm \Delta y)$ and from client node as $RSS_c^i(x \pm \Delta x, y \pm \Delta y)$ at instant i, the robust stochastic optimisation algorithm is expressed in algorithm 5. The aim of the algorithm is not to reach the global optimum in one iteration but to reach the global optimum progressively after several iterations. The proposed algorithm measures only the relative direction of the nodes and uses RSS measurements only in a very basic and thus robust way.
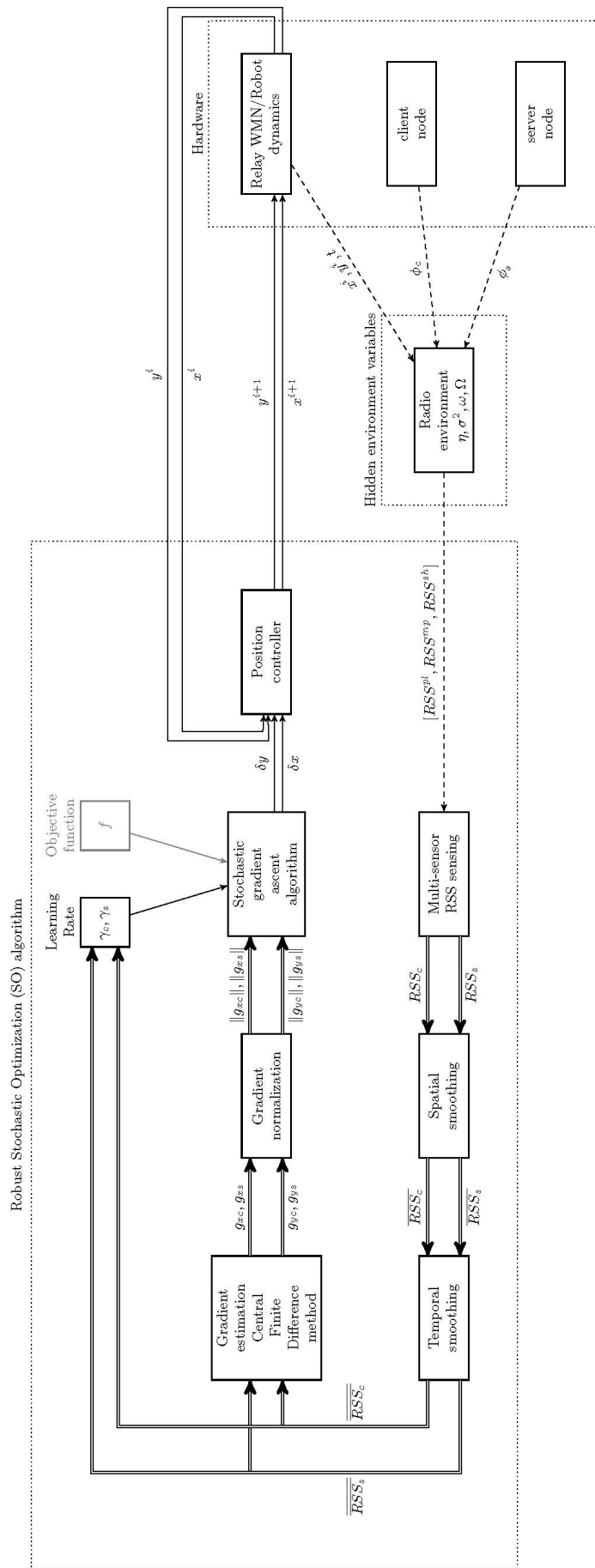
Figure 6.10: Schematic view of the proposed position controller implementing the robust stochastic optimisation (RSO) algorithm.

Algorithm 5 Robust stochastic optimisation (RSO) algorithm for RSS balancing between two mobile robot nodes.

1: Inputs: $x^i, y^i, RSS_c^i(x \pm \Delta x), RSS_c^i(y \pm \Delta y), RSS_s^i(x \pm \Delta x), RSS_s^i(y \pm \Delta y)$
2: Outputs: x^{i+1}, y^{i+1}
3: Parameters: $\Delta x, \Delta y,$
4: Multi-sensor spatial sampling ()
5: {
6: $RSS_c = [RSS_c(x + \Delta x), RSS_c(x - \Delta x), RSS_c(y + \Delta y), RSS_c(y - \Delta y)]$
7: $RSS_s = [RSS_s(x + \Delta x), RSS_s(x - \Delta x), RSS_s(y + \Delta y), RSS_s(y - \Delta y)]$
8: }
9: $[\overline{RSS_c}, \overline{RSS_s}] = $ Spatial Filtering(RSS_c, RSS_s)
10: $[\overline{\overline{RSS_c}}, \overline{\overline{RSS_s}}] = $ Temporal Filtering$(\overline{RSS_c}, \overline{RSS_s})$
11: **while** $(|average(RSS_s) - average(RSS_c)| \not\leq RSS_{\text{threshold}})$ and $(\|g^i\|_{l^2} \not\leq g_{\text{threshold}})$
    do
12:     Multi-sensor spatial sampling ( )
13:     Gradient Estimation $(\overline{\overline{RSS_c}}, \overline{\overline{RSS_s}})$
14:     {
15:     $\nabla_x RSS_c = \frac{\overline{\overline{RSS_c}}(x+\Delta x) - \overline{\overline{RSS_c}}(x-\Delta x)}{2\Delta x}, \nabla_y RSS_c = \frac{\overline{\overline{RSS_c}}(y+\Delta y) - \overline{\overline{RSS_c}}(y-\Delta y)}{2\Delta y}$
16:     $\nabla_x RSS_s = \frac{\overline{\overline{RSS_s}}(x+\Delta x) - \overline{\overline{RSS_s}}(x-\Delta x)}{2\Delta x}, \nabla_y RSS_s = \frac{\overline{\overline{RSS_s}}(y+\Delta y) - \overline{\overline{RSS_s}}(y-\Delta y)}{2\Delta y}$
17:     $\nabla_{RSS_c} f = \frac{e^{(RSS_s)}}{e^{(RSS_c)} + e^{(RSS_s)}}, \nabla_{RSS_s} f = \frac{e^{(RSS_c)}}{e^{(RSS_c)} + e^{(RSS_s)}}$
18:     }
19:     Gradient Normalisation $(\nabla_x RSS_c, \nabla_y RSS_c, \nabla_x RSS_s, \nabla_y RSS_s)$
20:     {
21:     $\nabla RSS_c = \sqrt{\nabla_x RSS_c^2 + \nabla_x RSS_c^2}, \nabla RSS_s = \sqrt{\nabla_x RSS_s^2 + \nabla_x RSS_s^2}$
22:     $\|\nabla_x RSS_c\| = \frac{\nabla_x RSS_c}{\nabla RSS_c}, \|\nabla_y RSS_c\| = \frac{\nabla_y RSS_c}{\nabla RSS_c}$
23:     $\|\nabla_x RSS_s\| = \frac{\nabla_x RSS_s}{\nabla RSS_s}, \|\nabla_y RSS_s\| = \frac{\nabla_y RSS_s}{\nabla RSS_s}$
24:     }
25:     Stochastic Gradient Descent $(\|\nabla_x RSS_c\|, \|\nabla_y RSS_c\|, \|\nabla_x RSS_s\|, \|\nabla_y RSS_s\|)$
26:     {
27:     $g_{xc} = \nabla_{RSS_c} f \cdot \nabla_x RSS_c, g_{xs} = \nabla_{RSS_s} f \cdot \nabla_x RSS_s$
28:     $g_{yc} = \nabla_{RSS_c} f \cdot \nabla_y RSS_c, g_{ys} = \nabla_{RSS_s} f \cdot \nabla_y RSS_s$
29:     $g_x = g_{xc} + g_{xs}, g_y = g_{yc} + g_{ys}, \|g\| = \sqrt{g_x^2 + g_y^2}$
30:     $\delta x = \gamma_c g_{xc} + \gamma_s g_{xs}, \delta y = \gamma_c g_{yc} + \gamma_s g_{ys}$
31:     }
32:     Relay Node Position Controller $(x^i, y^i, \delta x, \delta y)$
33:     {
34:     $x^{i+1} = x^i + \delta x$
35:     $y^{i+1} = y^i + \delta y$
36:     }
37:     Move the relay node to position (x^{i+1}, y^{i+1})
38: **end while**

Sensors spatial separations Δx and Δy depends on the physical constraints of the relay node. For instance, in the youBot, the feasible maximum values are $\Delta x \leq 0.38\,\text{m}$ and $\Delta y \leq 0.58\,\text{m}$. The $RSS_{\text{Threshold}}$ is an important factor that determines the stopping condition of the algorithm because only when the current RSS is below this threshold, improving the RSS will be fruitful

as can be inferred from figure 6.9. Another stop criterion is reaching the minimum gradient threshold, which is derived empirically.

6.4.3.1   Preprocessing of the RSS data

The RSS is measured using a metric called Radio Signal Strength Indicator (RSSI) [66]. As the RSSI metric need to be filtered for noise [176] in both spatial and temporal dimensions, separate RSS filters for spatial and temporal smoothing are integrated in the proposed algorithm such that the measurement noises and multipath fading effects can be mitigated. This preprocessing step is common to both simulation and experimental implementation.

Spatial smoothing   The multipath fading effects (RSS^{mp}) can be mitigated by linear spatial averaging of the RSS measurements with several measurements per wavelength λ of the radio signal used [177]. In [144], it is mentioned that there should be a minimum spacing of 0.38λ between two RSS spacial samples to obtain independent uncorrelated measurements. Therefore, assuming that the $2.4\,\text{GHz}$ ($\lambda = 12.5\,\text{cm}$) radio frequency band is used, the spatial sampling frequency (f_s) has been set to a value greater than or equal to $5\,\text{cm}$, meeting both the minimum spacing for uncorrelated measurements as well as the resolution needs of the linear spatial averaging (around 2.5 measurements per λ). An averaging filter is proposed for the RSS spatial smoothing when the relay node is moving from (x^i, y^i) to x^{i+1}, y^{i+1} as shown in the following equation:

$$\overline{RSS} = \sum_{k=1}^{N} RSS^k \quad \text{where, } N = \frac{\|((x^{i+1}, y^{i+1}) - (x^i, y^i)\|}{f_s}. \tag{6.18}$$

At each receiver, the RSS sampling time is $t_s = f_s \nu$ where ν being the velocity of the relay node. This means that the outcome of the smoothed $\overline{RSS}$ will be the RSS sample at $(x^{i+\frac{1}{2}}, y^{i+\frac{1}{2}})$ instead of (x^{i+1}, y^{i+1}). As the concentration is chiefly on the RSS gradient measurements, this spatial averaging has a positive impact [138].

Temporal smoothing   An exponential moving average (EMA) filter is proposed for smoothing large changes in the RSS over a given time. This temporal smoothing helps in mitigating temporal multipath fading effects and smoothing out noise in the measurements. The implementation is similar to a discrete first order Infinite Impulse Response (IIR) or a single-pole low-pass filter that has a recursive feedback. The filter is characterised by the equation (6.19).

$$RSS^i = \alpha RSS^i + (1 - \alpha)RSS^{i-1} = RSS^{i-1} + \alpha(RSS^i - RSS^{i-1}). \tag{6.19}$$

Where, $0 \leq \alpha \leq 1$ is the smoothness parameter that yields the filter time constant $\tau_f = \Delta_T(\frac{1-\alpha}{\alpha})$. Δ_T is the RSS sampling period used in the temporal smoothing.

6.4.4 Simulation experiments

The proposed Robust Stochastic Optimisation (RSO) algorithm is first evaluated with simulations before moving to field experiments. This section begins with presenting the types of simulation cases and evaluation methods and metrics. This is followed by presentation of the simulation setup and finally present the results with analysis. The following simulation cases are considered:

Case 1: Considering a LOS scenario without spatio-temporal noise

In this case, the radio signals are presumed to be not blocked by large obstacles and hence the RSS has line-of-sight propagation from the source to the destination device. Also, the RSS spatial variations due to shadowing effects (RSS^{sh}) are assumed to be negligible as the environment is free of obstacles, and the multipath fading effects on RSS (RSS^{mp}) is filtered out completely;

Case 2: Considering a LOS scenario with spatio-temporal noise

In Case 2, LOS conditions are presumed. However, the RSS spatial variations due to shadowing and multipath effects (RSS^{sh}) are considered to some extent in spite most of the variations in the RSS (including the measurements noise of the device) are presumed to be filtered out;

Case 3: Considering a NLOS scenario with spatio-temporal noise

In this case, the radio signals are presumed to have no direct line-of-sight between wireless devices and suffer blockage by several obstacles in the environment and hence qualify for NLOS conditions. Verifying the NLOS conditions are relevant to the algorithm because the relay node aims to overcome the NLOS barriers in radio propagation and convert the relayed channel to "LOS + LOS" (two LOS) links through relay node instead of a single (direct) NLOS link without relay node. The variations in RSS due to shadowing and multipath effects are considered similar to case 2.

6.4.4.1 Simulation setup

A realistic radio signal strength environment is simulated using Matlab. The pseudo-code in algorithm 6 shows the principle of the simulation setup. The simulation setup uses the extended log-normal shadowing model given in the equation (2.3). The radio environment parameters are set based on the empirical observations made in the section 4.1.2 and the Gaussian noises

(std_{space} and std_{time}) are set according to the simulation cases. The radio source (transmitter) is fixed at (0,0) and the distance from the source to the receiver (relay robot) is calculated based on Euclidean (l^2) norms.

Algorithm 6 Simulation setup for the 2D RSS environment.

```
receiver_position = (rx ry) % Initial position of the relay node
transmitter_position = (tx ty) % Initial position of the client node
P_t = 17 % Transmit power (dBm) of the transmitter
d_0 = 1 % Reference distance d_0 (m)
P_{d_0} = -25 % Received power at the distance d_0
PL_{d_0} = P_t - P_{d_0} % Path loss at the reference distance
n = 2.52 % Path loss exponent for LOS scenario
std_{space} = rand(x,y,2) % Std. deviation of Gaussian noise in spatial domain (x,y)
std_{time} = rand(2) % Std. deviation of Gaussian noise in temporal domain
for x in 1 to 100
    for y in 1 to 100
        if (x,y) == (rx,ry)
            rss(i,j) = 0
        elseif (x,y) == (tx,ty)
            rss(x,y) = P_t
        else
            rss(x,y) = P_t - PL_{d_0} - 10η log_10( (√((x-rx)²+(y-ry)²))/d_0 ) - std_space(x,y) - std_time
        end
    end
end
```

In the real simulation, there are two transmitter nodes, namely the server and client nodes. The receiver is the relay node. The positions of server node and client node are fixed at (-30,0) and (30,0) respectively. The position of the relay node is chosen randomly based on the simulation cases. The environmental path loss parameter η is chosen according to the real experimental observations in [18]. In a NLOS scenario, η is different for different links (relay-server link and relay-client link). The channel noise in the radio signals are not accurately measurable by most of the commercial wireless transceivers, therefore the measurements are restricted to only the RSS values as opposed to considerations in [141], [159].

Figure 6.11 plots the histogram of the standard deviation of the RSS values measured in a tunnel environment at CERN. As it is clear from the figure that the stochastic parts (Shadowing and multipath effects) of the RSS are indeed Gaussian [136], it is modelled as spatio-temporal noise in the RSS measurements using Gaussian random variables in the simulations. It is found in measurements that the standard deviation of the spatial RSS due to shadowing can be as low as $0.5\,\mathrm{dBm}$ to as high as $2\,\mathrm{dBm}$ with average of about $1\,\mathrm{dBm}$ at each point in space. Hence in simulations the stochastic noise in RSS as set $2\,\mathrm{dBm}$ to replicate an as realistic environment as possible. A simulated RSS environment for server and client nodes is shown in figure 6.12 with (a variance of $4\,\mathrm{dBm}^2$) and without Gaussian noise in the RSS.
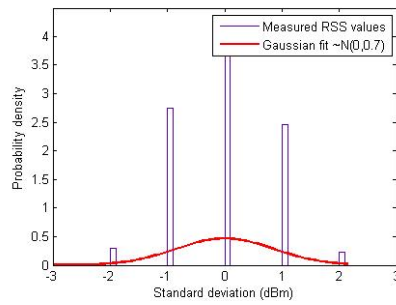
Figure 6.11: Histogram of the RSS variations.
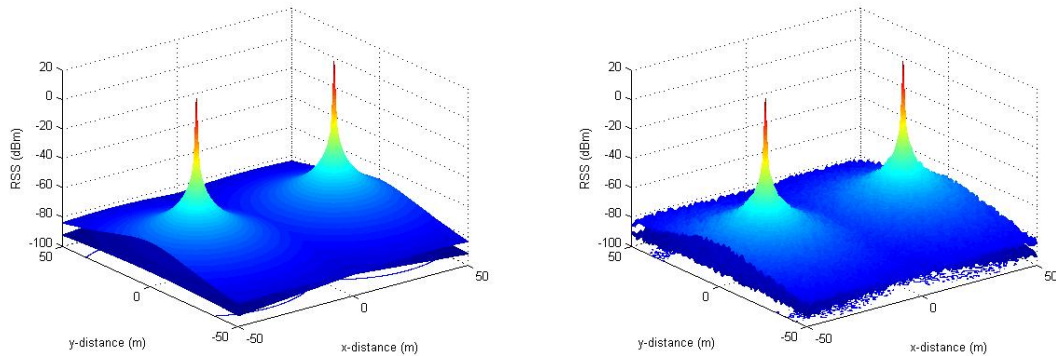
(a) 2D simulation without Gaussian noise.   (b) 2D simulation with a Gaussian noise $\mathbb{N}(0, 4)$.

Figure 6.12: Simulation of the radio field (environment) in 2D Cartesian space (x, y). The server node is placed at (30,0) and the client node is placed at (-30,0).

6.4.4.2 Simulation results

Algorithm 5 is also implemented in Matlab for evaluating its performance in the simulated RSS environment. Each simulation case is run for 100 trials and the average performance results are considered. The following metrics are considered for presenting and comparing the performance results for different cases and considerations.

MAE (m): The mean absolute distance error in reaching the theoretical global optimum position,

RMSE (m): The root mean squared error in reaching the global optimum position,

Success rate (%): The percentage of success in reaching a threshold zone around the theoretical global optimum. The threshold zone is the radial zone around the theoretical optimum and the radius is determined by considering the 10% of the total distance between the initial relay node position and the theoretical global optimum position,

Distance cost (m): The total distance (Euclidean norm) travelled from the initial position to the theoretical optimum position,

Time cost (#iter): Time taken in reaching the optimum, measured indirectly using the number of iterations,

Speed of convergence ($\frac{m}{\#iter}$): The speed at which the algorithm converges, measured as: Speed of convergence $= \frac{\text{Distance cost}}{\text{Time cost}}$.

Case 1: LOS scenario without noise The simulation case 1 is implemented as follows. The simulation is executed by placing the relay node initially at random locations all around the simulation grid area in each trial. The intention of this case is to understand the distance range of the relay node from the global optimum position over which the proposed algorithm can prove effective. Figure 6.13a presents the path taken by the relay node from its initial random position (red dots) to the optimum position (green dots) (the client node and server node are shown as blue dots). It can be observed from the figure 6.13b that the lower the initial distance of the relay node from the optimum position, the lower is the speed of convergence. The MAE obtained for this case is 1.7 m (the initial relay node located in a range of 10m to 50m from the optimum) which is well within the 10% threshold zone and the achieved average success rate is 83%.

In reality, the relay node is always at a lower distance range (usually within 5 m) to the global optimum at any given point of time, because the solution using relay node is implicitly dynamic in nature and the relay node keeps optimising its position to reflect the changes in the client or server node positions. Therefore in further simulations, the relay node initial position is fixed at (-15,15) to simulate the worst-case conditions in reality. The results of performance metrics for all the simulation cases are presented in table 6.1.

(a) Path taken by the relay node from an initial position (red) to an optimum position (green). Blue dots indicate the server and client node locations.

(b) Scatter plot of the distance of initial relay node position from the optimum position shown against the speed of convergence.
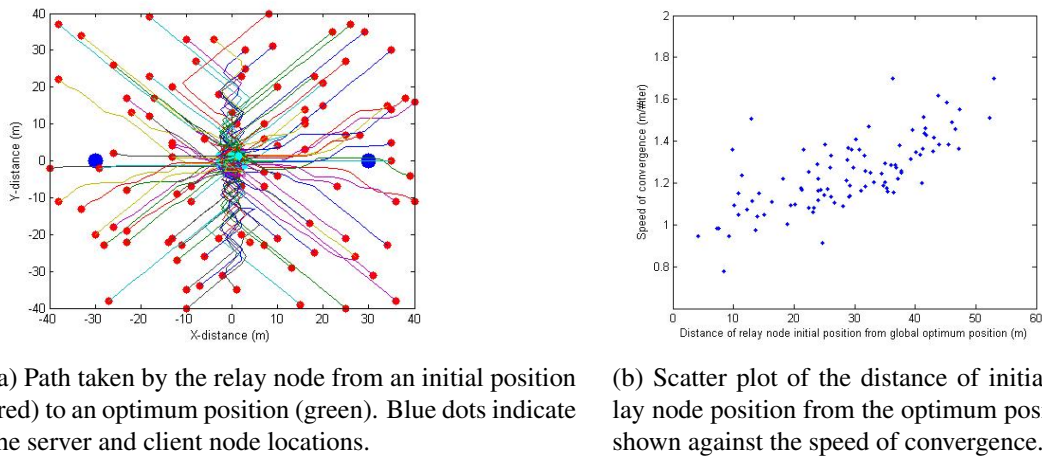
Figure 6.13: Case 1 simulation results for 100 trials with random relay node initial positions.

Case 2: LOS scenarios with Gaussian noises The case 2 is simulated by fixing the path loss parameter η as 2.54 [18]. Two different scenarios are considered, one is using the standard deviation σ of the spatio-temporal Gaussian noise as 1 dBm and another uses $\sigma = 2$ dBm. The

results of simulations are shown in figure 6.14. In both the plots of figure 6.14, the theoretical optimum position without noise is (0,0) and it can be observed that the relay node tries to reach that optimum position. Though the success rate has dropped compared to case 1 results, more than 75% success rate in reaching the optimum position is obtained in Case 2.
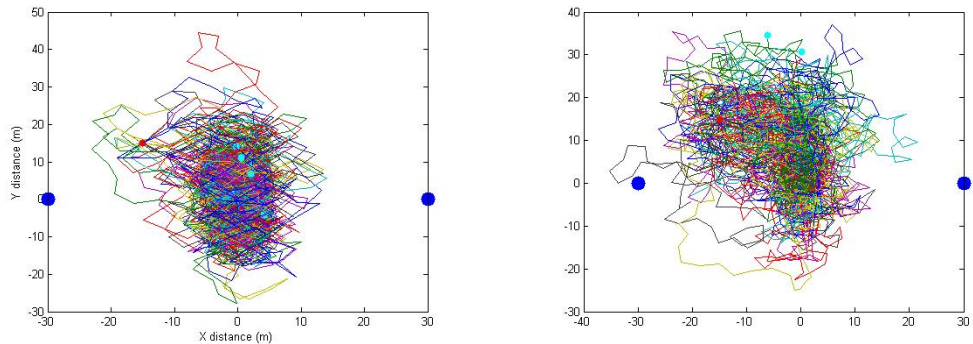
(a) LOS scenario with a 1 dBm spatio-temporal Gaussian noise in RSS.

(b) LOS scenario with a 2 dBm spatio-temporal Gaussian noise in RSS.

Figure 6.14: Case 2 simulation results showing 100 trials of two different noise conditions.

Case 3: NLOS scenarios with and without Gaussian noises In case 3, four different types of scenarios are attempted. The first two are for 1 dBm noise but with different path loss constants η between the relay-client and relay-server link to simulate the NLOS conditions. The last two scenarios are for 2 dBm noise with similar difference in path loss constants. A difference of 0.5 in η can differentiate between a LOS and NLOS condition and a difference of 2 in η (from a LOS condition) can represent a deep NLOS conditions [18]. The results of all the four scenarios are presented in the figure 6.15. The left figures presents the NLOS scenarios without noise so that the optimum position can be observed clearly. The centre figures presents the NLOS scenarios with 1 dBm noise. The right figures presents the NLOS scenarios with 2 dBm noise. These figures contains only the first 10 trials of the actual simulation so that the algorithm behaviour can be observed without ambiguity.

It can be observed from table 6.1 that, as the complexity increases, the success rate drops and the error increases. Figure 6.16 presents the relay node path for a random run in each simulation case overlaid on the value of the objective function (Equation (6.7)). The results show promising convergence to the maximum of the objective function value.

For all the simulation scenarios, the values for sensor separation distances δx and δy are fixed at 0.2 m. (The following) Figure 6.17 provides the influence of sensor separation on the error for LOS condition with 2 dBm noise. It is obvious from this figure that the higher the sensor separation, the lower the error. However the physical limitation of wireless nodes restricts the feasible sensor separation distances.
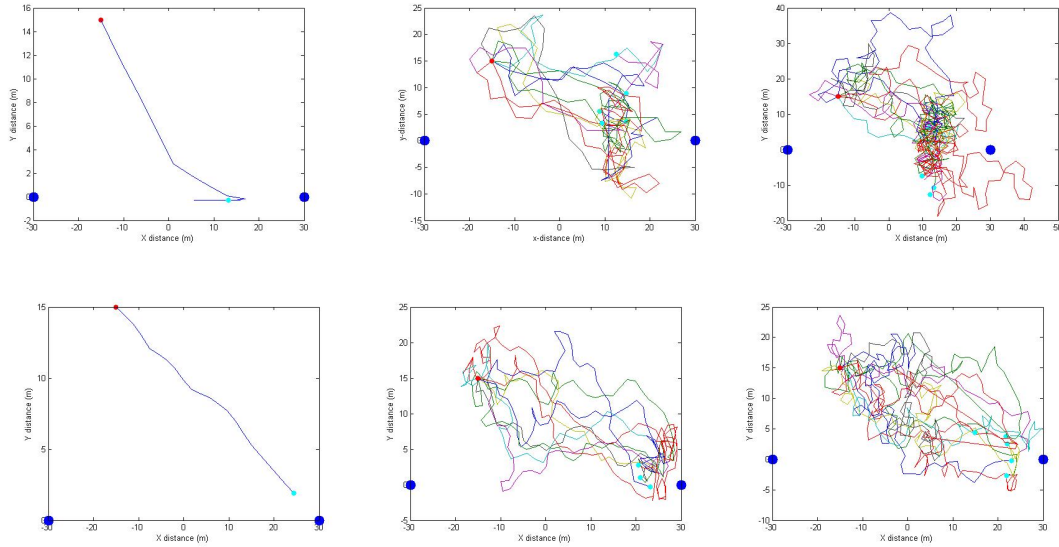
Figure 6.15: Case 3 simulation results showing 10 trials each. Simulation results without noise (Left), with a 1 dBm noise (centre), and with a 2 dBm noise (Right). The results of NLOS conditions are presented in the first row and in the second row, and the results of deep NLOS conditions are presented in the third row.

Scenarios	MAE (m)	RMSE (m)	Distance cost (m)	Time cost (#iter)	Success rate (%)	Speed of Convergence ($\frac{m}{\#iter}$)
Case 1: LOS without noise	1.7	2.1	65.6	49.1	88	1.3
Case 2: LOS with 1 dBm noise	2.3	3.2	120.7	69.0	81	1.7
Case 2: LOS with 2 dBm noise	4.7	7.2	128.3	98.4	76	1.3
Case 3: NLOS with 1 dBm noise	3.3	6.1	161.8	81.9	78	1.9
Case 3: NLOS with 2 dBm noise	6.4	8.6	179.8	90.9	72	1.9
Case 3: deep NLOS with 1 dBm noise	3.7	5.14	210.4	89.2	75	2.3
Case 3: deep NLOS with 2 dBm noise	6.9	9.5	210.1	95.5	65	2.2

Table 6.1: Results obtained for all simulation cases.

The proposed algorithm is principally designed for RSS measurements. However it can also handle SNR measurements without any modifications if the wireless transceivers are capable of measuring noise power (as in [141], [159]) as conveyed in the following discussions.

The RSS is simulated as before and simulate the received noise power (P_N) from a localised external noise source in the environment and then derive the SNR using the equation (2.4). There can be many external noise source depending on the environment. Even though the simulation shown uses one external noise source, the principle can be extended to multiple localised

(a) LOS without noise.

(b) LOS with a 1 dBm noise.

(c) LOS with a 2 dBm noise.

(d) NLOS without noise.

(e) Deep NLOS without noise.

(f) NLOS with a 1 dBm noise.

(g) Deep NLOS with a 1 dBm noise.

(h) NLOS with a 2 dBm noise.

(i) Deep NLOS with a 2 dBm noise.
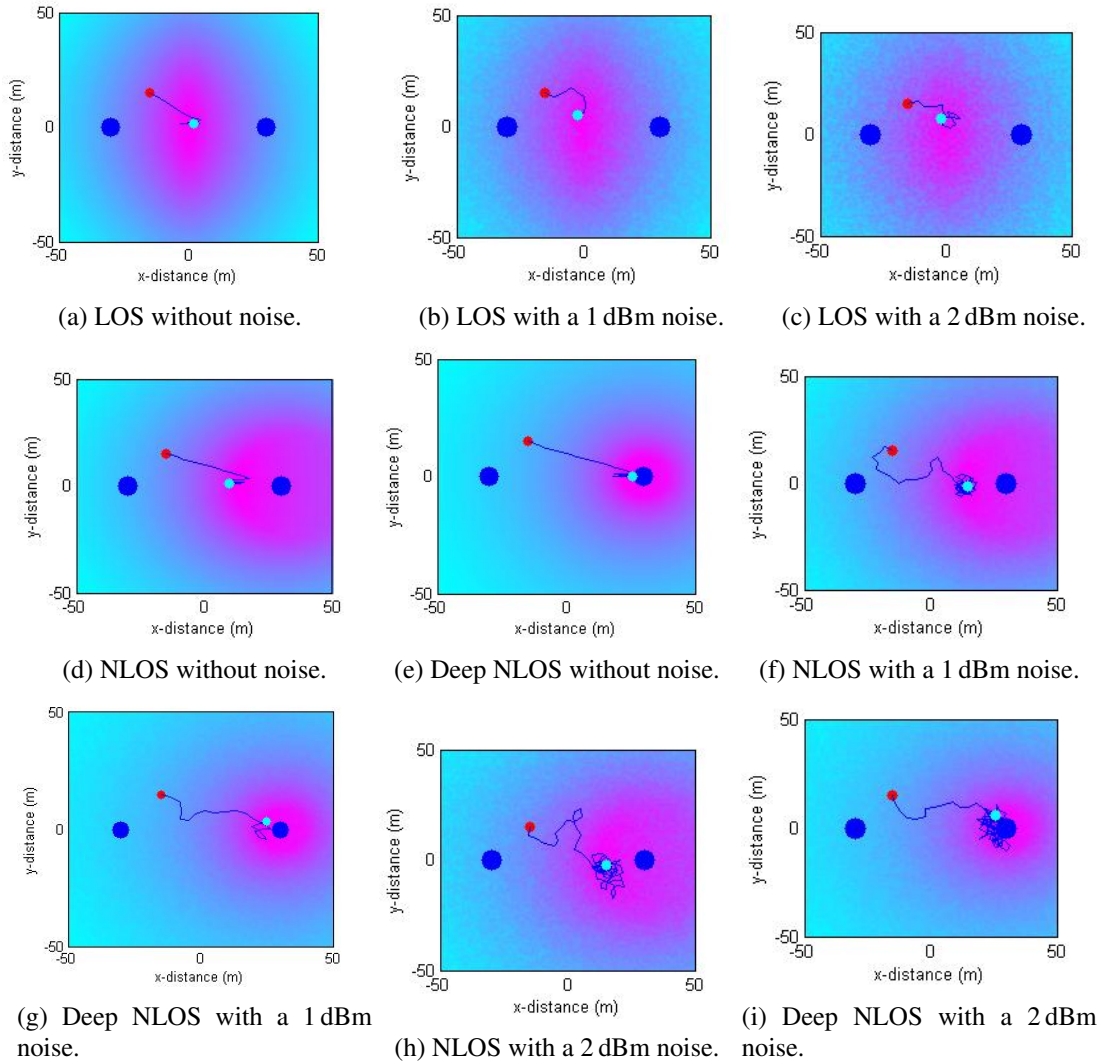
Figure 6.16: Path taken by the relay node and the objective function value for all scenarios during a simulation trial.
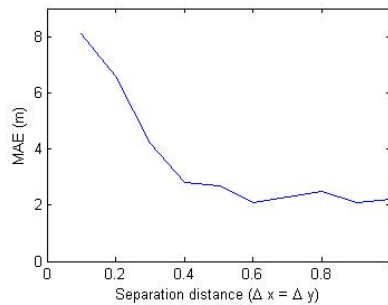
Figure 6.17: Influence of the sensors separation distance on the mean absolute error (MAE) in reaching optimum position.

external noise sources.

In addition to the simulated environment used before, a localised external noise source (with 10% of the power of the server/client signal) is added at $(5, 5)$ in the environment as can be seen

(a) Simulated 2D map of the SNR values. Server node at (-30,0), client node at (30,0), and a localised noise source at (5,5).

(b) Path taken by the relay node in reaching the global optimum overlaid on the objective function value.
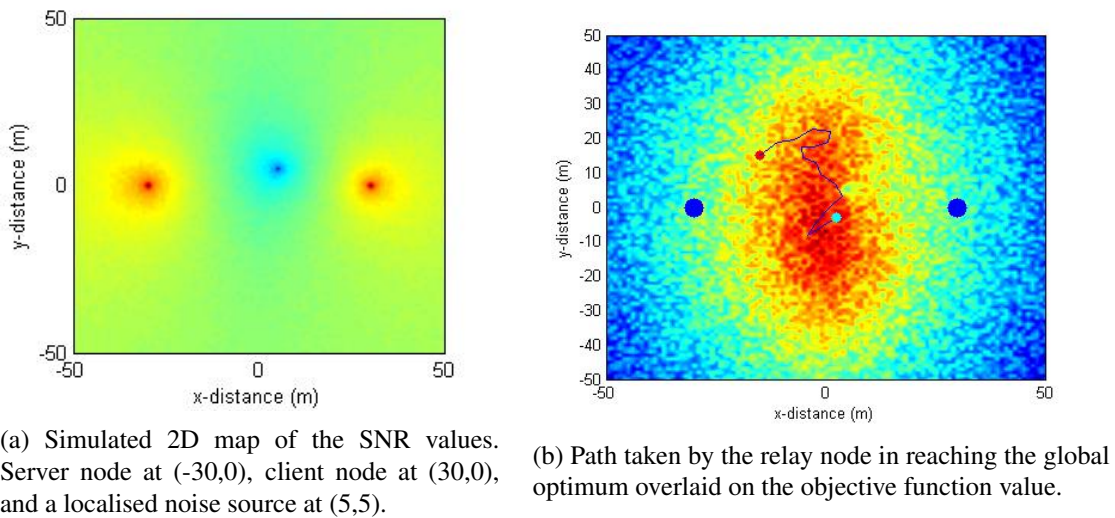
Figure 6.18: A sample simulation using SNR measurements for a LOS scenario with a 2 dBm Gaussian RSS noise and a localised external noise source.

in figure 6.18a. A sample output of simulation case 2 (LOS and Gaussian spatio-temporal noise of 2 dBm) using the SNR measurements is presented in figure 6.18b. The figure 6.18 shows the efficiency of the algorithm in avoiding the external noise location and driving the relay node towards the global optimum adapted to the noisy environment.

6.4.5   Field experiments

In this section, experiments carried out are presented along with the results and their implications. The experiments are conducted in CERN experimental test facilities. A youBot [58] mobile robot platform (shown in figure 6.6a) is used as the relay node and two stand-alone raspberry Pi mini-computers (shown in figure 6.6b) are used as the server and client nodes. As the youBot has omnidirectional wheels, navigation is efficient given the space restrictions in the intended hostile environments. Figure 6.19 show the experimental setup in an indoor facility containing large metallic objects. Due to the nature of the experiments and the confined space in the environment, the need to have an obstacle avoidance feature for the relay node is inevitable. The obstacles are detected if they are within 4 m range of the robot platform using a 2D laser range (LIDAR) sensor and make use of a basic obstacle avoidance system using the vector field histogram technique [178].

As the used robot platform is velocity-controlled, the position controller part of the algorithm is modified to a velocity controller using state-space transitions. The control equations for the relay node located in inertial frame of reference with pose (x, y, θ), are given in equation (5.1).

Because the laser sensor is fitted on the front side of the relay node, the relay robot is made to move only in the forward direction and therefore it will first turn towards the necessary control

direction and then move to the corresponding position. This means that the control output of algorithm has been transferred from the Cartesian space (x, y) to the polar domain (r, θ) as follows:

$$r = \sqrt{x^2 + y^2}, \quad \theta = \begin{cases} \tan^{-1}(y/x) \text{ if } x > 0, \\ \pi + \tan^{-1}(y/x) \text{ if } x < 0. \end{cases} \quad . \tag{6.20}$$
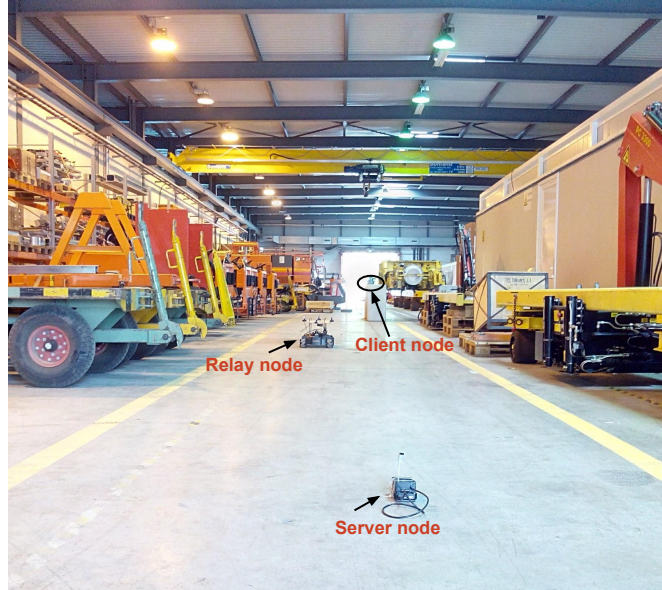
Figure 6.19: Experimental setup showing the server, relay, and client nodes at a CERN facility.

The wireless devices used are the following: Edimax EW-7811un Wi-Fi USB card as the "access points (transmitter)" on the client and server nodes and Zyxel NWD2105 Wi-Fi USB card as the "receiver stations" on the relay node and as RSS sensors. The spatial distribution of the RSS sensors on the relay node can be seen in the figure 6.6a. Each receiver is set to channel 3 in the IEEE 802.11n standard $2.4\,\text{GHz}$ spectrum and all the receivers have same characteristics (internal omnidirectional antenna, receiver sensitivity of -64 dBm). They are placed on the relay node with same orientations to minimise antenna orientation effects in the RSS. The RSS values from the access points at both the server and client nodes are obtained in the form of "received signal strength indicator" ($RSSI$) metric using the `iwlist` command in Linux (E.g., `iwlist interface-name scan`). The Zyxel NWD2105 receiver uses the RALink 2850 wireless driver and the $RSSI$ measurement is equal to the received power in dBm. Each $RSSI$ sample is measured at a $100\,\text{Hz}$ sampling rate and then the corresponding temporal and spatial RSS filters are employed as described in section 6.4.3.1.

As a minimum spacing of 0.38λ (where $\lambda = 12.5\,\text{cm}$ for $2.4\,\text{GHz}$ signal) between two RSS spacial samples is needed to obtain independent uncorrelated measurements [144], the receivers on the relay node are separated with the maximum feasible physical spacing on the robot platform of $20\,\text{cm}$ in each dimension, therefore $\Delta x = \Delta y = 20\,\text{cm}$. This is done to mitigate the effects of interferences between various receivers. It also means that the effects of channel noise and

inter-receiver interferences are negligible between each RSS spacial sample as each sample is measured at more than $\frac{\lambda}{2}$ spacing. Listed below are certain constraints in the experimental setup.

- Due to the fundamental nature of radio signal propagation in real environments, the theoretical global optimum position where the objective function value is maximum cannot be determined without extensive RSS sampling of the complete environment.

- Because of large metal objects in the environment, the radio reflections from such objects constitute a major part of the intensity in the received signal [18] and hence the direction of RSS determined using RSS gradients could point to the metal objects themselves instead of pointing to the actual radio source.

The above mentioned physical constraints and fundamental limitations complicates to determine the performance metrics used in section 6.4.4.2 and therefore mainly the success rate (reaching the 10% threshold of theoretical global optimum position) is reported and prove algorithm performance by showing the continuous improvements in the measured RSS values on both client and server sides.

6.4.5.1 Experimental results

Over 50 different field trials are conducted in both LOS and NLOS conditions to verify the efficiency of the proposed algorithm. The results of various trials are summarised in the table 6.2. An average of 78% success rate (determined based on the final optimal position and the RSS balancing behaviour) is obtained in the field trials. An average of 3.5 dBm improvement in RSS is obtained by a displacement of 1 m by the relay node. In the field experiments, the temporal performance is grounded based on the time taken by the algorithm instead of the number of iterations as used in the simulation trials.

	Mean	Standard deviation
RSS improvement (dBm)	16.7	6.6
Success rate %	78	6.7
Time taken (s)	10.6	3.9
Distance travelled (m)	4.7	4.4

Table 6.2: Summarised results obtained in the field trials.

The obstacle avoidance system also had some impact on the performance of the algorithm as it constrained the free control on the motion executed by the algorithm. Hence the presented results are selected carefully so that the impact on the performance due to obstacle avoidance system is negligible. It is important to note that the theoretical optimum is adjudged as the reference optimum in field experiments which need not be true due to the physical constraints mentioned before. Hence the percentage of cases that have not reached 10% of theoretical
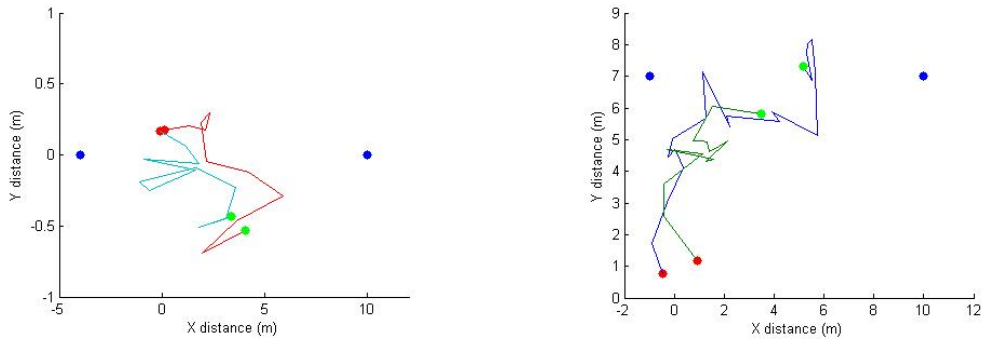
Figure 6.20: Path taken by the relay node when the initial positions are almost the same. Server and client node are shown as blue dots. Red and green dots indicate initial and final relay node position respectively.

global optimum does not necessarily mean that the algorithm failed, however, it means that the real global optimum could be at the position where the relay node reached, for instance, because of NLOS conditions.

Figure 6.20 presents two examples of path taken by the relay node for two similar trials experimented at different times. This is to show that a given radio environment doesn't change significantly with time because of which the path taken is similar.
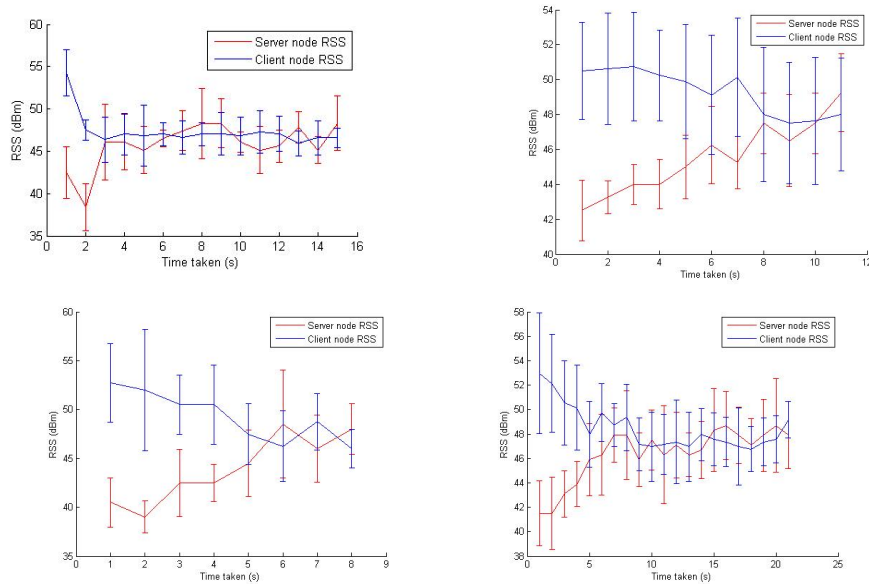
Figure 6.21: Changes in the RSS values of server and client nodes at the relay node during the execution of the algorithm 6.

In figure 6.21, some examples of the RSS balancing (and improvement) behaviour are shown. The error bars are used to represent variations in the RSS values from various sensors on the relay node. It can be observed from this figure that the RSS is balanced quickly within few iterations and then the algorithm maintains the balance in the RSS between server and client nodes.

As a fundamental advantage of the proposed multi-sensor method is the redundancy of wireless networks and the redundancy in communication channel, this method can be useful in environments with radiations which can affect the electronics in the nodes. This work is an initial step towards the goal of automatic optimisation adaptation of the wireless node to hostile environments.

6.5 Summary

This chapter exploited the use of relay robots in enhancing wireless communication qualities for mobile robots in radiation environments. It appeared on analysing the literature review that, the state-of-the-art research solutions possessed drawbacks such as the use of customised hardware with changes at the physical layer (for instance, using directional antennas) and impotent when the radio environment is noisy.

This chapter consisted of two parts. In the first part, a simple but efficient decentralised method inspired by Braitenberg vehicle controller was proposed to balance the RSS between two wireless nodes by optimising the wireless relay robot position. The performance of the proposed method had been experimentally shown. In the second part of this chapter, a robust stochastic optimisation (RSO) method using stochastic gradient ascent algorithm was proposed for RSS balancing and to maximise the wireless network goodput with the help of Server-Relay-Client framework. This method made use of a novel multi-sensor sampling method for measuring radio signal strengths (RSS) spatially distributed about the relay node and integrated special RSS preprocessing techniques such as exponential moving average temporal filter, and averaging spatial filter. The RSO algorithm was demonstrated using simulations and field experiments. The algorithms had been proven to be robust to noise and work effectively under both LOS and NLOS conditions. The algorithms proposed in this chapter could be applied directly at the application layer of the OSI reference model (as against the state-of-the-art solutions that act at the physical layer).

Chapter 7

Conclusions

In hostile or radiation environments, the mobile robots will be equipped with teleoperation capabilities and/or semi-autonomous features to ease the operator overload. This thesis focussed on improving the capabilities of mobile robots for use in CERN's accelerator tunnels where the presence of ionising radiation and the nature of the infrastructure and experimental structures lead to problems with the deployment of mobile robots. After gathering needs and requirements from the end users [31], the project work focussed on robotic applications for remote visual inspection and remote radiation survey tasks. The main research aims were to increase operating range and to avoid the need to send personnel into radiation areas to recover mobile robots in the event of failure during missions. The particular issues identified and addressed were wireless communication in curved and obstructed underground tunnels and problems encountered due to the relatively limited energy storage capabilities of batteries used in mobile robots. It should be noted that the problems have many similarities with those encountered during robotic search and rescue interventions [32].

This thesis provided introductory information on the infrastructures where mobile robots will need to operate, the tasks to be carried out by mobile robots in these environments and the problems encountered that were addressed in the research reported here. The reporting of research work carried out to improve wireless communication (the main subject of this work) comprised an introduction to the relevant radio signal propagation theory and technology followed by explanation of the researched methods. The outcome of the research in this thesis could be summarised by answering the research questions raised in the section 1.3 as follows:

- It was possible to predict the energy consumption of a mobile robot for an assigned task with the help of energy prediction models and such energy prediction models had been shown useful in choosing energy-efficient wireless communication strategies;

- Predicting the wireless communication range(s) of a mobile robot before and during the robotic mission was made possible by using the radio signal strength (RSS) models that incorporate deterministic and stochastic variations with respect to space and time;

- Possibility of optimising (improving) wireless communication qualities had been evaluated by making use of spatial sampling methods and exploiting mobility of the robot. Moreover, the practicality of optimising the communication qualities was demonstrated with a haptic teleoperation application;

- The use of relay robots (and multi-robot system) in enhancing the wireless communication range(s) had been substantiated by establishing an autonomous and robust relay robot positioning mechanism and validating its performance.

In summary, a set of tools are developed in this thesis for improving, easing and making safer robotic missions in hostile environments. Also, this thesis validated with theoretical and experimental procedures that mobile robots could indeed improve wireless communication quality by exploiting robots mobility to dynamically optimise their positions and maintain connectivity even when the (radio signal) environment possess non-line-of-sight characteristics.

The first chapter introduced the practical problems addressed in this thesis, and the motivations behind the research, the research objectives and their potential impacts. The second chapter provided a background on mobile robots and wireless communications, while it also introduced the typical wireless communication requirements for telerobotic applications at CERN and similar scientific facilities, and shown a comparison of available wireless technologies. Conclusions of all the research results contributed in the rest of the chapters of this thesis are presented below.

7.1   Energy prediction models for energy-efficient wireless communication strategies

The operational ranges (time and distance autonomy) of mobile robots are decided mainly by the limitations in the energy and communication devices. Chapter 3 dealt with the prediction of the energy consumption in advance which enables the estimation of energy autonomy of a mobile robot, chiefly to determine the time autonomy. Nonetheless, the distance (locomotion range) autonomy could also be deduced using the time autonomy presuming the velocities for the entire robot paths are known.

In the chapter 3, a generic approach for an on-line energy prediction modelling system for a mobile robot is presented along with applications to energy-efficient wireless communication strategies with an aim to provide increased safety and reliability for robots operating in hostile

environments. The proposed method demonstrated high accuracy ($\geq 96\%$) during tests and can also be used in saving energy by predicting and pre-planning the robotic mission. A simple but effective and adaptive approach is followed so that this energy management feature can be used by many types of small-scale mobile robot (such as differential/skid-steered, wheeled/tracked) as an additional module.

7.2 Radio propagation models for communication range prediction

Chapter 4 dealt with determining the practical communication ranges by predicting the RSS so that the distance autonomy of a mobile robot can be estimated in advance or during the missions.

The research in the first section of the chapter 4 attempted to characterise radio signal propagation in a typical underground scientific facility for telerobotic applications. An extended log-normal shadowing model (ELNSM) for the RSS was used and the model was validated with the experimental results. Considering the requirements for application of wireless video transmission, it is attempted to answer whether readily available wireless technologies such as Wi-Fi offer adequate performance and can be used for the case study application. Experiments have been performed to analyse and the temporal, spatial and environmental characteristics of the radio signal propagation in a ECN3 tunnel area using the link quality measurement parameters such as Received Signal Strength Indicator ($RSSI$), Link Quality Indicator (LQI) and Round Trip Time (RTT).

Eventually it was found that the data rate requirement for the ISOLDE case study application can be met with the present Wi-Fi based system used for the experiments. The distance requirement can be met only under line-of-sight conditions whereas the latency requirement can be met only if the quality of the transmitted videos is reduced. With all the observations, the conclusion is that the Wi-Fi devices used in the experiments can be used for ISOLDE vision system application only if there is a trade-off between the latency and data rate requirements or if a powerful wireless transmitter and receiver (with better transmit power and receive sensitivity) should be required. The HD video is needed because only HD video quality is sufficient to inspect small cracks in the target or the beam dump in the ISOLDE area. As inspecting a crack with a delay is acceptable, for such inspection, the latency requirements are not needed to be strictly met but the data rate has to be strictly met. On the other hand, for teleoperation of the robot, the HD video may not be strictly required and so the video quality can be reduced to meet the strict latency requirements but with a trade-off to the data rate. Even though the experiments were conducted in the ECN3 tunnel area, the results have given intuitive decisions on how to design a better wireless system in the ISOLDE facility.

In the second section of the chapter 4, a fast on-line RSS prediction method was presented. The proposed method took advantages of the Discrete Kalman Filters (DKF) and Radial Basis Function (RBF) kernel function for modelling the deterministic and stochastic (Gaussian process) variations of the RSS in both spatial and temporal domains. As the DKF is a stochastic tool, it integrated both the ELNSM and the stochastic variations of the RSS and provided better RSS filtering and prediction performances compared to the other state-of-the-art methods. A mean prediction accuracy of more than 90% has been achieved in predicting the RSS up to 20m in advance. These experiments validated the radio signal propagation models and exploited their use in off-line and on-line communication range predictions.

7.3   Spatial sampling methods for communication quality optimisation

Improvement of wireless network throughput and communication quality is achieved by improving the radio signal strength (RSS) at the receiver. In chapter 5, decentralised, time-independent, spatial diversity based spatial sampling methods for radio signal strength optimisation are presented. The proposed methods used multiple receivers on a wireless relay robot to improve network reliability and coverage range in challenging environments such as underground scientific facilities where the reflections, interferences and multipath effects of radio signals make wireless communication unreliable. The mobile robot's position was optimised using gradient ascent algorithms to search and receive the best RSS within a localised region. The performance of the proposed algorithms are experimentally demonstrated in the ECN3 tunnel facility at CERN. The proposed time-independent spatial sampling methods are observed to be more efficient than time-dependent methods. In the experiments, the gradient search method based on averaged central difference algorithm performed better than classical central difference and forward/backward difference algorithms in terms of time taken and improvement in the received signal strength. Using multiple wireless receivers also provided an advantage of having redundant networks, with which the chances of wireless network failure could be reduced and the possibilities to recover from failure situations could be increased. It is worth noting that this is a step towards a fully autonomous relay robot that follows the relay/end robots.

In the reminder of the chapter 5, a method that used haptic feedback to allow operators to perceive wireless signal strength when driving a field robot during rescue robot missions and avoid low-wireless signal regions, was proposed and demonstrated with simulated experiments. This type of feedback has shown to be effective as a natural and intuitive way to guide operators into areas with higher wireless signal strength and a series of tests were carried out on environments with randomly generated wireless signal strength maps to demonstrate the effectiveness of this approach. The haptic feedback helped the robot in avoiding the communication loses and helps

to avoid the manual recovery of the robot in case the robot loses communication link. As the mapping is highly customisable, the work performed in this study can be extended to use other types of sensors such as laser scan readings to avoid obstacles. The approach of the haptic feedback to the operator with the RSS, even though overloads the operator, could be influential and pivotal in the development of novel state-of-the-art methods for superior teleoperation of wireless mobile robots in environments with low-wireless signals.

7.4 Relay robots for communication quality enhancement

Research in chapter 6 concerned with the use of relay robots for wireless tethering of radio signals from a server robot (command station) to a client robot (robot performing the actual inspection or manipulation task). As the first contribution of this chapter, a simple but efficient decentralised method was proposed to balance the radio signal strength between two wireless nodes by optimising the wireless relay robot position. The proposed method could improve network reliability and coverage range in challenging environments such as underground scientific facilities where the reflections, interferences and multipath effects of radio signals make wireless communication unreliable. The relay mobile robot's position was optimised by devising a reactive motion controller (to equalise the RSS at both server and client nodes) that used the RSS measurement from two identical wireless transceivers each connected to either client or server node. The performance of the method was proved experimentally using a youBot mobile robot as the relay node and two Raspberry Pi computers as the client and server nodes.

The rest of chapter 6 presented one of the main contribution of this thesis, where a novel method for improving the connectivity of mobile wireless robot nodes was considered. Specifically, a robust stochastic optimisation (RSO) algorithm was proposed, using a stochastic gradient ascent algorithm, for balancing and boosting the received Signal Strength (RSS) between two nodes by optimising the position of the relay node. For the implementation of this algorithm, a multi-sensor setup for the measurement of the received radio signal strengths (RSS) was devised. The sensors were hereby spatially distributed on the relay node, and dedicated preprocessing techniques such as an exponential moving average temporal filtering and an averaging spatial filtering were applied. The proposed method can in principle be implemented in any movable robot platform. The effectiveness of the proposed solution for connectivity improvement was validated, both with simulations and field experiments at a CERN facility, using a mobile robot platform as the relay node and two stand-alone Raspberry Pi computers as the server and client nodes. Around 88% of the experimented simulation cases reached the theoretical optimal position (where the RSS of the relay robot is mathematically optimal and well-balanced between other two wireless nodes) with more than 90% accuracy (N.B. The error is measured in terms of radial distance around the theoretical optimum), whereas the similar rate of success obtained

in the field experiments was 78%. Nevertheless, in the rest of the simulation and field experiment cases (that were considered as non-successful based on the success rate), the algorithm had considerably improved the RSS on both the server and client sides. It should be worth noting that the actual optimum position and theoretical optimum might be different owing to the hostile structure and objects of the environment. Related work was referred to and compared with throughout the development of the algorithm and implementation.

Another fundamental advantage of the proposed solution was the redundancy in the wireless network setup, which implies an increase in robustness. This robustness is needed in hostile environments where fail-safe operations of mobile robot nodes are of supreme importance. This is precisely the application aimed for.

7.5   Future research

The proposed methods were not only intended to be deployed on ground wireless nodes (field robots), but also on unmanned aerial nodes such as in quad-rotors, for example. These proposed solutions can be applied to radiation environments and urban search and rescue robotics scenarios. They have potential to improve wireless communication reliability and redundancy in mobile robots, especially at the environments such as underground facilities where the reflections, interference and multipath effects of radio signals makes the wireless communication unreliable.

Concerning the communication range prediction techniques, further studies could possibly consider the use of directional antennas (on both the transmitter and the receiver robots) so that the radio signals from the transmitter are concentrated only to the receiver and increase the RSS. The main limitation of the proposed on-line RSS prediction method was that it can predict the RSS only in the direction of travel. Therefore, the future plan in this research is to overcome this limitation and to implement a two-dimensional RSS prediction using multi-sensor RSS sampling. Work has already been going on towards this aim.

In communication quality optimisation methods, the main challenges are to develop a cooperative framework and integrating the proposed method with the existing localisation techniques such as Simultaneous Localisation and Mapping (SLAM) methods. This should be addressed in further work. Investigating the burden of cognitive load to the operator when haptic feedback is used for perceiving wireless signal strength can also be nice research in itself.

Regarding the communication quality enhancement methods, future works include the implementation of the current developments in dynamic (changing) environments and improving the algorithm performance by integrating it with SLAM algorithms for better obstacle detection and management. Extension to multi-tier architectures are also an avenue for future research.

Appendix A

Requirements for mobile robots at CERN facilities

A systems engineering V-model (shown in figure A.1) is followed in the research progress in this thesis. As part of the systems engineering process, a survey for needs and requirements for mobile robots in CERN tunnel facilities from the end users are conducted. The summary of the gathered needs is presented in the table A.1.
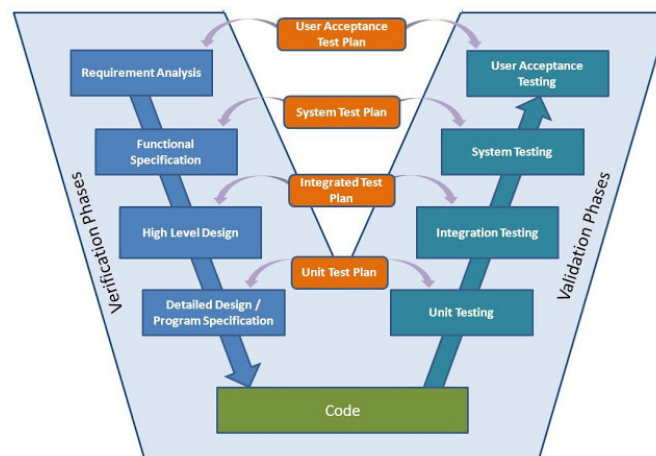
Figure A.1: Systems engineering V-model for life-cycle of product development [29]

A.1 Functions to be performed by the mobile robot

Based on the needs gathered from the end users of robotic applications at CERN, the following are the generic functions needed to be performed by a mobile robot.

- Visual inspection: Visual inspection shall be in colour and the image quality (at least VGA 640x480p in 16 colours) shall permit the assessment of corrosion and small defects (0.5mm at 50cm) with the following needs:

    1. Reach: Visual inspection may be possible behind accelerator equipment such as magnets. The robot shall provide the necessary camera views to allow the operator to position the probe next to relatively delicate beamline equipment;

    2. Lighting: The mobile robot shall be equipped with on-board lighting to ensure that the visual inspection requirements can be met in the absence of ambient lighting.

- Radiation Measurements: The mobile robot shall be able to carry out two types of radiation surveys:

    1. Sparse radiation survey of a zone: for example, follows a path running parallel to the accelerator beamline;

    2. Manipulation of a radiation dose rate monitoring probe: To allow detailed local point measurements to be taken.

- Manipulation: Optionally, the robot may be equipped with a manipulator arm for performing teleoperation with force feedback from the slave arm.

- Surface Contamination measurement: Optionally, the robot may be useful to measure the surface contamination on the floor with the special probe for the surface contamination with the radiation measuring device.

- Finding Hotspots: Optionally, with added intelligence features, the robot may be used to locate the radiation hotspot or the source of radiation leakage when the situation demands.

The requirements and constraints for a communication system is presented below. For control signals, data and camera images between the operator controls and the robot, the following requirements applies for normal operation.

- Radio communication : Bidirectional and Full duplex,

- Minimum line-of-sight distance range: 300 m. Minimum non-line-of-sight distance range: 100 m,

- Use only unlicensed ISM bands,

- Maximum delay (at maximum distance) in video transmission 1000ms (Round Trip Time),

- Maximum delay (at maximum distance) in control movement response 200ms (Round Trip Time),

- Minimum number of channels capable: 02,

- Minimum required data transfer rate (at maximum distance): 1 Mbps,

- Maximum required data transfer rate (at 10 m distance): 10 Mbps,

- Permit safe emergency stop from operator console,

- Provide operator warning before losing signal,

- Have inbuilt redundancy.

A summary of the gathered needs is presented in table A.1. This table shows the information on the functions to be performed by a mobile robot in the intended CERN locations. For the LHC facility, the needs of a ground mobile robot (remote mobile vehicle - RMV) are compared against the needs of the existing TIM robot [3]. More detailed needs and requirements are provided in the requirements document of the concerned research project RP6 in the PURESAFE network reference [30].

A.2 Summary of technical and mission requirements for mobile robots at CERN

A summary of technical and mission requirements for a mobile robot application at CERN are given in tables A.2 and A.3 respectively for two important places (ISOLDE and TDC2) where the mobile robot could greatly help in remote radiation surveys [27], [28]. The table A.2 presents the mobile robot platform requirements such as the payload capability, control and sensing requirements. In the table A.3, the mission requirements such as the type of missions to be performed including the constraints on space and communication are presented.

RMV – NEEDS SPECIFICATION TABLE

Area	Item		Needs for various facilities at CERN						
			LHC		**PS/SPS**	**AD**	**ISOLDE**		**TDC2, CNGS, ELENA, HiRadMat, etc.**
			TIM	**RMV**			**RP**	**Operation**	
Function	Role	Remote visual inspection	1. View whole tunnel section from **any side** (PTZ camera) of the robot. 2. Inspect beam line equipment						
		Remote measurements /other needs	Radiation detailed survey, quick radiation map, Inspect CE pressure gauges.	Radiation detailed survey, quick radiation map	Detailed radiation survey	Detailed radiation survey	Detailed radiation survey	Inspect the ISOLDE robot, Rescue operation when ISOLDE robot fails, Handling the target to transfer to Hotcell	Detailed radiation survey
		Air sampling	No	No	No	Yes	Yes (rare)	No	No
		Contamination measurement	No	Yes	Yes	No	Yes (rare)	No	Yes
	Autonomous capabilities	Finding Hot spot	No	Yes	Yes	Yes	Yes	No	Yes
		Localization	Yes	Yes	Yes	Yes	Yes	Yes	Yes
		Navigation	No	Yes	Yes	Yes	Yes	Yes	Yes
		Repeating tasks	No	Yes	Yes	Yes	Yes	No	Yes

	Speed		Max 12km/h variable down to zero	Max speed = Biking speed (~ 12kmph)	Max speed = Biking speed (~ 12kmph)	Max speed = Walking speed (~ 6kmph)	Max speed = Walking speed (~ 6kmph)	Max speed = Walking speed (~ 6kmph)	Max speed = Walking speed (~ 6kmph)
	Smallest movement		10mm	5cm	5cm	5cm	5cm	5mm	5cm
	Max Payload	**For radiation detectors (500g), cameras (500g * 4), etc.**	Able to pull client wagon of 500kg.	5kg	5kg	5kg	5kg	30kg (weight of Target)	5kg
		Max slope	6.1% Max lateral curvature:2985mm	1.4%	-	-	-		2.7%
		Type of floor	Support rail: LHC monorail IPER180	Mostly flat and smooth	Mostly flat and smooth	Flat. But rough (plastic covers) in some places	Flat and smooth		Mostly flat and smooth
	Space restrictions – cross section for door passage etc.		Pass though opening as defined in LHCHMURT0127	No	No	No	Cables *diameter ~25cm		Ramps used for routing cables/pipeline Width: <1m Length: <1.5m Height: <20cm

Area	Item		Needs for various facilities at CERN						
			LHC – TIM	LHC – RMV	PS/SPS	AD	ISOLDE – RP	ISOLDE – Operation	TDC2, CNGS, ELENA, HiRadMat, etc.
	Space restrictions – length etc		Pass aiguillages Pass toboggan P4 Pass tremies Pass quai P6 Fit in Lift Pass SAS access in RA's etc.	Fit in Lift Pass SAS access in RA's etc.	Pass all the doors (sector and access doors)	Pass all the doors (access doors)	Pass all the doors (access doors)		Pass all the doors (access doors)
	Width restrictions		30cm	Door's width (~80cm)	Door's width	50cm	50cm		Based on Ramp's width
	Height restrictions	Beam-line height	30cm	~120cm	~120cm	~120cm	~120cm		~120cm
		Ability to go under beam line	No	~30cm	<1m	<1m	<1m		~30cm to 1m
	Compatibility with other RMV elements.	Modular concept design	Yes	Yes	Yes	Yes	Yes		Yes
		Compatible with TIM	Yes	Yes	No	No	No		No
	Weight (Self load)	Minimise weight to maximize autonomy	As low as possible. Monorail capacity 2.4t per 4.2m	As low as possible	As low as possible	As low as possible	As low as possible		As low as possible
	Light conditions		Poor	Poor	Poor	Poor	Poor		Poor
Communication and position measurement	Communication with control station	CERN's GSM network available (Present technology used: EDGE, Future: UMTS900)	Yes	Yes	Yes	Yes	Yes		Yes
		WiFi Available	Yes (very limited)	Yes (very limited)	No	No	Yes		May be
Electrical System and autonomy	Battery Charging	Charging when the device is not in operation	Charge batteries remotely from monorail power supply rail when stationary	Manual. Possible to charge through TIM	Manual charging	Manual charging	Manual charging		Manual charging
	Autonomy (between charges)	Max distance for continuous running	15km continuous running without client wagon. 10 days PLC / camera operation without client wagon	2.6km (if sector doors closed) 6 km (return, if sector doors open)	700m (PS, SPS if doors closed) 7 km (if doors open)	200m	200m		1km
Safety	Anti collision	self protection + Protect all other equipments inside the operating area	Yes	Yes	Yes	Yes	Yes		Yes

Table A.1: Summary of needs gathered from the end users of mobile robot applications at CERN

	ISOLDE Facility	SPS North Area (TDC2)
Working time autonomy	Minimum 2 hours	Minimum 2 hours
Communication link	Wireless	Wireless
Remote control distance	Up to 200 m	Up to 200 m
Vision performance	• See features of less than 0.5mm at 50 cm distance • Min. image quality of VGA 640x480p in 16 colours resolution	• See features of less than 0.5mm at 50 cm distance • Min. image quality of VGA 640x480p in 16 colours resolution
Sound capture	Yes	Yes
On-board lighting	Yes	Yes
Control station	Portable station	Portable station
Navigation control	On-board camera	On-board camera
SLAM (self-mapping)	Yes (Optional)	Yes (Optional)
Autonomous anticollision	Yes (optional)	Yes (optional)
Travel speed range	From 0.01m/s to 1 m/s	From 0.01m/s to 1m/s
Stair climbing	No	No
Maximum slope	10%	10%
Minimum Payload	20 kg	20 kg
Minimum self-weight	30 kg	30 kg
Maximum width	600 mm	600 mm
Observation height	Up to 1500 mm	Up to 1500 mm
Vehicle self-rescue	Human intervention	Human intervention

Table A.2: Summary of technical requirements for deploying mobile robots at CERN
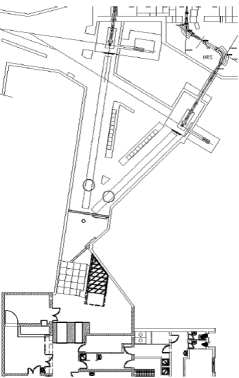
	ISOLDE Facility	SPS North Area
Mission of the RIV	Radiation measurement and Visual and audio inspection during shut downs / technical stops in view of RP, repair and maintenance interventions	Radiation measurement and Visual and audio inspection during shut downs / technical stops in view of RP, repair and maintenance interventions
Examples of missions	• Radiation survey of the area before allowing personnel for interventions • RMV can be used as a base for remote manipulation of tasks (telemanipulation)	• Quick RP survey • Detailed radiation survey around collimators when there is need • Surface contamination measurements
Intervention scene		
Building configuration		
Equivalent dose rate	Up to 300 mSv/h at 40 cm	Up to 150 mSv/h at 10cm
Floor obstacles	Groove (12cm x 4cm), Cables (< 2cm diameter)	Cables, ramps, cable trays, supporting feet, waste
Floor quality	Painted concrete, clean, dry, dust free	Concrete, dirty, possible water leaks
Height limitation	1000 mm	500 mm
Width limitation	600 mm	600 mm
Communication network	• No GPRS (GSM) • No WiFi, but it can be added on purpose	• GPRS (GSM) • No WiFi, but it can be added on purpose

Table A.3: Summary of mission requirements for deploying mobile robots at CERN

A.3   Selection of a mobile platform for use at CERN

Table A.4 shows a comparison of specifications of the mobile robot platforms commercially available. Out of these mobile robotic platforms surveyed, while applying the first selection filter which is the size of the robot (Length<60cm; Width<50cm ; Height<100cm), only the following platforms meets the CERN requirements: Adept's Pioneer DX and AT, KUKA Youbot, Coroware's Corobots, Superdroid's LT treaded robot, K-team's Koala and Khopher, iRobot's iCreate.

The smaller robots like iRobot's iCreate, K-teams' Khoala and Khopher robots cannot carry a payload of more than few Kg, but for the intended applications, payload carrying capacity of greater than 10 Kg is needed. Also, the Coroware's products (Corobots and Explorer) have low payload capacity because of which, they are not suitable for the telerobotic applications at CERN.

The next main filter in the selection is the drive mechanism, which should be either a 4 wheel skid-steered or omni-drive platform so that the robot can easily pass over the obstacles on the floor. The Superdro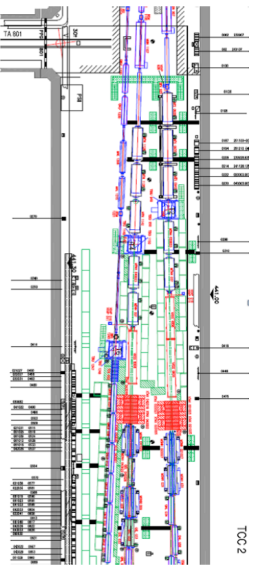id robot is significantly more expensive than the Pioneer AT or youBot robots. Summing up all these criteria, only two robots: Adept's Pioneer AT robot and KUKA youBot, are suitable for the application requirements.

Comparing both these robot's drive mechanisms, omni-drive is preferred because of flexible navigational capabilities. In addition, the user interface (or the human-machine interface (HMI)) can be lot simpler if omni-wheeled movement is used rather than skid-steered movements. Also, ease of navigation with the omni-drive platform will be very useful in radiation measurement applications. The 24V battery voltage of youBot is compatible with wider range of sensors compared to Pioneer AT robot powered by a 12V battery pack. Also, the KUKA youBot platform comes with an inbuilt mini-PC/computer whereas, for Pioneer AT, a laptop/computer has to be purchased additionally to work with. This feature makes the price of Pioneer AT and youBot similar if both the platforms is considered along with a computer.

In addition to all these, the Pioneer AT is a USA product and the KUKA youBot is a German product. Since CERN purchases products from member states where possible, the youBot is preferred to the Pioneer AT. The KUKA youBot is a newly launched product in the market and it is targeted to education, research and training. Hence, the KUKA's youBot mobile base platform has been selected to suit the requirements and environment constraints in the PURESAFE research project.

Robot	Design	Cost	Size (cm3) L.W.H	Weight (self) & Payload	Battery/ Autonomy	Max. Speed	Max. Slope	Motor & Control	Sensors	Onboard Processor	Software	Accessories	Typical Applications	Miscellaneous
Adept "Pioneer DX"	2-Wheel	€4k	L:46 W:40 H:24	W: 9Kg P: 17 Kg	12V 7.2 Ah *2 8-10 hours	4.32 kmph	25%	2-Motor Differen tial Drive	Sonar, Encoder, Laser, Bumper	Optional	ARCOS, Pioneer SDK	Robotic Arm, Audio and Vision, Gyroscopes, etc.	Indoor lab research	Country: USA Warranty: 1 year
Adept "Pioneer AT"	4-Wheel	€8k	L:50 W:49 H:26	W: 12Kg P: 15 Kg	12V 7.2 Ah *2 8-10 hours	2.52 kmph	35%	4-Motor Skid Steer Drive	Sonar, Encoder, Laser, Bumper	Optional	ARCOS, Pioneer SDK	Robotic Arm, Audio and Vision, Gyroscopes, etc.	All terrain operation, lab experiments	Country: USA Warranty: 1 year
CoroWare "CoroBot"	4-Wheel	$8k	L:30 W:33 H:25 H:41 (with arm) H:84 (with kinect	W: 5.5Kg P: 2.2 Kg P(arm): 225g	12V, 10 Ah 2.5 hours	1.64 kmph	-	4-Motor Skid-Steer Drive	4 DOF Gripper Arm with Pressure sensor, Sonar, Encoder, Laser, Bumper	1.2GHz dual-core	Kinect, MRS	Microsoft Kinect, GPS, sensors, etc.	Swarms, manipulation, research, expandable platform	Country: CA Warranty: 90 days, +500$ for 1 year.
CoroWare "CoroBot"	4-Wheel	$8k	L:58 W:53 H:41	W: 13Kg P: 6.8Kg	12V, 13 Ah 2.5-4 hours	2.2 kmph	-	4-Motor Skid-Steer Drive	Sonar, Encoder, Laser, Bumper	533MHz dual-core	MRS	GPS, sensors, etc.	Swarms, manipulation, research, expandable platform	Country: CA Warranty: 90 days, +500$ for 1 year.
Metralabs "SCITOS G5"		€13k	L:58 W:74 H:62	W: 60Kg P: 50Kg	26 V Li-Po 2072Wh 24 hours	5 kmph	-	Differen tial drive	Sonar, Bumper	iPC, Core 2 Duo 2.16 GHz	Kinect, MRS	Laser, cameras, etc.	Mobile monitoring	Country: DE Warranty: 5 years
Superdrio d LT treaded	Tracked wheels	$16k	L:51 W:42 H:19	W: 18Kg	22V 10Ah Li-ion, 3 to 8 hours	5.5 kmph	-	Two (2) planetar y IG52-04 285RPM 24VDC gear motors	4 DOF Flipper/stabi liser arm, includes Control station, 8 channel 2.4GHz PTZ camera, IR sonar, laser, etc.	-	-	Optional: Laser, cameras, etc		Country: USA
K-team "Koala II"	4-Wheel	$11k	L:32 W:32 H:20	W: 4Kg P: 3Kg	4 hours	2.16 kmph	43deg	Differen tial Drive	IR, Sonar, Encoder, Laser	Optional		Various sensors		Country: CH Warranty: 1 year
K-team "Khopher a III)		$6k	Dia: 13 H:7	W: 700g P: 2Kg	1.35Ah 8 hours	1.8 kmph	-	-	IR, Sonar, Encoder, Laser	Optional	Embedde d Linux, VREP 3D	Various sensors		Country: CH Warranty: 1 year
Bluebotics "AMV1"		-	L:67 W:56	P: 150Kg	24V, 10km	5 kmph	10.5%	High torque 24V DC motors	ANT Autonomous navigation	Optional	-	Various sensors		Country: CH Warranty: 1 year
Bluebotics "AMV1"		-	Dia: 70 H: 70	W: 100Kg P: 50Kg	24V, 12 hours	3.6 kmph	-	High torque 24V DC motors	ANT, Laser, encoders, bumpers	Optional	-	Various sensors		Country: CH Warranty: 1 year
Adept "PatrolBot "		$15k		P: 40kg		2 m/s								
KUKA youBot		€10k	58x38 x14	24 Kg 24 Kg	90 minutes	0,8 m/s	30%	4-Wheel Omni drive	Optional	Mini iTX PC-Board Intel Atom	Linux	Various sensors, Wireless Joystick	Education & Research, Flexible navigation	Country: DE Warranty: 1 year
iRobot ICreate		$300	H: 8cm	W: 6Kg	-	-	-	4 wheels	Avoids obstacles, stairs, walls, vacuum cleaning,30 built in sensors	-	iRobot Comman d module			Country: USA Warranty: 1 yr

Table A.4: Comparison of the specifications of commercially available mobile robot platforms

Appendix B

List of publications

Journal papers

- R.Parasuraman, K.Kershaw, and M.Ferre. Experimental Investigation of Radio Signal Propagation in Scientific Facilities for Telerobotic Applications. Int J Adv Robot Syst, 2013, 10:364. doi: 10.5772/56847

- R.Parasuraman, T.Fabry, L.Molinari, M.Di Castro, A.Masi, K.Kershaw, and M.Ferre. A robust multi-sensor RSS spatial sensing method for enhanced wireless tethering in harsh environments. Sensors MDPI, 2014 (Under review)

- R.Parasuraman, L.Molinari, M.Di Castro, A.Masi, and M.Ferre. 2D prediction of radio signal strength for mobile robots in unknown environments. J. Sensors, IEEE, 2014 (To be submitted)

Book Chapters

- R.Parasuraman, P.Pagala, K.Kershaw, and M.Ferre. Energy Management Module for Mobile Robots in Hostile Environments. Advances in Autonomous Robotics, Lecture Notes in Computer Science Volume 7429, 2012, pp 430-431. Springer Berlin Heidelberg. doi: 10.1007/978-3-642-32527-4_45.

Conference papers

- R.Parasuraman, T.Fabry, K.Kershaw, and M.Ferre. Spatial Sampling Methods for Improved Communication for Wireless Relay Robots. 2013 International Conference on Connected Vehicles and Expo (ICCVE), Las Vegas (USA), 2-6 Dec. 2013. doi: 10.1109/ICCVE.2013.6799919

- A.Owen-Hill, R.Parasuraman, and M.Ferre. Haptic Teleoperation of Mobile Robots for Augmentation of Operator Perception in Environments with Low-Wireless Signal. 2013 IEEE International Symposium on Safety, Security, and Rescue Robotics (SSRR), Linköping (Sweden), 21-26 Oct. 2013. doi: 10.1109/SSRR.2013.6719329

- R.Parasuraman, P.Pagala, K.Kershaw, and M.Ferre. Model Based On-Line Energy Prediction System for Semi-Autonomous Mobile Robots. 2014 5th International Conference on Intelligent Systems, Modelling and Simulation (ISMS), IEEE, Langkawi (Malaysia), 27-19 Jan 2014.

Workshop papers and posters

- R.Parasuraman, K.Kershaw, and M.Ferre. Wireless communication for mobile robots in hostile environments. International workshop on telerobotics and systems engineering for scientific facilities, UPM Madrid, Spain. 4th Oct 2012.

- R.Parasuraman, L.Molinari, M.Di Castro, A.Masi, and K.Kershaw. A Fast Radio Signal Strength Prediction Algorithm for Mobile Robots in Unknown Environments. Communication-aware Robotics: New Tools for Multi-Robot Networks, Autonomous Vehicles, and Localization (CarNet) workshop, Robotics: Science and Systems Conference 2014, Berkeley, USA.

Internal reports

- R.Parasuraman. Needs gathered for a mobile platform to be used in remote radiation survey and inspection applications at CERN. CERN EDMS, 1326585, 2011.

- R.Parasuraman. TIM Pre-series energy management system specifications. CERN EDMS, 1318898, 2013.

- R.Parasuraman and A.Stadler. Wireless Video transmission tests in ISOLDE: Remote handling test of ISOLDE target units using radio controlled forklift vehicle with wireless video feedback. CERN EDMS, 1209799, 2012.

- R.Parasuraman. TIM power requirements. CERN EDMS, 1282313, 2013.

- R.Parasuraman. TIM energy management tests protocol. CERN EDMS, 1280191, 2013.

- R.Parasuraman. Selection of commercial mobile platform for PURESAFE research project. CERN EDMS, 1179574, 2012.

Bibliography

[1] K. Nagatani, S. Kiribayashi, Y. Okada, *et al.*, "Redesign of rescue mobile robot Quince", in *2011 IEEE International Symposium on Safety Security and Rescue Robotics*, 2011, pp. 13–18.

[2] R. Murphy, J. Kravitz, S. Stover, *et al.*, "Mobile robots in mine rescue and recovery", *Robotics Automation Magazine, IEEE*, vol. 16, no. 2, pp. 91–103, Jun. 2009.

[3] K. Kershaw, C. Bertone, P. Bestmann, *et al.*, "Remotely Operated Train for Inspection and Measurement in CERN's LHC Tunnel", in *Particle Accelerator Conference 2009, Vancouver, Canada*, Apr. 2009.

[4] K. Nagatani, S. Kiribayashi, Y. Okada, *et al.*, "Emergency response to the nuclear accident at the fukushima daiichi nuclear power plants using mobile rescue robots", *Journal of Field Robotics*, vol. 30, no. 1, pp. 44–63, 2013.

[5] "2007 recommendations of the International Commission on Radiological Protection", *ICRP Publication 103 in Annals of the ICRP*, Feb. 2008.

[6] A. Sullivan, *A guide to radiation and radioactivity levels near high energy particle accelerators*. Nuclear Technology Publishing, 1992.

[7] C. Grupen, *Introduction to Radiation Protection: Practical Knowledge for Handling Radioactive Sources*. Springer Berlin Heidelberg, 2010.

[8] International Atomic Energy Agency, "Occupational radiation protection: protecting workers against exposure to ionizing radiation", in *International Atomic Energy Agency, Vienna. Held in Geneva, 26-30 August*, 2002.

[9] *CERN Safety Code F/Rev. on Radiation Protection*. CERN, Nov. 2006.

[10] T. Wijnands, "ALARA principles: CERN ALARA approach", in *SPS technical coordination meeting 10*, CERN, Oct. 2011.

[11] A. Holmes-Siedle and L. Adams, *Handbook of radiation effects*. Oxford University Press, UK, 1993.

[12]   S. Richard and D. Marc, "Radiation tolerance of components and materials in nuclear robot applications", *Reliability Engineering & System Safety*, vol. 53, no. 3, pp. 291–299, 1996, Safety of Robotic Systems.

[13]   R.A. Horne, "Teleoperator evolution at CERN", in *Proceedings of the International Symposium on Teleoperation and Control, Bristol, UK*, Jul. 1988.

[14]   L. Scibile, D. Forkel-Wirth, H. Menzel, *et al.*, "The LHC radiation monitoring system for the environment and safety", in *Proc. EPAC*, 2004.

[15]   G. Segura Millan, D. Perrin, and L. Scibile, "RAMSES: the LHC radiation monitoring system for the environment and safety", in *Proceedings of the 10th ICALEPS Int. Conf. on Accelerator & Large Expt. Physics Control Systems*, 2005.

[16]   K. Kershaw, F. Chapron, A. Coin, *et al.*, "Remote inspection, measurement and handling for LHC", in *Particle Accelerator Conference, 2007. PAC. IEEE*, Jun. 2007, pp. 332–334.

[17]   K. Kershaw, B. Feral, J.-L. Grenard, *et al.*, "Remote Inspection, Measurement and Handling for Maintenance and Operation at CERN", *Int J Adv Robot Syst*, vol. 10, no. 382, 2013.

[18]   R. Parasuraman, K. Kershaw, and M. Ferre, "Experimental investigation of radio signal propagation in scientific facilities for telerobotic applications", *Int J Adv Robot Syst*, vol. 10, no. 364, 2013.

[19]   S. Duzellier, "Radiation effects on electronic devices in space", *Aerospace Science and Technology*, vol. 9, no. 1, pp. 93–99, 2005.

[20]   R. Schrimpf, "Radiation effects in microelectronics", in *Radiation Effects on Embedded Systems*, Springer, 2007, pp. 11–29.

[21]   J. Carlson and R. R. Murphy, "How UGVs physically fail in the field", *IEEE Transactions on Robotics*, vol. 21, no. 3, pp. 423–437, 2005.

[22]   R. R. Murphy, "Proposals for New UGV, UMV, UAV, and HRI Standards for Rescue Robots", in *Proceedings of the 10th Performance Metrics for Intelligent Systems Workshop*, ACM, 2010, pp. 9–13.

[23]   S. Yarkan, S. Guzelgoz, H. Arslan, *et al.*, "Underground Mine Communications: A Survey", *IEEE Communications Surveys & Tutorials*, vol. 11, no. 3, pp. 125–142, 2009.

[24]   M. Boutin and A. Benzakour, "Radio wave characterization and modeling in underground mine tunnels", *IEEE Transactions on Antennas and Propagation*, vol. 56, no. 2, pp. 540–549, Feb. 2008.

[25]   I. Efthymiopoulos, "The SPS North Area Beams", in *SPS Training Lecture Program*, CERN, Mar. 2006.

[26] G. Battistoni, S. Muraro, P. R. Sala, *et al.*, "The FLUKA code: Description and benchmarking", in *Proceedings of the Hadronic Shower Simulation Workshop 2006, Fermilab, AIP Conference Proceeding 896*, 2007, pp. 31–49.

[27] K. Tsoulou, "Simulation studies of the mixed radiation field in TCC2 area", in *Joint RADWG and RADMON Working Group Day, CERN*, Dec. 2003.

[28] J. Vollaire, "Calculations of the radiological environment for handling of ISOLDE targets", *4th High Power Targetry Workshop, Malmo*, May 2011.

[29] K. J. Schlager, "Systems engineering-key to modern development", *IRE Transactions on Engineering Management*, vol. EM-3, no. 3, pp. 64–66, Jul. 1956.

[30] R. Parasuraman, "Requirements specification document", in *Deliverable RP6 D2.2*, EU-FP7-PURESAFE, 2014.

[31] R. Parasuraman, "Technical specifications document", in *Deliverable RP6 D2.1*, EU-FP7-PURESAFE, 2014.

[32] S.Y. Nof, *Handbook of Industrial Robotics*, ser. Electrical and electronic engineering v. 1. Wiley, 1999.

[33] J. Suomela, "Tele-presence aided teleoperation of semi-autonomous work vehicles", Helsinki University of Technology, Espoo, Finland, Licenciate thesis, 2001.

[34] R. Parasuraman, K. Kershaw, and M. Ferre, "Wireless communication for mobile robots in hostile environments", in *International workshop on telerobotics and systems engineering for scientific facilities*, UPM Madrid, Spain, Oct. 2012.

[35] R. Parasuraman, P. Pagala, K. Kershaw, *et al.*, "Energy Management Module for Mobile Robots in Hostile Environments", in *Advances in Autonomous Robotics*, ser. Lecture Notes in Computer Science, vol. 7429, Springer Berlin / Heidelberg, 2012, pp. 430–431.

[36] R. Parasuraman, P. Pagala, K. Kershaw, *et al.*, "Model Based On-Line Energy Prediction System for Semi-Autonomous Mobile Robots", in *International Conference on Intelligent Systems, Modelling and Simulation (ISMS), IEEE*, 2014.

[37] R. Parasuraman, L. Molinari, M. Di Castro, *et al.*, "A Fast Radio Signal Strength Prediction Algorithm for Mobile Robots in Unknown Environments", in *Communication-aware Robotics: New Tools for Multi-Robot Networks, Autonomous Vehicles, and Localization (CarNet) workshop, Robotics: Science and Systems Conference 2014, Berkeley, USA*, Jul. 2014.

[38] R. Parasuraman, T. Fabry, K. Kershaw, *et al.*, "Spatial sampling methods for improved communication for wireless relay robots", in *2013 International Conference on Connected Vehicles and Expo (ICCVE)*, IEEE, Dec. 2013, pp. 874–880.

[39] A. Owen-Hill, R. Parasuraman, and M. Ferre, "Haptic teleoperation of mobile robots for augmentation of operator perception in environments with low-wireless signal", in *2013 IEEE International Symposium on Safety, Security, and Rescue Robotics (SSRR)*, Oct. 2013.

[40] R. Parasuraman, T. Fabry, L. Molinari, *et al.*, "A multi-sensor RSS spatial sensing based robust stochastic optimization algorithm for enhanced wireless tethering", *Sensors*, 2014, Under review.

[41] F. Riccardo, *Introduction to Mobile Robotics*. Dipartimento di Elettronica, Informatica e Sistemistica (DEIS), Universita di Bologna, Course Handout.

[42] P. Lime and M. I. Ribeiro, *Mobile Robotics*. Instituto Superior Técnico/Instituto de Sistemas e Robótica, 2002, Course Handout.

[43] P. J. McKerrow, *Introduction to Robotics*. Addison-Wesley, 1991.

[44] H. Choset, K. M. Lynch, S. Hutchinson, *et al.*, *Principles of Robot Motion: Theory, Algorithms, and Implementations*. Cambridge, MA: MIT Press, Jun. 2005.

[45] R. Siegwart and I. R. Nourbakhsh, *Introduction to Autonomous Mobile Robots*. Scituate, MA, USA: Bradford Company, 2004.

[46] R. Siegwart, I. R. Nourbakhsh, and D. Scaramuzza, *Introduction to autonomous mobile robots*. MIT press, 2011.

[47] J. Ebken, M. Bruch, and J. Lum, "Applying unmanned ground vehicle technologies to unmanned surface vehicles", in *Proc. SPIE*, vol. 5804, 2005, pp. 585–596.

[48] A. De Luca, G. Oriolo, and M. Vendittelli, "Control of wheeled mobile robots: an experimental overview", English, in *RAMSETE*, ser. Lecture Notes in Control and Information Sciences, vol. 270, Springer Berlin Heidelberg, 2001, pp. 181–226.

[49] W. A. Aviles, T. W. Hughes, H. R. Everett, *et al.*, "Issues in mobile robotics: the unmanned ground vehicle program teleoperated vehicle", in *Proc. SPIE*, vol. 1388, 1991, pp. 587–597.

[50] P. Fahlstrom and T. Gleason, *Introduction to UAV systems*. John Wiley & Sons, 2012.

[51] M. Caccia, M. Bibuli, R. Bono, *et al.*, "Basic navigation, guidance and control of an unmanned surface vehicle", English, *Autonomous Robots*, vol. 25, no. 4, pp. 349–365, 2008.

[52] N. K. Dhiman, D. Deodhare, and D. Khemani, "A review of path planning and mapping technologies for autonomous mobile robot systems", in *Proceedings of the 5th ACM COMPUTE Conference: Intelligent & Scalable System Technologies*, ser. COMPUTE '12, Pune, India: ACM, 2012, 3:1–3:8.

[53] G. Dudek and M. Jenkin, *Computational Principles of Mobile Robotics*. New York, NY, USA: Cambridge University Press, 2000.

[54] P. Michelman and P. Allen, "Shared autonomy in a robot hand teleoperation system", in *Proceedings of the IEEE/RSJ/GI International Conference on Intelligent Robots and Systems '94. 'Advanced Robotic Systems and the Real World', IROS '94*, vol. 1, Sep. 1994, pp. 253–259.

[55] H. R. Everett, *Sensors for Mobile Robots: Theory and Application*. Natick, MA, USA: A. K. Peters, Ltd., 1995.

[56] M. Kam, X. Zhu, and P. Kalata, "Sensor fusion for mobile robot navigation", *Proceedings of the IEEE*, vol. 85, no. 1, pp. 108–119, Jan. 1997.

[57] R. Bajcsy, "Active perception", *Proceedings of the IEEE*, vol. 76, no. 8, pp. 966–1005, Aug. 1988.

[58] R. Bischoff, U. Huggenberger, and E. Prassler, "KUKA youBot - a mobile manipulator for research and education", in *2011 IEEE International Conference on Robotics and Automation (ICRA)*, May 2011.

[59] P. F. Muir and C. P. Neuman, "Kinematic modeling of wheeled mobile robots", *Journal of robotic systems*, vol. 4, no. 2, pp. 281–340, 1987.

[60] F. Mondada, E. Franzi, and P. Ienne, *Mobile robot miniaturisation: A tool for investigation in control algorithms*. Springer Berlin Heidelberg, 1994.

[61] R. M. Harlan, D. B. Levine, and S. McClarigan, "The Khepera robot and the kRobot class: a platform for introducing robotics in the undergraduate curriculum", in *ACM SIGCSE Bulletin*, ACM, vol. 33, 2001, pp. 105–109.

[62] K. Kershaw, F. Chapron, a. Coin, *et al.*, "Remote inspection, measurement and handling for LHC", *2007 IEEE Particle Accelerator Conference (PAC)*, pp. 332–334, 2007.

[63] T. S. Rappaport, *Wireless Communications: Principles and Practice*. Prentice Hall, 1996, vol. 207.

[64] A. Fink, H. Beikirch, M. Voss, *et al.*, "RSSI-based indoor positioning using diversity and Inertial Navigation", in *International Conference on Indoor Positioning and Indoor Navigation (IPIN)*, Sep. 2010.

[65] R. Katz, "CS 294-7: Radio Propagation", *White Paper, University of California - Berkeley*, pp. 1–20, 1996.

[66] A. Vlavianos and L. Law, "Assessing link quality in IEEE 802.11 wireless networks: Which is the right metric?", in *IEEE 19th International Symposium on Personal, Indoor and Mobile Radio Communications (PIMRC)*, Sep. 2008.

[67] D. G. Dudley, S. Mahmoud, M. Lienard, *et al.*, "On wireless communication in tunnels", *IEEE Antennas and Propagation International Symposium*, pp. 3305–3308, Jun. 2007.

[68] P. Tao, "Technology Study of Wireless Communication System under the Coal Mine Tunnel", *2010 International Conference on Intelligent System Design and Engineering Application*, pp. 553–556, Oct. 2010.

[69] A. Emslie, R. Lagace, and P. Strong, "Theory of the propagation of UHF radio waves in coal mine tunnels", *IEEE Transactions on Antennas and Propagation*, vol. 23, no. 2, pp. 192–205, Mar. 1975.

[70] P. Delogne, "EM propagation in tunnels", *IEEE Transactions on Antennas and Propagation*, vol. 39, no. 3, pp. 401–406, Mar. 1991.

[71] D. J. R. Martin, "Leaky-feeder radio communication: a historical review", in *Vehicular Technology Conference, 1984. 34th IEEE*, vol. 34, May 1984, pp. 25–30.

[72] C. Shannon, "Communication in the presence of noise", *Proceedings of the IRE*, vol. 37, pp. 10–21, 1949.

[73] H. Zimmermann, "OSI reference model–The ISO model of architecture for open systems interconnection", *IEEE Transactions on Communications*, vol. 28, no. 4, pp. 425–432, 1980.

[74] A. Tanenbaum, *Computer Networks*, 4th. Prentice Hall Professional Technical Reference, 2002.

[75] R. Wirz, R. Marín, J. M. Claver, *et al.*, "End-to-end congestion control protocols for remote programming of robots, using heterogeneous networks: a comparative analysis", *Robotics and Autonomous Systems*, vol. 56, no. 10, pp. 865 –874, 2008.

[76] G. Cermak, M. Pinson, and S. Wolf, "The relationship among video quality, screen resolution, and bit rate", *IEEE Transactions on Broadcasting*, vol. 57, no. 2, pp. 258–262, Jun. 2011.

[77] A. Stadler and R. Parasuraman, "Wireless video transmission tests in ISOLDE: Remote handling test of ISOLDE target units using radio controlled forklift vehicle with wireless video feedback", *CERN EDMS*, no. 1209799, 2012.

[78] C. Jay, M. Glencross, and R. Hubbold, "Modeling the effects of delayed haptic and visual feedback in a collaborative virtual environment", *ACM Trans. Comput.-Hum. Interact.*, vol. 14, no. 2, Aug. 2007.

[79] B. Sidhu, H. Singh, and A. Chhabra, "Emerging Wireless Standards-WiFi, ZigBee and WiMAX", *Int. J. Applied Science, Engineering and Technology*, vol. 4, no. 1, pp. 308–313, 2007.

[80] J. Sammarco, R. Paddock, E. Fries, *et al.*, *A Technology Review of Smart Sensors with Wireless Networks for Applications in Hazardous Work Environments*, ser. Information Circular 9496. Department of Health and Human Services, Pittsburgh, Apr. 2007.

[81] H. Schióler and T. S. Toftegaard, "Wireless Communication in Mobile Robotics: A Case for Standardization", *Wireless Personal Communications*, vol. 64, no. 3, pp. 583–596, Apr. 2012.

[82] E. Ferro and F. Potorti, "Bluetooth and Wi-Fi wireless protocols: a survey and a comparison", *Wireless Communications, IEEE*, pp. 1–24, 2005.

[83] D. Raychaudhuri and N. Mandayam, "Frontiers of wireless and mobile communications", *Proceedings of the IEEE*, vol. 100, no. 4, pp. 824–840, Apr. 2012.

[84] D. Porcino and W. Hirt, "Ultra-wideband radio technology: potential and challenges ahead", *Communications Magazine, IEEE*, pp. 66–74, Jul. 2003.

[85] J. H. Stott, "The how and why of COFDM", *EBU Technical Review*, pp. 43–50, 1998.

[86] M. D. Arthur M, "Non-Line-of-Sight (NLOS) communications - COFDM field testing results", 2010.

[87] "WirelessHD Specification Version 1.1 Overview May 2010 Notice", May 2010.

[88] V. L. Duc, O. Hoon, and Y. Seokhoon, "Reinforcing wireless links using controllable mobility of robotic relays", in *2012 18th Asia-Pacific Conference on Communications (APCC)*, Oct. 2012, pp. 23–28.

[89] S. Hert and V. Lumelsky, "Moving multiple tethered robots between arbitrary configurations", in *1995 IEEE/RSJ International Conference on Intelligent Robots and Systems 95. 'Human Robot Interaction and Cooperative Robots', Proceedings.*, vol. 2, Aug. 1995, pp. 280–285.

[90] S. Hert and V. Lumelsky, "Motion planning in R3 for multiple tethered robots", *IEEE Transactions on Robotics and Automation*, vol. 15, no. 4, pp. 623–639, Aug. 1999.

[91] N. Pezeshkian, H. G. Nguyen, and A. Burmeister, "Unmanned ground vehicle radio relay deployment system for non-line-of-sight operations", DTIC Document, Tech. Rep., 2007.

[92] A. Deshmukh, P. Vargas, R. Aylett, *et al.*, "Towards Socially Constrained Power Management for Long-Term Operation of Mobile Robots", in *Towards Autonomous Robotic Systems (TAROS) Conference, UK*, 2010.

[93] D. Austin and K. Kouzoubo, "Robust, Long Term Navigation of a Mobile Robot", in *IARP/IEE-RAS Joint Workshop on Technical Challenges for Dependable Robots in Human Environments*, 2002.

[94] S. Oh and A. Zelinsky, "Autonomous Battery Recharging for Indoor Mobile Robots", in *Australian Conference on Robotics and Automation*, 2000.

[95] Y. Mei, Y.-H. Lu, Y. Hu, *et al.*, "Energy-efficient motion planning for mobile robots", in *IEEE International Conference on Robotics and Automation*, vol. 5, 2004, pp. 4344–4349.

[96] C. H. Kim and B. K. Kim, "Minimum-Energy Motion Planning for Differential-Driven Wheeled Mobile Robots", in *Mobile Robots Motion Planning, New Challenges*, Intechopen, 2008, pp. 193–226.

[97] H. Wei, B. Wang, Y. Wang, *et al.*, "Staying-alive path planning with energy optimization for mobile robots", *Expert Systems with Applications*, vol. 39, no. 3, pp. 3559 –3571, 2012.

[98] Z. Hui-zhong, D. Shu-xin, and W. Tie-jun, "Energy-efficient motion planning for mobile robots", in *International Conference on Machine Learning and Cybernetics*, 2005.

[99] Y. Wei, C. Emmanuel, and C. Oscar, "Dynamic Modeling and Power Modeling of Robotic Skid-Steered Wheeled Vehicles", *Mobile Robots - Current Trends*, 2011.

[100] O. Chuy, J. Collins E.G., W. Yu, *et al.*, "Power modeling of a skid steered wheeled robotic ground vehicle", in *IEEE International Conference on Robotics and Automation*, 2009, pp. 4118–4123.

[101] J. Morales, J. Martinez, A. Mandow, *et al.*, "Power consumption modeling of skid-steer tracked mobile robots on rigid terrain", *IEEE Transactions on Robotics*, vol. 25, no. 5, pp. 1098–1108, 2009.

[102] J. Liu, P. Chou, N. Bagherzadeh, *et al.*, "Power-aware scheduling under timing constraints for mission-critical embedded systems", in *Design Automation Conference*, 2001, pp. 840–845.

[103] P. Lamon, "The solero rover", in *3D-Position Tracking and Control for All-Terrain Robots*, ser. Springer Tracts in Advanced Robotics, vol. 43, Springer Berlin Heidelberg, 2008, pp. 7–19.

[104] Y. Mei, Y. Yung-Hsiang Lu Hu, and C. Lee, "A case study of mobile robot's energy consumption and conservation techniques", in *12th International Connference on Advanced Robotics*, 2005, pp. 492–497.

[105] Y. Mei, Y.-H. Lu, Y. Hu, *et al.*, "Deployment of mobile robots with energy and timing constraints", *IEEE Transactions on Robotics*, vol. 22, no. 3, pp. 507–522, 2006.

[106] M. Bonani, V. Longchamp, S. Magnenat, *et al.*, "The MarXbot, a Miniature Mobile Robot Opening new Perspectives for the Collective-robotic Research", in *International Conference on Intelligent Robots and Systems, IROS, Taiwan*, 2010.

[107] J. Wawerla and R. T. Vaughan, "Optimal robot recharging strategies for time discounted labour", in *Artificial Life XI: Proceedings of the Eleventh International Conference on the Simulation and Synthesis of Living Systems*, 2008, pp. 670–677.

[108] P. Tokekar, N. Karnad, and V. Isler, "Energy-optimal velocity profiles for car-like robots", in *International Conference on Robotics and Automation*, 2011, pp. 1457–1462.

[109] R. Parasuraman, "TIM Pre-series energy management system specifications", *CERN EDMS*, no. 1318898, 2012.

[110] R. Rao, S. Vrudhula, and D. N. Rakhmatov, "Battery modeling for energy aware system design", *Computer*, vol. 36, no. 12, pp. 77–87, 2003.

[111] R. Vaughan, "Massively multi-robot simulation in stage", *Swarm Intelligence*, vol. 2, pp. 189–208, 2008.

[112] M. Quigley, B. Gerkey, K. Conley, *et al.*, "ROS: an open-source Robot Operating System", *ICRA Workshop on Open Source Software*, 2009.

[113] D. Gossow, A. Leeper, D. Hershberger, *et al.*, "Interactive Markers: 3-D User Interfaces for ROS Applications", *IEEE Robotics and Automation Magazine*, no. December, pp. 14–15, 2011.

[114] R. Wirz, R. Marín, M. Ferre, *et al.*, "Bidirectional transport protocol for teleoperated robots", *IEE Transactions on Industrial Electronics*, vol. 56, p. 10, Oct. 2009.

[115] C. U. Bas and S. C. Ergen, "Spatio-temporal characteristics of link quality in wireless sensor networks", *2012 IEEE Wireless Communications and Networking Conference (WCNC)*, pp. 1152–1157, Apr. 2012.

[116] R. Catherall, "Future Developments at ISOLDE", *ISOLDE Workshop and Users meeting*, Dec. 2012.

[117] Y. Chapre, P. Mohapatra, S. Jha, *et al.*, "Received signal strength indicator and its analysis in a typical WLAN system (short paper)", in *2013 IEEE 38th Conference on Local Computer Networks (LCN)*, Oct. 2013, pp. 304–307.

[118] M. Baunach, C. Mühlberger, C. Appold, *et al.*, "Analysis of Radio Signal Parameters for Calibrating RSSI Localization Systems", *Institut für Informatik, Universität Würzburg, Tech. Rep*, vol. 455, 2009.

[119] S. J. Fortune, D. M. Gay, B. W. Kernighan, *et al.*, "WISE design of indoor wireless systems: practical computation and optimization", *Computational Science Engineering, IEEE*, vol. 2, no. 1, pp. 58–68, 1995.

[120] C. T. Chou, A. Misra, and J. Qadir, "Low-Latency Broadcast in Multirate Wireless Mesh Networks", *IEEE Journal on Selected Areas in Communications*, vol. 24, no. 11, pp. 2081–2091, Nov. 2006.

[121] *ProSafe Dual Band Wireless-N Access Point WNDAP350, Reference Manual*. Netgear Inc., Nov. 2009.

[122] *NWD2105 - Wireless N-lite USB Adapter, User Guide*. Zyxel Communication Corp., Sep. 2011.

[123] K. Srinivasan and P. Levis, "RSSI is Under Appreciated", in *Proceedings of the Third Workshop on Embedded Networked Sensors (EmNets)*, 2006.

[124]   *Wireless link budget analysis : How to calculate link budget for your wireless network, Whitepaper*. Tranzeo Wireless Technologies Inc., 2010.

[125]   R. Murphy and J. Burke, "From remote tool to shared roles", *Robotics & Automation Magazine*, vol. 15, no. 4, pp. 39–49, Dec. 2008.

[126]   J. Geissbühler, "Wireless multihop communications for first responder connectivity", Master's thesis, Swiss Federal Institute of Technology (ETH) Zürich, Zurich, Switzerland, 2006.

[127]   K. Hee Sung, L. Binghao, C. Wan Sik, *et al.*, "Spatiotemporal location fingerprint generation using extended signal propagation model", *Journal of Electrical Engineering & Technology*, vol. 7, no. 5, pp. 789–796, 2012.

[128]   X. Long and S. B, "A real-time algorithm for long range signal strength prediction in wireless networks", in *Wireless Communications and Networking Conference, 2008. WCNC 2008. IEEE*, Mar. 2008, pp. 1120–1125.

[129]   K. Farkas, T. Hossmann, F. Legendre, *et al.*, "Link quality prediction in mesh networks", *Computer Communications*, vol. 31, no. 8, pp. 1497 –1512, 2008.

[130]   M. Malmirchegini and Y. Mostofi, "On the spatial predictability of communication channels", *IEEE Transactions on Wireless Communications*, vol. 11, no. 3, pp. 964–978, Mar. 2012.

[131]   Y. Mostofi, A. Gonzalez-Ruiz, A. Gaffarkhah, *et al.*, "Characterization and modeling of wireless channels for networked robotic and control systems - a comprehensive overview", in *IEEE/RSJ International Conference on Intelligent Robots and Systems IROS*, Oct. 2009, pp. 4849–4854.

[132]   A. Ghaffarkhah and Y. Mostofi, "Channel learning and communication-aware motion planning in mobile networks", in *American Control Conference (ACC), 2010*, Jun. 2010, pp. 5413–5420.

[133]   T. Fabry, L. Vanherpe, M. Baudin, *et al.*, "Interactive intervention planning in particle accelerator environments with ionizing radiation", *Nuclear Instruments and Methods in Physics Research Section A: Accelerators, Spectrometers, Detectors and Associated Equipment*, vol. 708, pp. 32–38, 2013.

[134]   N. Bezzo and R. Fierro, "Tethering of mobile router networks", *American Control Conference (ACC), 2010*, 2010.

[135]   M. Omiya, "Throughput Measurements and Numerical Prediction Methods for IEEE802.11n Wireless LAN Installations at 2.4 GHz in a Residential Two-Story House", in *International symposium on Antennas and Propagation (ISAP)*, Oct. 2011.

[136] J. Fink, A. Ribeiro, and V. Kumar, "Motion planning for robust wireless networking", in *Robotics and Automation (ICRA), 2012 IEEE International Conference on*, 2012, pp. 2419–2426.

[137] N. Bezzo, B. Griffin, P. Cruz, *et al.*, "A cooperative heterogeneous mobile wireless mechatronic system", *IEEE/ASME Transactions on Mechatronics*, vol. 99, 2012.

[138] J. N. Twigg, J. R. Fink, P. Yu, *et al.*, "RSS gradient-assisted frontier exploration and radio source localization", in *Robotics and Automation (ICRA), 2012 IEEE International Conference on*, IEEE, 2012, pp. 889–895.

[139] B.-C. Min, J. Lewis, D. Schrader, *et al.*, "Self-orientation of directional antennas, assisted by mobile robots, for receiving the best wireless signal strength", in *Sensors Applications Symposium (SAS), 2012 IEEE*, 2012.

[140] S. Venkateswaran, J. T. Isaacs, B. M. Sadler, *et al.*, "RF source-seeking by a micro aerial vehicle using rotation-based angle of arrival estimates", in *Proc. of the 2013 Amer. Contr. Conf.*, Jun. 2013.

[141] B. Griffin, R. Fierro, and I. Palunko, "An autonomous communications relay in GPS-denied environments via antenna diversity", *The Journal of Defense Modeling and Simulation: Applications, Methodology, Technology*, vol. 9, no. 1, pp. 33–44, Jun. 2011.

[142] S. Gil, M. Schwager, B. J. Julian, *et al.*, "Optimizing communication in air-ground robot networks using decentralized control", in *IEEE International Conference on Robotics and Automation (ICRA)*, May 2010, pp. 1964–1971.

[143] M. Avriel, *Nonlinear programming. Analysis and methods.* Ser. Prentice-Hall Series in Automatic Computation. Prentice-Hall, Inc., 1976.

[144] M. Lindhè, K. H. Johansson, and A. Bicchi, "An experimental study of exploiting multipath fading for robot communications", in *Proceedings of Robotics: Science and Systems*, Jun. 2007.

[145] D.G. Brennan, "Linear diversity combining techniques", in *Proc. IRE*, vol. 47, Jun. 1959, pp. 1075–1102.

[146] A. Birk and H. Kenn, "A rescue robot control architecture ensuring safe semi-autonomous operation", *RoboCup 2002. Robot Soccer World Cup VI*, 2003.

[147] E. Slawinki, V. Mut, and J. Postigo, "Teleoperation of mobile robots with time-varying delay", *IEEE Transactions on Robotics*, vol. 23, no. 5, pp. 1071–1082, 2007.

[148] R. Wegner and J. Anderson, "Agent-Based Support for Balancing Teleoperation and Autonomy in Urban Search and Rescue", *International Journal of Robotics and Automation*, vol. 21, no. 2, pp. 1–19, 2006.

[149]   S. Muszynski, J. Stuckler, and S. Behnke, "Adjustable autonomy for mobile teleoperation of personal service robots", *2012 IEEE RO-MAN: The 21st IEEE International Symposium on Robot and Human Interactive Communication*, pp. 933–940, Sep. 2012.

[150]   I. Farkhatdinov and J. Ryu, "Improving mobile robot bilateral teleoperation by introducing variable force feedback gain", *2010 IEEE/RSJ International Conference on Intelligent Robots and Systems*, pp. 5812–5817, Oct. 2010.

[151]   I. Farkhatdinov and J.-H. Ryu, "A preliminary experimental study on haptic teleoperation of mobile robot with variable force feedback gain", *2010 IEEE Haptics Symposium*, pp. 251–256, Mar. 2010.

[152]   H. Wang and X. P. Liu, "Design of a novel mobile assistive robot with haptic interaction", *2012 IEEE International Conference on Virtual Environments Human-Computer Interfaces and Measurement Systems (VECIMS) Proceedings*, pp. 115–120, Jul. 2012.

[153]   S. Lee, G. Sukhatme, G. Kim, *et al.*, "Haptic control of a mobile robot: A user study", in *Intelligent Robots and Systems, 2002. IEEE/RSJ International Conference on*, vol. 3, IEEE, Jun. 2002, pp. 2867–2874.

[154]   Ö. Çayırpunar, B. Tavlı, and V. Gazi, "Dynamic Robot Networks for Search and Rescue Operations", in *EURONIIARP International Workshop on Robotics for Risky Interventions and Surveillance of the Environment, Benicassim, Spain*, Jan. 2008.

[155]   S. Lichiardopol, "A Survey on Teleoperation", in *DCT 2007.155*, Technische Universiteit Eindhoven, 34 p.

[156]   A. J. Silva, O. a. D. Ramirez, V. P. Vega, *et al.*, "PHANToM OMNI Haptic Device: Kinematic and Manipulability", *2009 Electronics, Robotics and Automotive Mechanics Conference (CERMA)*, pp. 193–198, Sep. 2009.

[157]   G. Tuna, K. Gulez, T. V. Mumcu, *et al.*, "Mobile Robot Aided Self-Deploying Wireless Sensor Networks for Radiation Leak Detection", *2012 5th International Conference on New Technologies, Mobility and Security (NTMS)*, May 2012.

[158]   S. Timotheou and G. Loukas, "Autonomous networked robots for the establishment of wireless communication in uncertain emergency response scenarios", in *Proceedings of the 2009 ACM symposium on Applied Computing - SAC '09*, ACM Press, 2009.

[159]   C. Dixon and E. Frew, "Optimizing cascaded chains of unmanned aircraft acting as communication relays", *IEEE Journal on Selected Areas in Communications*, vol. 30, no. 5, pp. 883–898, Jun. 2012.

[160]   N. Bezzo, B. Griffin, P. Cruz, *et al.*, "A cooperative heterogeneous mobile wireless mechatronic system", *IEEE/ASME Transactions on Mechatronics*, vol. 19, no. 1, pp. 20–31, Feb. 2014.

[161] S. Zickler and M. Veloso, "RSS-based relative localization and tethering for moving robots in unknown environments", in *Robotics and Automation (ICRA), 2010 IEEE International Conference on*, 2010, pp. 5466–5471.

[162] D. Corbett, D. Gage, and D. Hackett, "Robotic Communications and Surveillance - The DARPA LANdroids Program", in *AI 2011: Advances in Artificial Intelligence*, ser. Lecture Notes in Computer Science, D. Wang and M. Reynolds, Eds., vol. 7106, Springer Berlin Heidelberg, 2011, pp. 749–758.

[163] H. G. Nguyen, N. Pezeshkian, A. Gupta, *et al.*, "Maintaining communication link for a robot operating in a hazardous environment", in *ANS 10th Int. Conf. on Robotics and Remote Systems for Hazardous Environments*, 2004, pp. 28–31.

[164] G. Antonelli, F. Arrichiello, S. Chiaverini, *et al.*, "Coordinated Control of Mobile Antennas for Ad-Hoc Networks Coordination of Multi-Vehicle Systems", 2005.

[165] C. Rizzo, J. Villarroel, and D. Tardioli, "Spatial diversity based coverage map building in complex tunnel environments", in *2012 International Conference on Wireless Communications in Unusual and Confined Areas (ICWCUCA)*, Aug. 2012.

[166] S. Hara, H. Sugano, T. Inoue, *et al.*, "A receiver diversity technique for ensuring high reliability of wireless vital data gathering in hospital rooms", in *2010 Annual International Conference of the IEEE Engineering in Medicine and Biology Society (EMBC)*, Aug. 2010, pp. 348–351.

[167] V. Braitenberg, *Vehicles: Experiments in synthetic psychology*. Cambridge, MA: MIT Press, 1984, pp. 1–164.

[168] I. E. Paromtchik and U. M. Nassal, "Reactive motion control for an omnidirectional mobile robot", in *Proc. of the Third European Control Conference*, 1995, pp. 5–8.

[169] G. Mester, "Intelligent mobile robot control in unknown environments", in *Intelligent Engineering Systems and Computational Cybernetics*, Springer, 2009, pp. 15–26.

[170] A. So and L. Ben, "Effect of relaying on capacity improvement in wireless local area networks", in *Wireless Communications and Networking Conference, 2005 IEEE*, vol. 3, Mar. 2005, pp. 1539–1544.

[171] Y. Nesterov, "Smooth minimization of non-smooth functions", *Mathematical Programming*, vol. 103, no. 1, pp. 127–152, 2005.

[172] J. D. Cook, "Basic properties of the soft maximum", in *UT MD Anderson Cancer Center Department of Biostatistics Working Paper Series*, ser. Working paper 70, Bepress, 2011.

[173] R. Brekelmans, L. Driessen, H. Hamers, *et al.*, "Gradient estimation schemes for noisy functions", *Journal of Optimization Theory and Applications*, vol. 126, no. 3, pp. 529–551, 2005.

[174] L. Bottou, "Online algorithms and stochastic approximations", in *Online Learning and Neural Networks*, D. Saad, Ed., revised, oct 2012, Cambridge, UK: Cambridge University Press, 1998.

[175] X. Zhang, Y. Sun, J. Xiao, *et al.*, "Theseus gradient guide: an indoor transmitter searching approach using received signal strength", in *2011 IEEE International Conference on Robotics and Automation (ICRA)*, May 2011, pp. 2560–2565.

[176] G. Deak, K. Curran, and J. Condell, "Filters for rssi-based measurements in a device-free passive localisation scenario", *International Journal on Image Processing & Communications*, vol. 15, no. 1, pp. 23–34, 2011.

[177] R. Valenzuela, O. Landron, and D. L. Jacobs, "Estimating local mean signal strength of indoor multipath propagation", *IEEE Transactions on Vehicular Technology*, vol. 46, no. 1, pp. 203–212, Feb. 1997.

[178] J. Borenstein and Y. Koren, "The vector field histogram-fast obstacle avoidance for mobile robots", *IEEE Transactions on Robotics and Automation*, vol. 7, no. 3, pp. 278–288, Jun. 1991.